ineering
brary

JUL 13 1937

UNITED STATES DEPARTMENT OF COMMERCE

Journal of Research

of the

National Bureau of Standards

Vol. 18, No. 6 June 1937

CONTENTS

RP	TITLE AND AUTHOR	Page
1000.	Study of the crystal behavior of hydrocarbons. Robert T. Leslie and Wilson W. Heuer ..... [Price 10c]	639
1001.	Characteristics of the ionosphere and their application to radio transmission. Theodore R. Gilliland, Samuel S. Kirby, Newbern Smith, and Stephen E. Reymer ..... [Price 10c]	645
1002.	Accelerated weathering tests of mineral-surfaced asphalt shingles. Hubert R. Snoke and Braxton E. Gallup ..... [Price 10c]	669
1003.	Compressibility of fused-quartz glass at atmospheric pressure. Walter B. Emerson ..... [Price 10c]	683
1004.	Behavior of leather in the oxygen bomb. Joseph R. Kanagy [Price 5c]	713
1005.	Compensation of strain gages for vibration and impact. William M. Bleakney ..... [Price 5c]	723
	Index to volume 18 (January 1937 to June 1937) Research Papers 957 to 1005	731

The articles listed above may be purchased separately (see cover page II) at the prices listed in the table of contents

A monthly periodical of pure and applied science published by our National Government

Journal of Research

of the

National Bureau of Standards

The January 1937 issue of the Journal of Research of the National Bureau of Standards began the eighteenth semiannual volume of this periodical. Fundamental researches in progress in the Bureau's laboratories are reported in this JOURNAL. If you are interested in new developments in science and technology, you should receive the JOURNAL. If you are not already a subscriber you are invited to send in your subscription.

Technical News Bulletin

This is a monthly publication containing short articles reporting progress of work in the Bureau laboratories, abstracts of papers which appear in the Journal of Research, accounts of scientific and technical meetings in which the Bureau has taken part, a list of all publications by members of the staff, and other items within the Bureau's fields. The BULLETIN is designed primarily to give a general and timely review of the activities of the Bureau in brief form. It is a prompt and reliable source of official information. If you have not already subscribed for the BULLETIN, you are invited to do so.

ANNUAL SUBSCRIPTION	Prices	
	United States, Canada, Cuba, Mexico, Newfoundland, Republic of Panama	Other countries
Journal of Research of the National Bureau of Standards:		
12 monthly issues (2 volumes), paper covers	$2.50	$3.25
Bound volume (½ year, 1 volume), blue buckram . . .	3.00	3.50
Technical News Bulletin, 12 monthly issues	.50	.70

Research Papers, reprinted individual articles appearing in the Journal of Research, are available from the Superintendent of Documents shortly after appearance of monthly issue of the JOURNAL.

Address orders only to
Superintendent of Documents, U. S. Government Printing Office,
Washington, D. C.

UNITED STATES DEPARTMENT OF COMMERCE
DANIEL C. ROPER, Secretary
NATIONAL BUREAU OF STANDARDS
Lyman J. Briggs, Director

✦

Journal of Research

of the

National Bureau of Standards

✦

Volume 18, Number 6

June 1937

UNITED STATES
GOVERNMENT PRINTING OFFICE
WASHINGTON : 1937

For sale by the Superintendent of Documents, Washington, D. C. - - - - - Price 25 cents
$2.50 per year on subscription

The prices of the separate Research Papers appearing in this JOURNAL are given on the front cover page. If 100 or more copies of any separate are ordered, a discount of 25 percent is allowed. Those who desire copies of separate Research Papers should send their orders and remittances without delay to the Superintendent of Documents, U. S. Government Printing Office, Washington, D. C. This will aid him to determine the number of copies to be printed for sale. Research Papers are not printed from electrotypes, and usually no more reprints can be had when the first and only printing is exhausted.

U. S. Department of Commerce National Bureau of Standards

RESEARCH PAPER RP1000

Part of Journal of Research of the National Bureau of Standards, Volume 18, June 1937

STUDY OF THE CRYSTAL BEHAVIOR OF HYDROCARBONS [1]

By Robert T. Leslie [2] and Wilson W. Heuer [3]

ABSTRACT

The construction and operation of a microscope for the observation of the growth of crystals at low temperatures are described. Photomicrographs of nine aromatic, six cycloparaffinic, eight normal paraffinic, and five branched-chain paraffinic hydrocarbons of known structure were obtained. It was shown that successive members of the homologous series of normal paraffins did not differ in crystal appearance. It was observed, however, that condensed molecules tended to crystallize in polyhedrons of about equal dimensions, whereas molecules with long chains tended to form long prisms. Mixed molecules showed modified forms depending on the relative influence of the chain and the condensed groups.

CONTENTS

	Page
I. Introduction	639
II. Apparatus and method	640
1. Crystallization without solvents	641
2. Crystallization with solvents	641
III. Discussion of crystal behavior	642
IV. Conclusions	643

I. INTRODUCTION

The identification of hydrocarbons by other than physical properties is difficult because of their inertness to chemical reactions which might serve as tests. Furthermore, identification by physical properties requires a high degree of purity of the sample and accurate data on compounds of known structure for comparison. The study of the properties of the crystals offers a possible means of identifying the chief constituents of a mixture without actually isolating the materials. A number of experimenters have studied the crystal behavior of hydrocarbon waxes,[4,5] and some observations have been made on lower-melting hydrocarbons.[6,7] In this work an attempt has been made to obtain a series of photomicrographs of the crystals of the low-melting paraffinic, cycloparaffinic, and aromatic hydrocarbons for use in comparison with materials isolated from the naphtha fraction of petroleum and to correlate the crystal habit with molecular structure, if possible.

[1] Financial assistance has been received from the research fund of the American Petroleum Institute. This is part of Project 6, the Separation, Identification, and Determination of the Constituents of Petroleum.

[2] [3] Research Associates at the National Bureau of Standards, representing the American Petroleum Institute.

[4] S. W. Ferris, A. C. Cowles, Jr., and L. M. Henderson, Ind. Eng. Chem. **23**, 681 (1931).

[5] G. D. Graves, Ind. Eng. Chem. **23**, 762 (1931).

[6] R. T. Leslie, J. Research NBS **15**, 41 (1935) RP808.

[7] R. T. Leslie, J. Research NBS **17**, 761 (1936) RP943.

While the difficulties in measuring extinction angles at low temperatures are not insuperable, some modification of the apparatus would be necessary, and this work is confined to the study of the appearances of the characteristic crystal forms.

II. APPARATUS AND METHOD

Figure 1 is a diagram of the apparatus used in securing the photographs. Its final form resulted from a number of attempts to build an apparatus which was convenient, economical, and rapid in operation. Some of the photographs shown in a previous work by the author were made by C. P. Saylor in an apparatus designed for observing crystals of rubber.[8] The chief differences are in the placing of the microscope objective within the cold chamber, the somewhat more compact cooling unit, and the side opening in the vacuum chamber for ease in manipulation of the sample. A microscope suitable for work at low temperatures has also been described by S. Erk,[9] which involves the use of a cooling unit submerged in a Dewar tube in place of the ordinary microscope stage. The experience of the present authors indicates that difficulty would be encountered with frost in such an arrangement during the time necessary to grow crystals of hydrocarbons.

The diagram of the apparatus is self-explanatory, and only a few details of construction will be emphasized. With some microscope objectives it was found that the low temperatures affected the canada balsam and caused the lenses to separate. Such lenses could be restored to usefulness by clamping them together and warming in an oven. Satisfactory lenses which will not split with large temperature changes are obtainable from some manufacturers, however. A 10× objective with a camera arrangement equivalent to a 10× ocular giving a magnification of about 100 times was used in this work. The bottoms of the vacuum jacket through which the illumination passed were made by sealing in disks of optically polished glass. It was found that simple flattening of the bottoms and polishing on the outsides before making the seal at the top of the dewar tube, leaving the inside unpolished, gave surfaces which distorted the light beam and produced nonuniformly illuminated fields. The evacuated tube in the barrel of the microscope was made by placing polished glass disks on the ends of the tube, heating in an electric furnace almost to their softening temperature, and sealing with a tiny gas flame while still in the furnace (Fairchild furnace method).[10] A practically undistorted surface was obtained by this means. The Polaroid screen (iodoquinine sulphate crystals on cellulose acetate) was found to be effective as a polarizing agent. The glass "stage", *R*, was a polished disk of such a diameter that it could be removed from the apparatus through the side tube, *P*. A variable resistance was placed in series with the Photoflood light, C_1, and it was burned at full capacity only during the exposure of the plates. With the single light it was found that exposures of 1 or 2 minutes were required for "process panchromatic" plates. Only 3 to 20 seconds were required for "superpanchromatic" plates, and most of the photographs were made with the latter. The cryostat was made from a single rod of brass, by boring out the center, turning recesses

[8] W. H. Smith, C. P. Saylor, and H. J. Wing, B.S J. Research **10**, 479 (1933) RP544.
[9] S. Erk, Physik Z. **36**, 451 (1935).
[10] C. O. Fairchild, J. Opt. Soc. Am. **4**, 496 (1920).

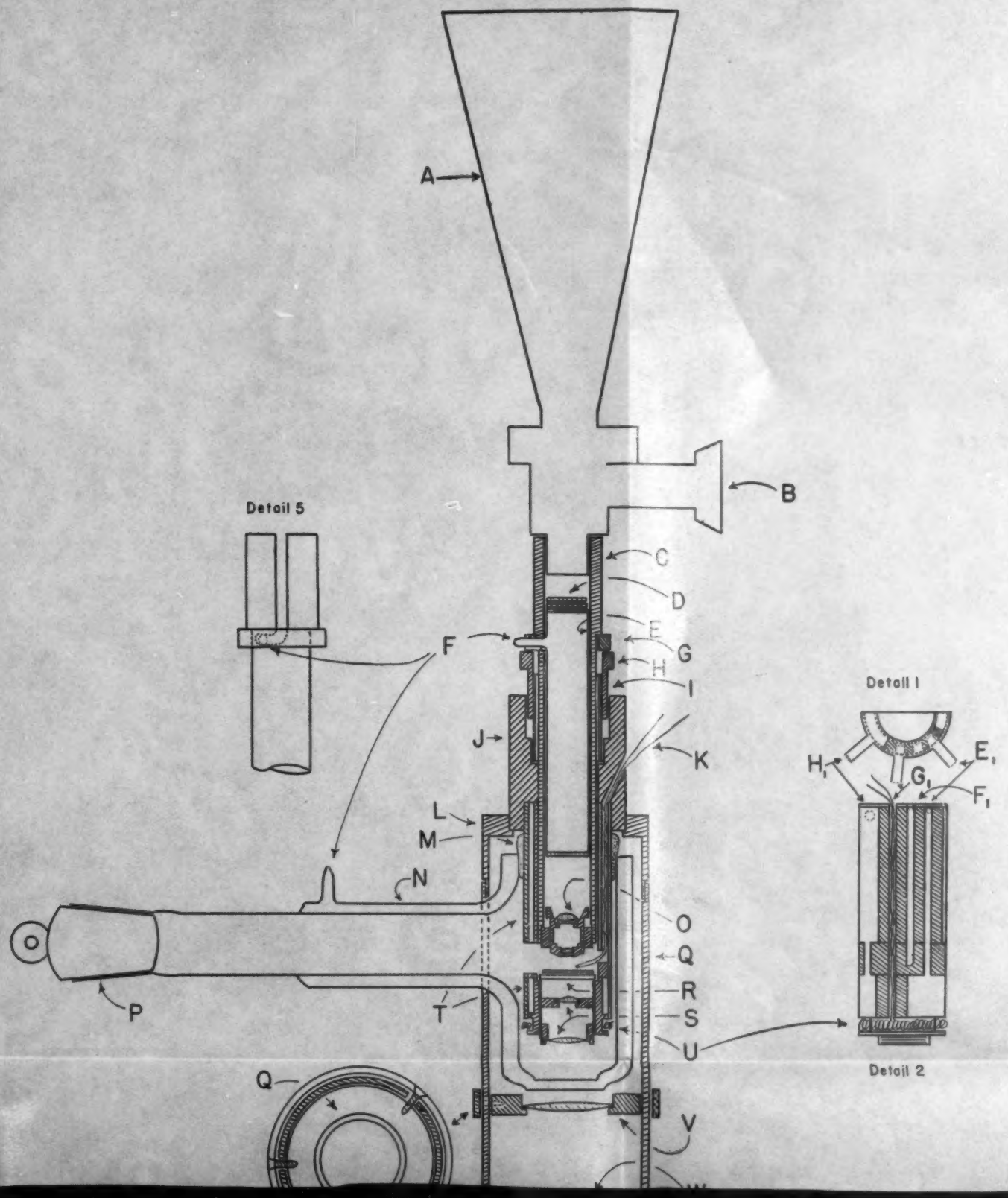
A
B
C
D
E
F
G
H
I
J
K
L
M
N
O
Q
R
S
T
U
V
W
P
Q
Detail 5
Detail 1
H_1
E_1
G_1
F_1
Detail 2

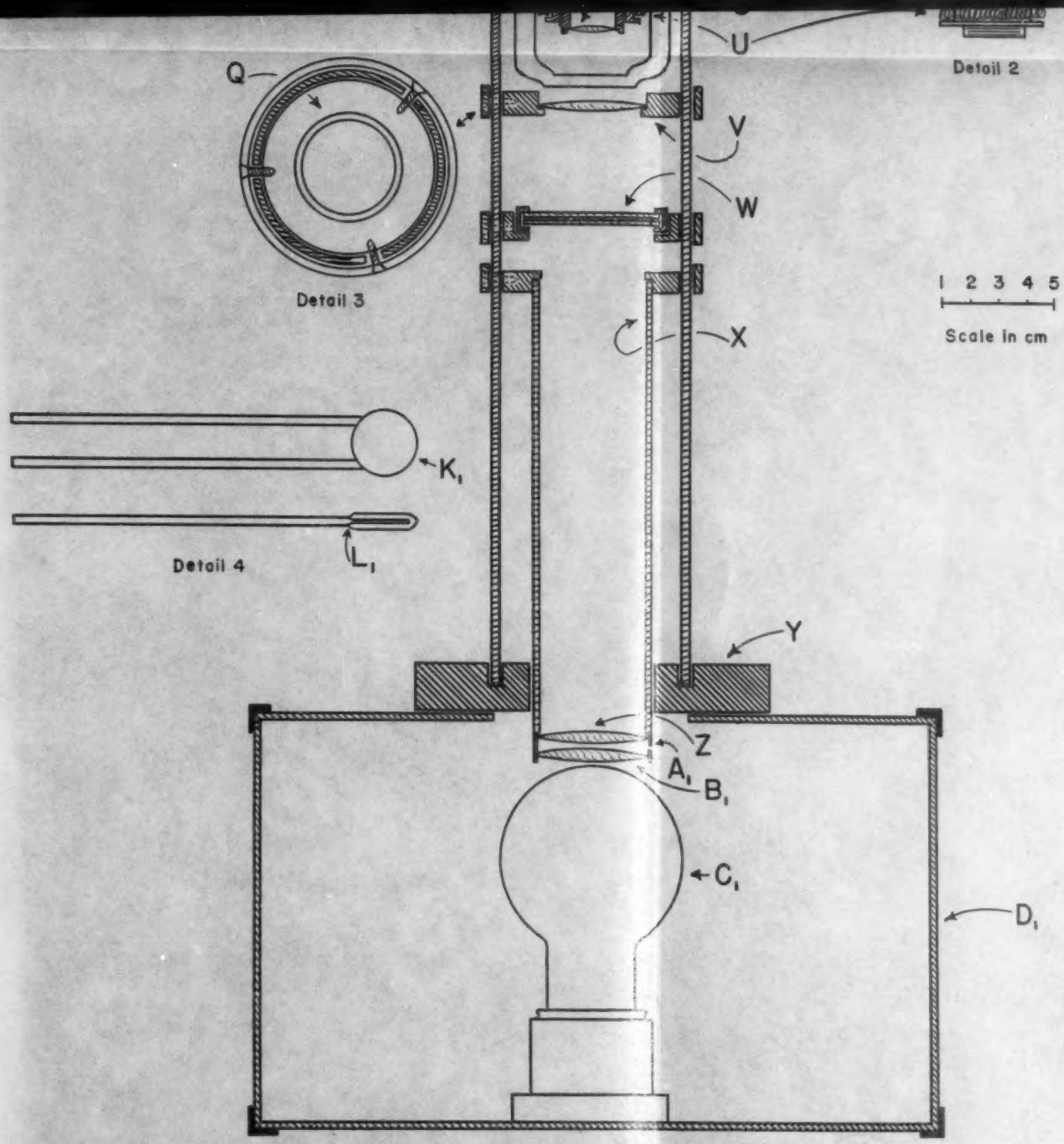

FIGURE 1.—*Microscope for studying crystallization at low temperatures.*

A, camera attachment for microscope; *B*, eyepiece; *C*, Bakelite tube of microscope; *D*, Polaroid analyzer; *E*, evacuated tube with optically clear ends (made by Fairchild oven technique; see reference 10) for thermal insulation in tube; *F*, seal after evacuation of *E*; *G*, Bakelite collar; *H*, threaded brass sleeve for focusing; *I*, screw threads (40/inch); *J*, Bakelite tube for thermal insulation; *K*, thermocouple; *L*, Bakelite cap; *M*, soft-rubber air seal; *N*, evacuated glass jacket; *O*, microscope objective; *P*, opening for manipulating sample; *Q*, Bakelite case; *R*, optically clear glass disk "stage" with thin glass cover; *S*, condensing lenses; *T*, chambers in cooler for cold air vapors; *U*, electrical heating coil insulated from cooler with mica; *V*, 10 diopter condensing lens; *W*, Polaroid polarizer; *X*, Bakelite tube holding lenses *Z* and B_1; *Z*, 5 diopter lens; A_1, ventilating hole; B_1, 20 diopter lens; C_1, Photoflood lamp; D_1, Transit board illuminator box; E_1, cold-air inlet; F_1, thermocouple well; G_1, dry-air inlet and conduit for heater leads; H_1, air outlet from cooler; K_1, cell for observing crystallization from solution; L_1, space for liquids (0.001 inch).

Detail 1.—Top view of cooler, showing position of inlet and outlet tubes.
Detail 2.—Section of cooler, showing conduits for air and electrical connections.
Detail 3.—Top view of holders for condensing lenses and polarizer showing means for adjusting position for focusing.
Detail 4.—Glass cell for observation of crystallization from solution.
Detail 5.—Microscope tube showing method of locking evacuated tube in position.

138329—37 (Face p. 640)

UNIV. OF MICH.

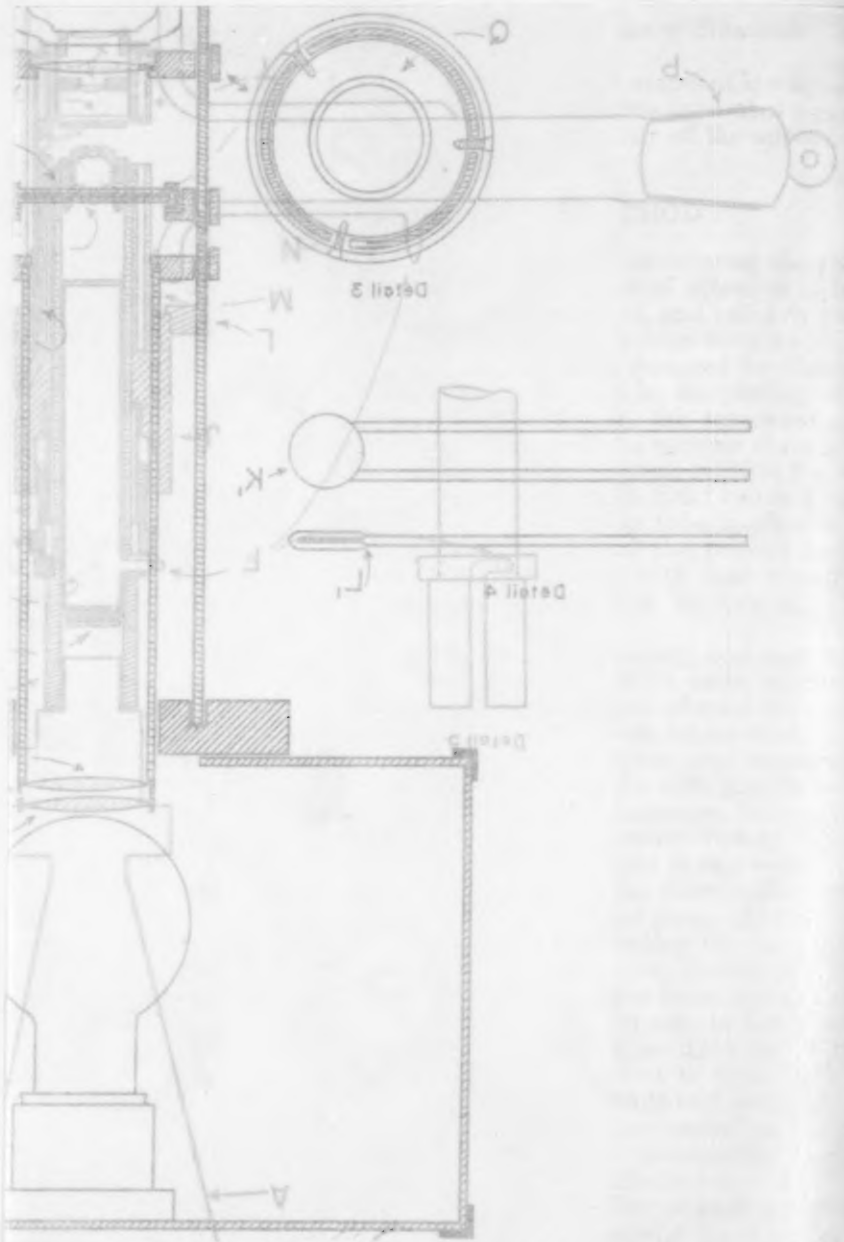
Detail 3
Detail 4

for the liquid air chambers, hard-soldering in blocks of brass into which the various channels for air, etc., were milled, and soft-soldering the jacket over the outside. It was found necessary to allow at least half a centimeter between each channel in order to be sure of a seal between them. The glass cells shown in detail 4 were made by spacing the polished disks with platinum foil or steel ribbon of the desired thickness and sealing most of the circumference of the beveled edges. The spacing ribbon was then withdrawn and the side tubes joined. Cells of 0.01 and 0.001 inch were tried. For most hydrocarbons, however, the cells were found impractical because of the necessity for seeding and otherwise manipulating the samples to produce cyrstal growth. A positive pressure of dry air was maintained within the apparatus by attaching a poorly evacuated dewar tube containing boiling liquid air to G_1. The liquid air for cooling was drawn into the apparatus by suction at H_1, and the temperature was controlled by varying the suction and the current through the heating coil, U.

A great deal of experience was required to grow crystals which were satisfactory for study, and the hydrocarbons differed greatly in the ease with which they formed large easily observable crystals. As much as 3 or 4 hours of patient warming and cooling was required for many of the crystals. Prolonged observation was also necessary in many cases to determine the characteristic behavior, since the crystals sometimes grow in anomalous and misleading forms. Repeated crystallizations generally make the distinguishing crystal forms obvious. No rigorous procedure can be described which will insure satisfactory results but the following are two of the methods which were found useful.

1. CRYSTALLIZATION WITHOUT SOLVENTS

Hydrocarbons which crystallized readily (generally above $-100°$ C) were observed by introducing a very small amount into the stage with an "eyedropper" drawn out to a very long capillary. The material was introduced after the apparatus had almost reached the freezing temperature, to avoid evaporation and condensation on the lenses. The first crystals generally appeared as masses of small size. The apparatus was then allowed to warm very gradually until most of the mass was melted, and the few remaining crystals formed nuclei for the growth of better formed ones on second cooling. The thin glass cover on the stage shown in the figure aided in obtaining a field with little depth which could be focused readily, but it was not necessary and sometimes interfered with crystal growth. If great undercooling occurred, it was found that crystallization could be induced by touching the edge of the stage with a chilled glass rod or introducing a few seed crystals from a mass which had been formed outside the instrument, from solvents if necessary.

2. CRYSTALLIZATION WITH SOLVENTS

Materials which form glasses or poorly developed crystals could generally be crystallized from solvents outside the apparatus, some of the crystals being then transferred to the stage with a little of the solvent by drawing them up into a glass tube of about 1-mm bore and discharging them by forcing a small glass rod down the tube. This procedure prevented the formation of much ice in the transfer.

The crystals were then improved by alternate warming and cooling, as described above. For the photographs shown in this work, small quantities of the hydrocarbons in propane were poured into a few milliliters of liquid methane. When this procedure is followed, the electric heater should not be used, because of the danger of igniting the gases.

III. DISCUSSION OF CRYSTAL BEHAVIOR

The photomicrographs have been grouped according to type and homologous series as much as possible. Thus from the upper-left cut of figure 2 to the upper-left view of figure 5, inclusive, are crystals of aromatic hydrocarbons; from the upper left of figure 5 to the middle left of figure 6 are cycloparaffins; from the middle right of figure 6 to the upper left of figure 9 are normal paraffins; and from the upper-right cut of figure 9 through figure 10 are branched-chain paraffins. More than one photograph of some of the compounds are shown to give an idea of the different appearance which the crystals may be expected to present. Because of interference patterns most of the crystals produced highly colored kaleidoscopic effects. All except cyclohexane were visible between crossed polarizing screens, indicating that they were birefringent (transmitted light at different velocities along different axes). Cyclohexane crystals, which have cubic structure, were only slightly birefringent and were nearly invisible with polarized light. They also showed no pronounced symmetry of crystal appearance with unpolarized light, though the material had other characteristics of a very pure, easily crystallized substance (white appearance and good cooling curve). The round, pebble-like grains which were photographed were obtained only after careful growth, the tendency being to form masses of very tiny crystals.

The aromatic hydrocarbons, with the exception of ethylbenzene, formed crystals, highly colored under polarized light, which grew rather easily. The cycloparaffins, except cyclohexane, were also readily crystallized, though they generally require seeding and some manipulation to cause them to grow. It is to be noted that the crystals of the aromatic and the corresponding cycloparaffins bear no resemblances. The normal paraffins tended to crystallize readily as masses in most cases, and dilution with solvent was necessary to form single crystals which could be studied. They crystallized readily in most cases. The branched-chain hydrocarbons were more difficult to crystallize. All of these crystals were obtained from solvents. *n*-Pentane, 2-methylbutane, and methylcyclopentane were particularly difficult to crystallize. They appeared to have less tendency to orient in individual crystal units than the other materials. No very good photographs of these substances were obtained, partly because of lack of time.

Examination of the normal hydrocarbons shows that they tend to form long prismatic crystals, while the hydrocarbons with closed chains, such as benzene, toluene, methylcyclohexane, etc., form more nearly equidimensional polyhedrons. With increasing number and length of the side chains on the rings, there seems to be an increased

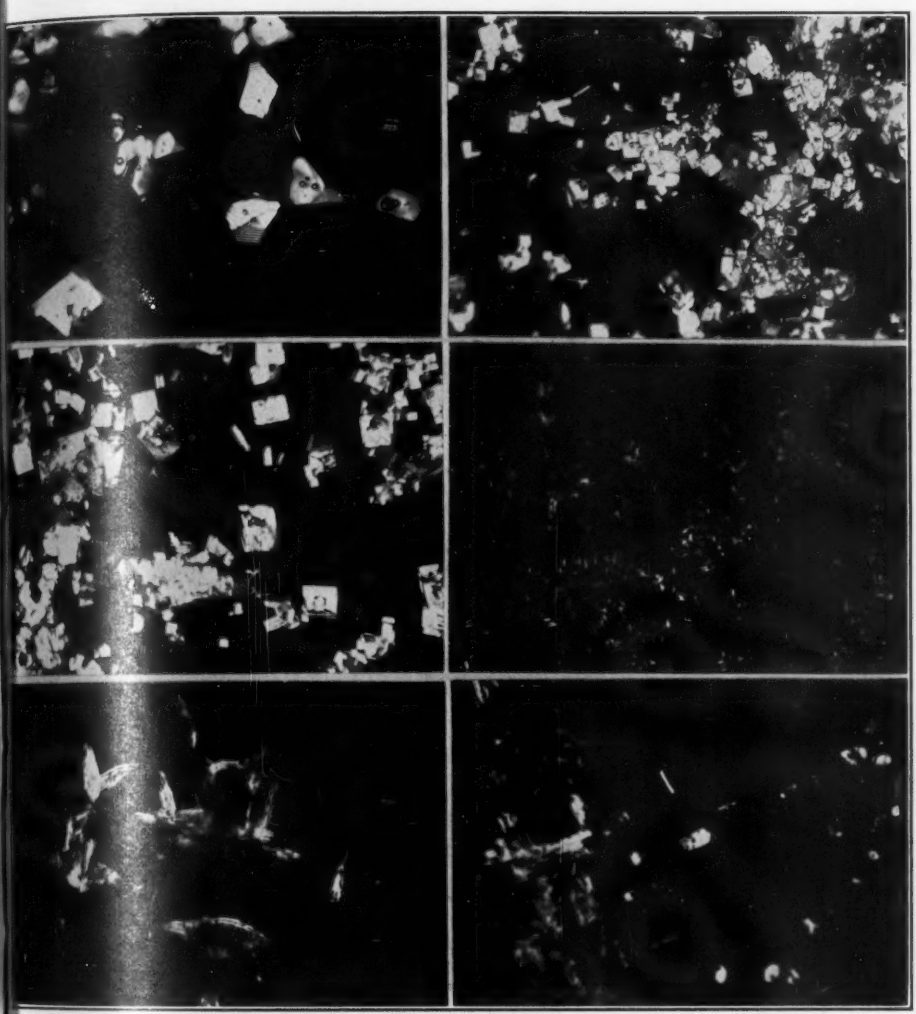

FIGURE 2.—*Crystals of aromatic hydrocarbons, benzene, toluene, ethylbenzene, and o-xylene.*

Upper left, benzene crystals (fp −5.5° C) grown from a solution containing a small quantity of petroleum distillate (bp 117 to 118° C, no freezing point); upper right, toluene (fp −95° C) crystallized by dilution as with benzene; middle left, toluene crystallized by dilution with a mixture of the petroleum hydrocarbon and propane; middle right, ethylbenzene (fp −92° C) crystallized from a solution of propane, showing very fine crystals which appeared first before growth; lower left, ethylbenzene crystallized from propane and grown by warming almost to the melting point and cooling slowly; lower right, o-xylene (fp −25° C) crystallized from solution in petroleum ether.

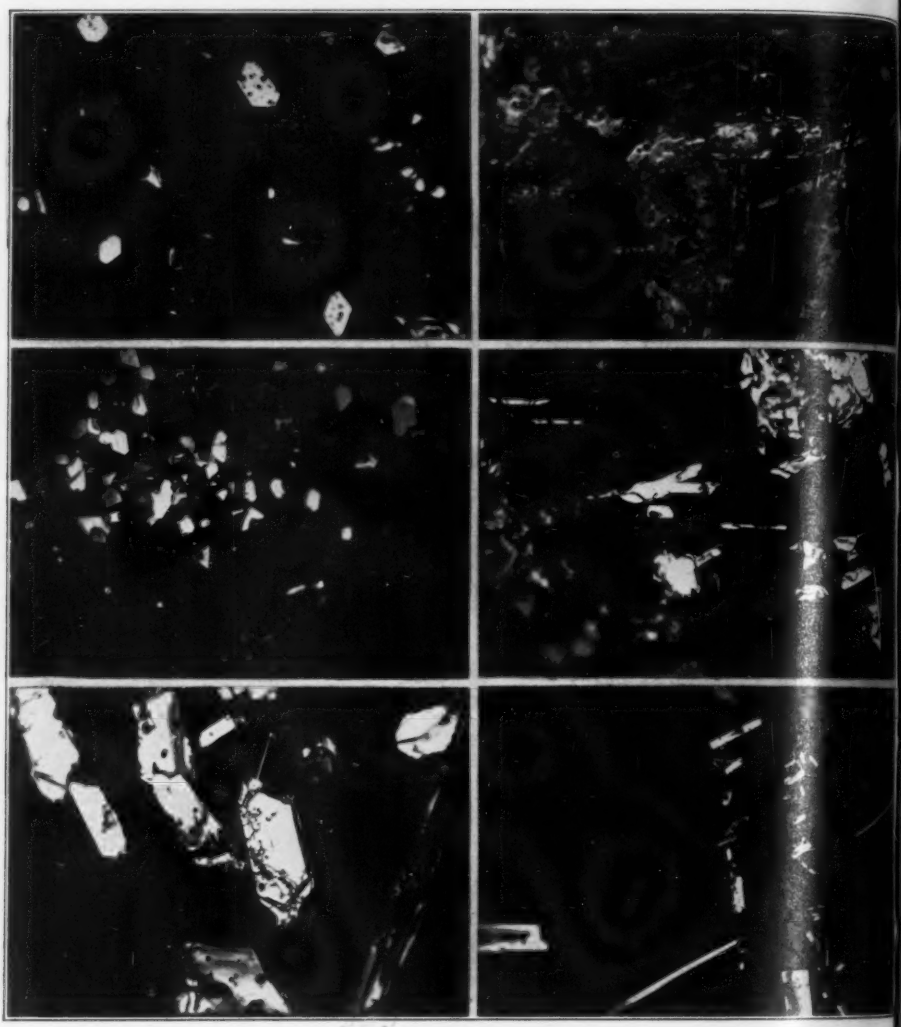

FIGURE 3.—*Crystals of aromatic hydrocarbons, o- and m-xylene.*

Upper left, *o*-xylene crystallized from petroleum ether; upper right, *m*-xylene crystallized alone, showing masses of crystals with frost present; middle left, *m*-xylene crystallized from petroleum ether, some of the crystals bearing resemblances to those of benzene; middle right, *m*-xylene crystallized from propane; lower left, *m*-xylene crystallized from propane and crystals grown; lower right, *p*-xylene (fp −13° C) crystallized from propane.

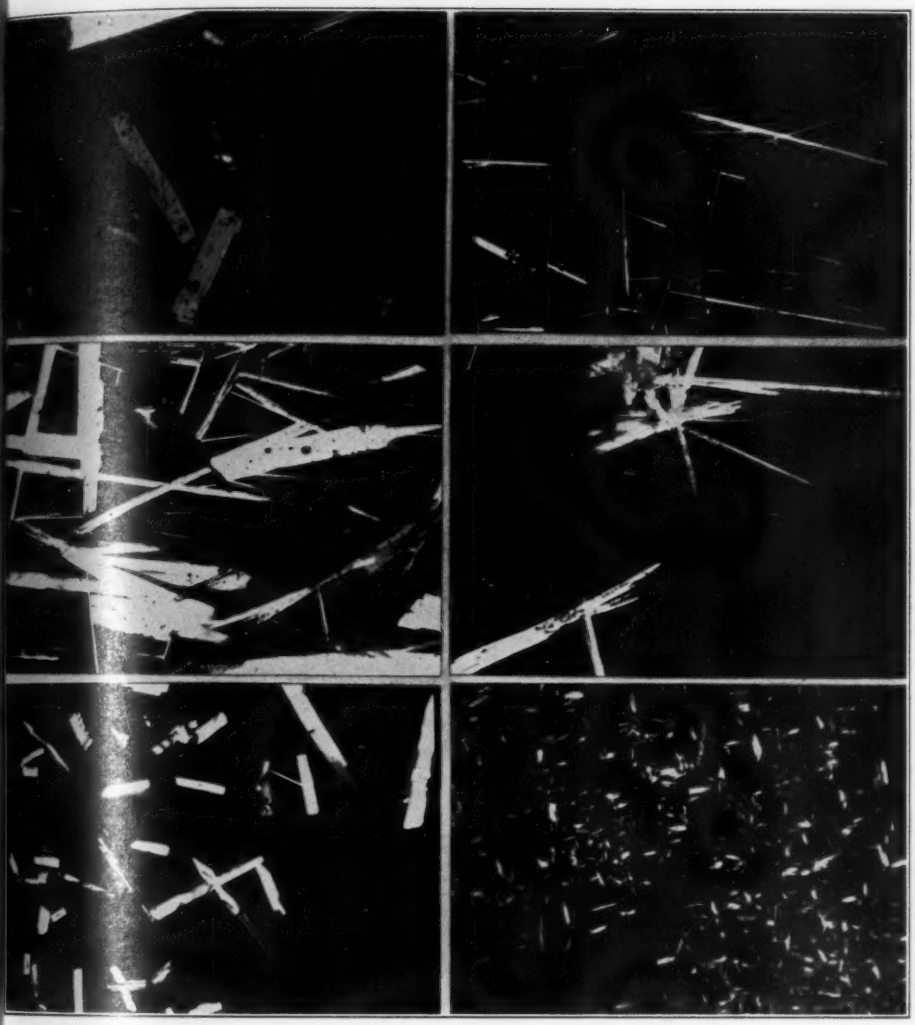

FIGURE 4.—*Crystals of aromatic hydrocarbons, p-xylene, mesitylene, hemimellitene, pseudocumene.*

Upper left, *p*-xylene crystallized from propane and crystals grown; upper right, mesitylene (fp −44.8° C) crystallized from mixture of petroleum and propane (see toluene), showing fine crystals which appeared on cooling without seeding; middle left, mesitylene crystallized from petroleum and propane, showing coarse crystals which appeared on continued cooling; middle right, mesitylene from petroleum and propane, showing coarse crystals which remain after warming; lower left, hemimellitene (fp −25.4° C) crystallized from petroleum distillate (bp 117 to 118° C); lower right, pseudocumene (fp −45° C) with petroleum distillate and propane.

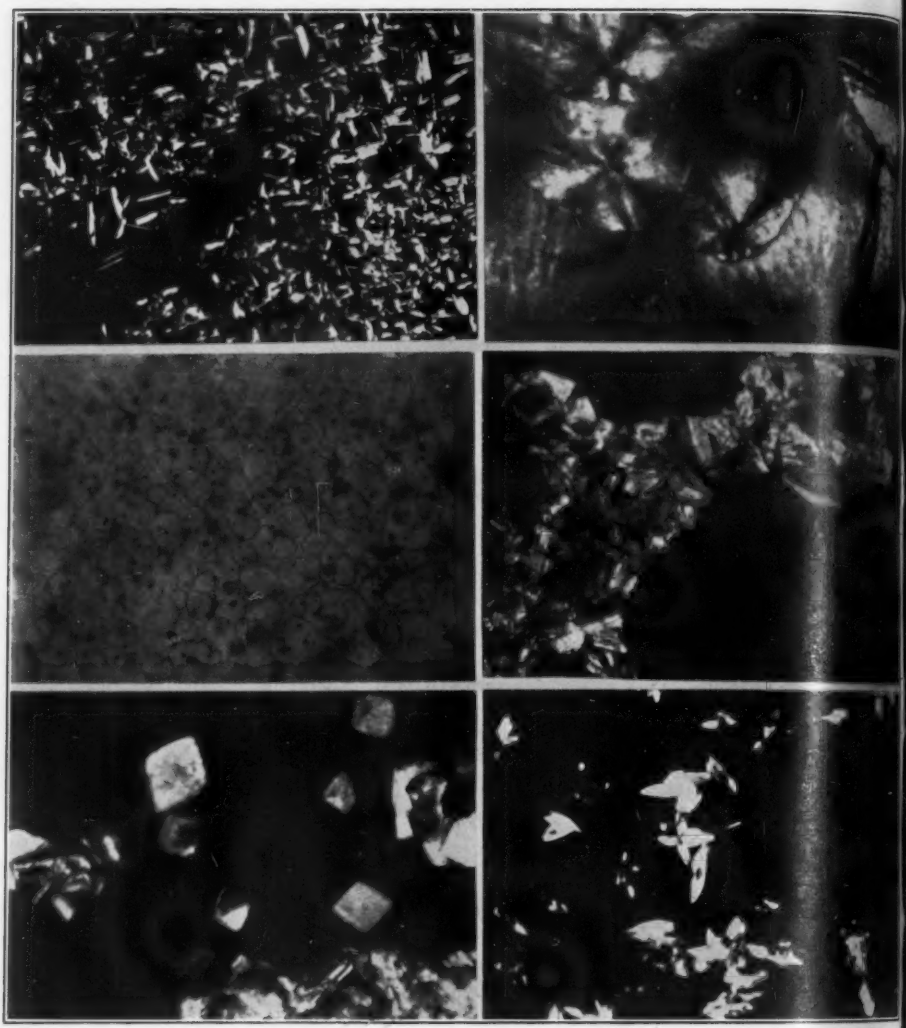

FIGURE 5.—*Crystals of aromatic and cycloparaffinic hydrocarbons, pseudocumene, methylcyclopentane, cyclohexane, methylcyclohexane, and ethylcyclohexane.*

Upper left, pseudocumene, second view; upper right, methylcyclopentane (fp −141° C) crystallized with methane and propane as solvents; middle left cyclohexane (fp −6.4° C) crystallized from petroleum distillate and viewed with unpolarized light; middle right, methylcyclohexane (fp −126.4° C) crystallized from solution in methane and propane; lower left, methylcyclohexane, second view; lower right, ethylcyclohexane (fp −111.4° C) crystallized from solution in methane and propane.

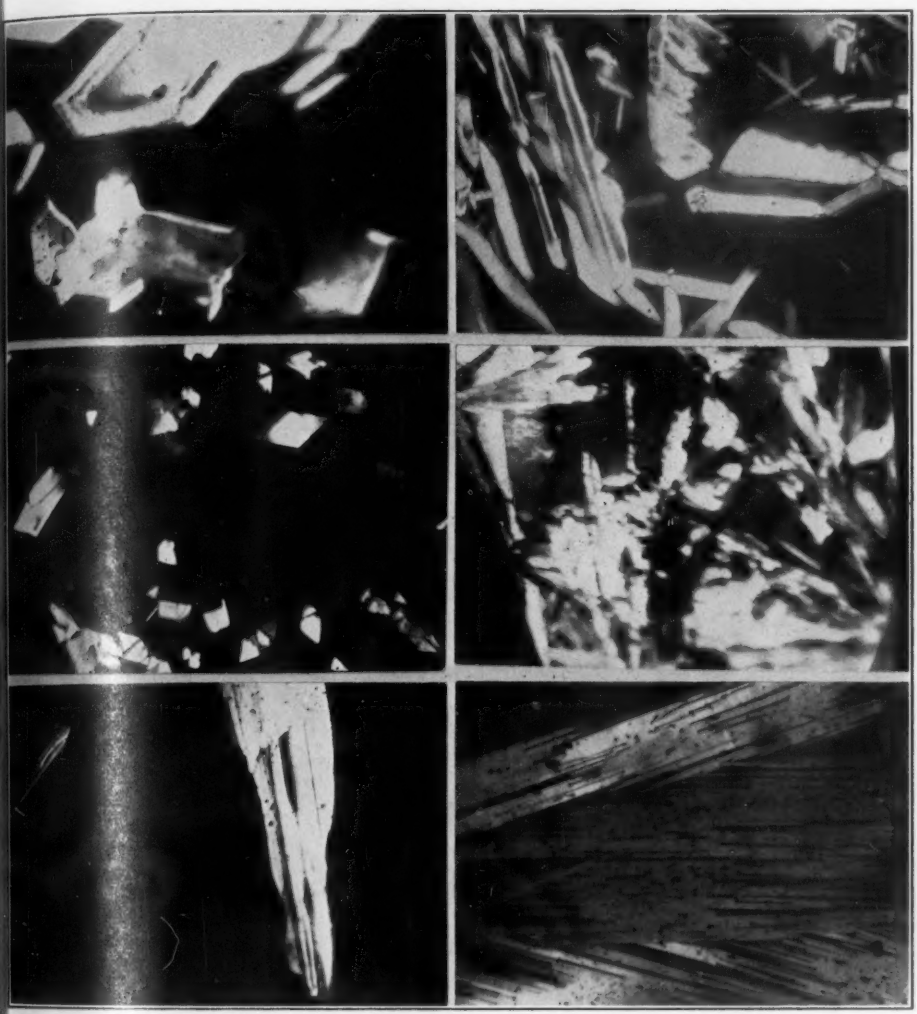

FIGURE 6.—*Crystals of cycloparaffinic and normal hydrocarbons, ethylcyclohexane, m- and p-dimethylcyclohexane, n-pentane, and n-hexane.*

Upper left, crystals of ethylcyclohexane grown by warming and refreezing; upper right, *m*-dimethylcyclohexane (fp −79° C) seeded with crystals grown from solution in propane; middle left, *p*-dimethylcyclohexane (fp −37° C) from solution in propane; middle right, *n*-pentane (fp −129° C) crystallized without solvent showing masses which appear after undercooling; lower left, *n*-pentane showing crystals formed after careful growth; lower right, *n*-hexane (fp −95° C) crystallized without solvent showing parts of large crystals.

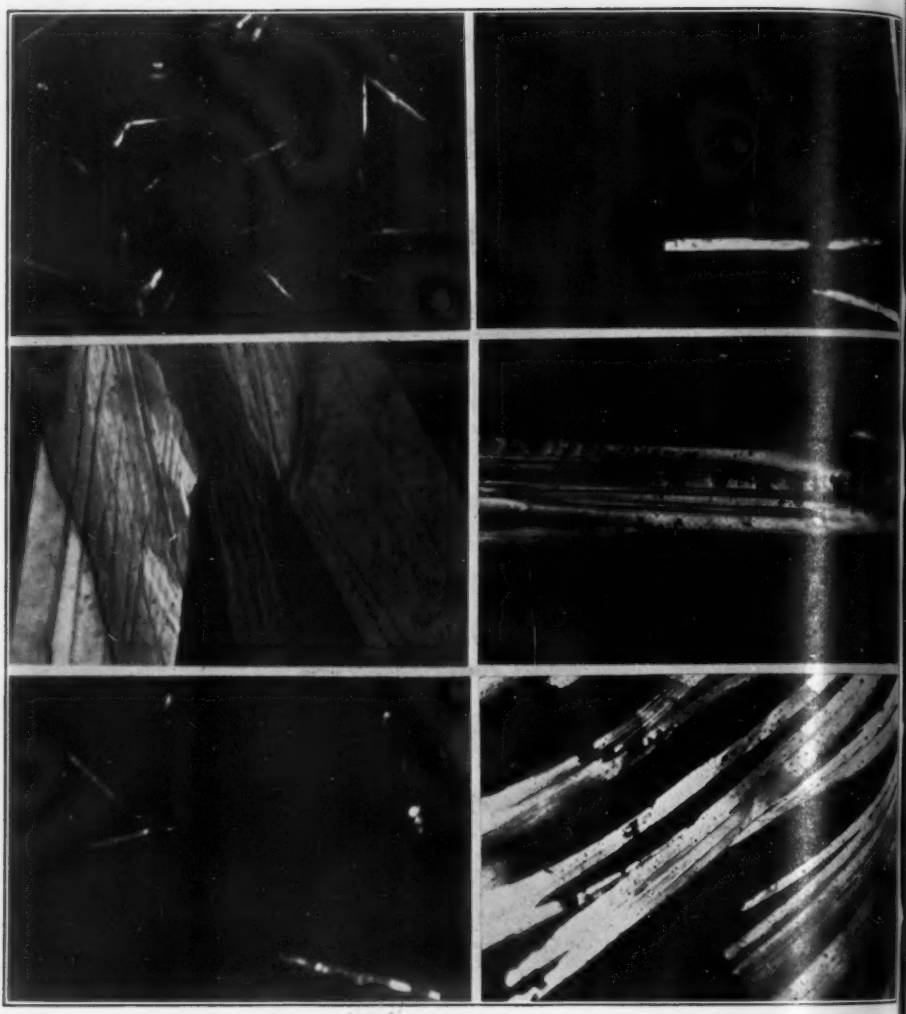

FIGURE 7.—*Crystals of normal hydrocarbons, n-hexane to n-nonane.*

Upper left, *n*-hexane crystallized from propane, showing smaller crystals; upper right, *n*-heptane (fp −90° C) crystallized from solution in propane; middle left, *n*-octane (fp −56° C) frozen without solvent, showing parts of large crystals; middle right, *n*-octane without solvent; lower left, *n*-octane crystallized from propane; lower right, *n*-nonane (fp −53° C) crystallized without solvent.

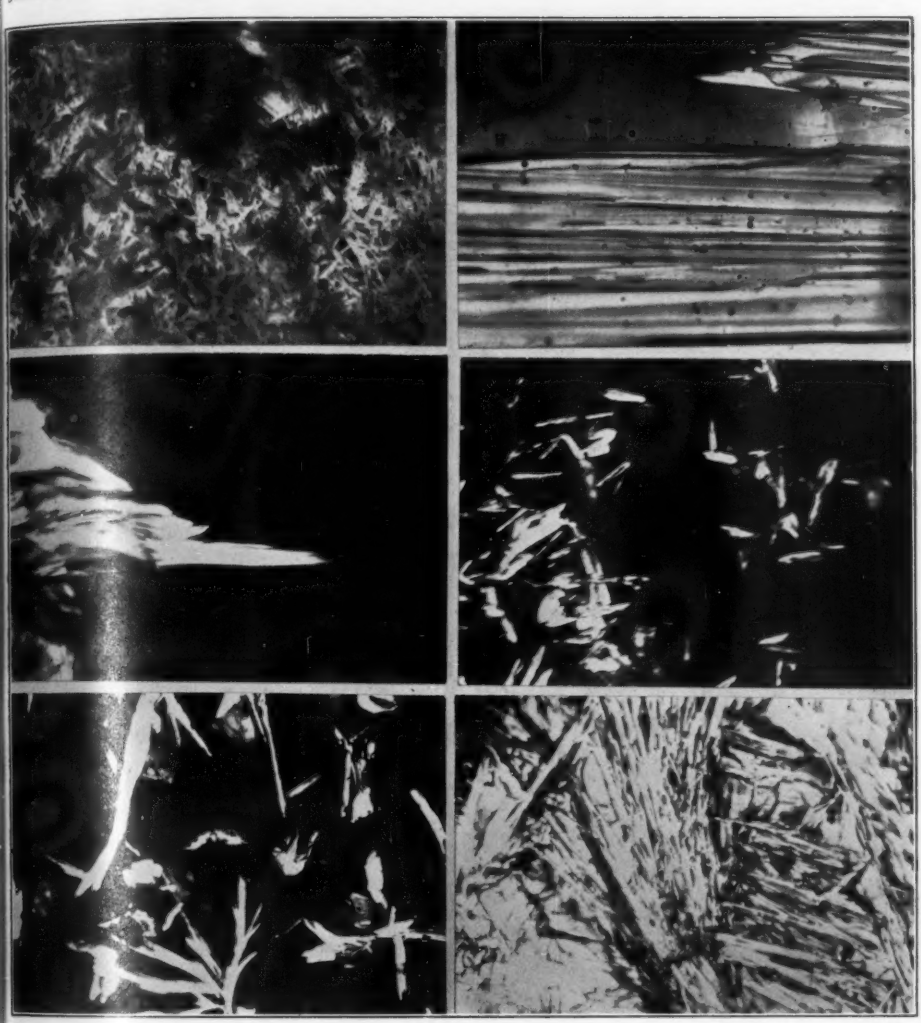

FIGURE 8.—*Crystals of normal hydrocarbons, n-decane to n-dodecane.*

Upper left, *n*-decane (fp −29° C) without solvent, showing masses of crystals resulting from undercooling; upper right, *n*-decane without solvent, showing large crystals; middle left, *n*-undecane (fp −25° C) without solvent, showing massive growth; middle right, *n*-undecane without solvent (this sample was difficult to grow in regular crystals); lower left, *n*-undecane without solvent, showing small crystals; lower right, *n*-dodecane (fp −10° C), showing masses of crystals.

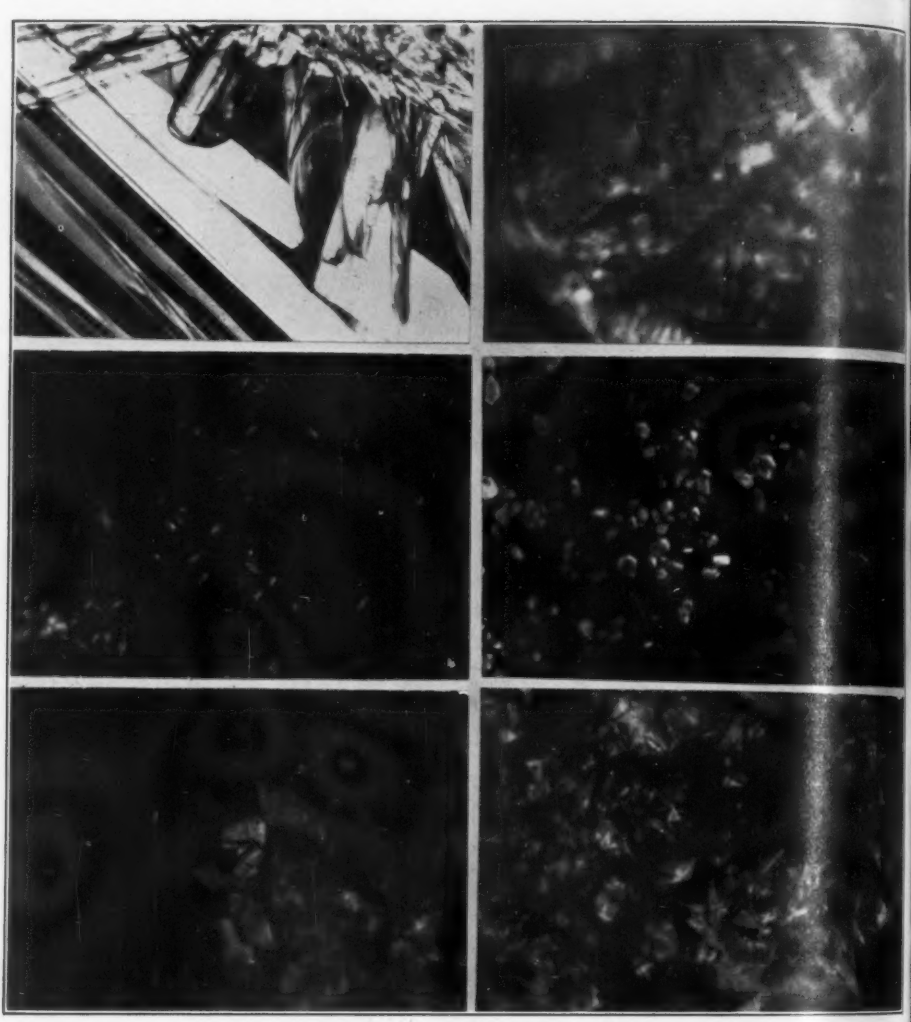

FIGURE 9.—*Crystals of normal and branched-chain hydrocarbons, n-dodecane, 2-methylbutane, 2,4-dimethylpentane, and 2,2,4-trimethylpentane.*

Upper left, *n*-dodecane showing large, isolated crystals; upper right, 2-methylbutane (fp −159° C) crystallized from methane and propane and transferred to the microscope (no single crystals are visible); middle left, 2-methylbutane crystallized from methane and propane, showing small crystals; middle right, 2,4-dimethylpentane (fp −119° C) crystallized from methane and propane, showing small crystals of about equidimensional section; lower left, 2,2,4-trimethylpentane (fp −107° C) crystallized from methane and propane, showing the typical crystals of quadrilateral section; lower right, 2,2,4-trimethylpentane, second view.

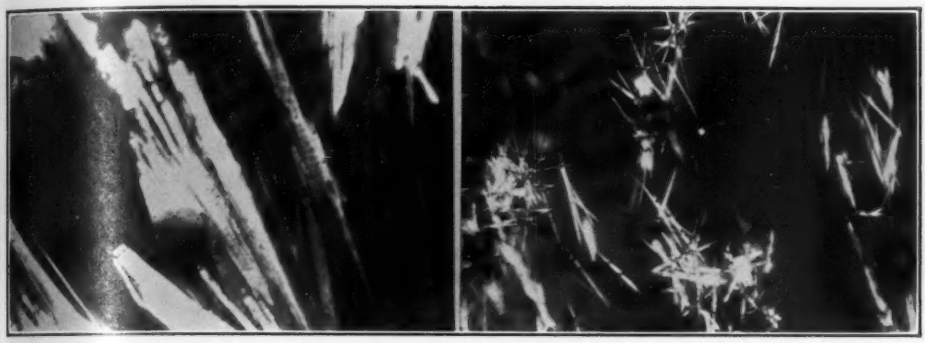

FIGURE 10.—*Crystals of branched-chain hydrocarbons, 2,2,5-trimethylhexane and 2-methylheptane.*

Left, 2,2,5-trimethylhexane (fp −106° C) crystallized from methane and propane, showing crystals which resemble those of normal hydrocarbons; right, 2-methylheptane (fp −111° C) crystallized from methane and propane, showing small prisms.

UNIV. OF MICH.

tendency to crystallize in the long forms of the normal paraffins; cf. dimethyl- and trimethylbenzene and the corresponding cycloparaffins. Examination of the highly branched paraffins with short chains (condensed molecules) shows that they also tend to crystallize in equidimensional polyhedrons, cf. isopentane, 2,4-dimethylpentane and 2,2,4-trimethylpentane, while the hydrocarbons with longer chains and fewer branches, such as 2,2,5-trimethylhexane and 2-methylheptane, resemble the normal compounds in their tendencies to the long flat shapes.

The crystals of mesitylene are interesting because they are known to undergo a transition in form, and the sample used for this work showed an anomalous behavior of the freezing curve. When cooled after fresh distillation the freezing began at −51.7°, whereas, if freezing was induced by plunging a chilled rod into the material, the freezing halt occurred at about −44.7.[11] Once crystals of the higher-melting form had been induced, they reappeared on refreezing unless the sample was redistilled. It is possible that the upper-right and the middle cuts of figure 4 show what occur. The needle-like crystals of the upper-right cut occur on gradual cooling without seeding, whereas if crystallization is induced by a cooled rod, the lath-like crystals of the middle-left cut appear. Warming the material causes the needle-like crystals to melt before the lath-like ones, as shown by the middle-right cut, indicating that the latter were stable at higher temperatures than the former ones.

Examination of the photographs of paraffin waxes shown by Ferris, Cowles, and Henderson [12] shows quadrilateral shapes somewhat similar to methylcyclohexane, 2,2,4-trimethylpentane and hydrogenated *p*-xylene, whereas the elongated six-sided crystals are similar to *m*-xylene. The more nearly equilateral hexagons shown by these investigators resemble none of the crystals of the hydrocarbons examined in this work, but resemble those of an unidentified hydrocarbon isolated by the author from a fraction of petroleum distilling between 119 and 120° C.[13]

IV. CONCLUSIONS

From the study of a number of hydrocarbons of known structure it is concluded that the behavior on crystallization depends somewhat on the nature of the molecule, condensed molecules tending to form nearly equidimensional polyhedrons, while open chains form elongated prisms. Mixed molecules (molecules in which chains are attached to groups with condensed structure) show modified forms depending on the relative influence of the chains and the condensed groups.

Successive members of the homologous series of the normal paraffins can not be distinguished by the appearance of their crystals, and hydrocarbons of different types but probably of the same classifications (condensed or open structure) may bear considerable superficial resemblance as, for example, methylcyclohexane and 2,2,4-trimethylpentane.

[11] B. J. Mair, BS J. Research **11**, 665 (1933) RP614.
[12] Ind. Eng. Chem. **23**, 681, (1931).
[13] R. T. Leslie, J. Research NBS **15**, 41 (1935) RP808.

Hydrocarbons differ considerably in the ease with which their crystals tend to grow. The normal paraffinic and aromatic hydrocarbons grow more readily than the cycloparaffins or the hydrocarbons with branched open chains. The low-freezing pentanes and their derivatives do not grow readily.

Crystal behavior can be used in conjunction with other physical properties to identify the chief constituents in mixtures of hydrocarbons.

The authors are much indebted to C. P. Saylor of this Bureau for his technical advice and assistance in this work.

WASHINGTON, March 15, 1937.

U. S. DEPARTMENT OF COMMERCE NATIONAL BUREAU OF STANDARDS

RESEARCH PAPER RP1001

Part of Journal of Research of the National Bureau of Standards, Volume 18, June 1937

CHARACTERISTICS OF THE IONOSPHERE AND THEIR APPLICATION TO RADIO TRANSMISSION

By Theodore R. Gilliland, Samuel S. Kirby, Newbern Smith, and Stephen E. Reymer

ABSTRACT

Results of ionosphere measurements near Washington, D. C., made at normal incidence over the period May 1934 to December 1936, inclusive, are presented in graphical form as monthly averages for each hour of the day. The general forms of the diurnal and seasonal variations of the critical frequencies and virtual heights have recurred from year to year. In addition to the seasonal variation there has been a continuous long-time increase of critical frequencies which is associated with the 11-year sunspot cycle. Data are given only for those layers which are fairly regular in behavior—the normal E, F, F_1, and F_2 layers.

The interpretation of properties of the ionosphere in terms of radio transmission over medium and long distances is discussed. The properties considered are absorption, virtual height, and critical frequency. It is pointed out that the long-time increase of critical frequencies indicates a corresponding rise in useful transmission frequencies. The paper also describes briefly two types of irregular disturbances of the ionosphere which affect radio transmission.

CONTENTS

		Page
I.	Introduction	645
II.	Virtual heights	662
III.	Critical frequencies	662
IV.	Long-time effects	664
V.	Interpretation and applications	664
VI.	Transmission irregularities	667
VII.	Conclusions	667

I. INTRODUCTION

A program of measurement of critical frequencies and virtual heights of the ionosphere has been carried on at Washington, D. C., by the National Bureau of Standards since January 1930. Results have been given from time to time in a number of published papers. One of these papers [1] gives systematic data on critical frequencies of the various regions of the ionosphere for the year May 1933 to April 1934, inclusive. These data were obtained with the multifrequency automatic recorder originated and developed [2] at the National Bureau of Standards in 1932. Experimental evidence of the beginning of a long-time increase of average critical frequencies was also given in that paper.

The use of the multifrequency automatic recorder has made it possible to secure hourly ionosphere records at the National Bureau

[1] T. R. Gilliland, *Multifrequency ionosphere recording and its significance.* J. Research NBS **14**, 283 (1935); Proc. Inst. Radio Engrs. **23**, 1076 (1935).

[2] T. R. Gilliland, *Note on a multifrequency automatic recorder of ionosphere heights.* BS J. Research **11**, 561 (1933); Proc. Inst. Radio Engrs. **22**, 236 (1934).

of Standards since May 1933. The recent adoption of the idea of multifrequency automatic recording and the principle of this recorder by the Carnegie Institution of Washington, British Radio Research Board, Australian Radio Research Board, and Harvard University will increase enormously the continuity and value of ionosphere data, which will, in turn, greatly increase our understanding of world-wide ionosphere and radio transmission conditions.

The graphs of the present paper present the results of observations continued since April 1934 through December 1936 and an extension of the F data to each hour of the day. The average, for each hour, of the critical frequencies and virtual heights of the three principal strata, the normal E, F_1, and F_2 regions, is given for each month. Curves are not plotted for the sporadic E, since its appearance was so erratic that average results would not be reasonably dependable, although it is known that sporadic E frequently determined the upper frequency limit of sky-wave transmission, especially during the summer. These graphs are intended to show the average diurnal variation of ionosphere characteristics for each month of the year, as well as long-period changes. It is believed that the information will be useful in predicting propagation conditions.

Following the precedent established in earlier papers, the critical frequency for the ordinary ray is given for the F_1 layer, while that for the extraordinary ray is given for the F_2 and F layers. In the case of the F_1 layer the ordinary ray is the more suitable for the purpose of averaging since it is much stronger and is therefore more frequently observed than the extraordinary ray. With regard to the F_2 and F layers the critical frequency for the extraordinary ray is, with the exception of irregular scattered reflection, the highest frequency returned at normal incidence. Its value gives a measure of the highest usable frequency for short-distance transmission. For long-distance transmission the extraordinary ray may however be expected to extend the usable frequency limit very little, if any, above that for the ordinary ray. If the critical frequency for either ray is known, that for the other may be determined by a simple calculation. At Washington the critical frequency for the extraordinary ray is roughly 800 kc/s higher than that for the ordinary ray, for ordinary-ray critical frequencies above 2,500 kc/s.

The graphs represent measurements obtained both with the multifrequency automatic recorder and by manual observations. The automatic recorder was arranged to cover the frequency band 2,500 to 4,400 kc/s once each hour. The manual measurements were usually made during one day each week and principally at frequencies above 4,400 kc/s.

The results of the manual observations are averages for a 60-minute interval centered on the hour. The automatic records began on the hour and lasted 4¾ minutes. Although the upper limit of the automatic recorder was 4,400 kc/s, the critical frequency for the extraordinary ray could be determined to as high as 5,200 kc/s, by the 800 kc/s separation relation mentioned above. Since December 1935, the multifrequency records have been supplemented by measurements with a fixed-frequency recorder operating either on 7,250 or 6,200 kc/s, giving a record of a few seconds duration every 4½ minutes.

The symbols used are:

h_E=*E*-region virtual height (lowest measured height).
h_{F_1}=F_1-region virtual height (lowest measured height).
h_{F_2}=F_2-region virtual height (lowest measured height).
h_F=night *F*-region virtual height (lowest measured height).
f_E=*E*-region critical frequency, in kilocycles per second, ordinary ray.

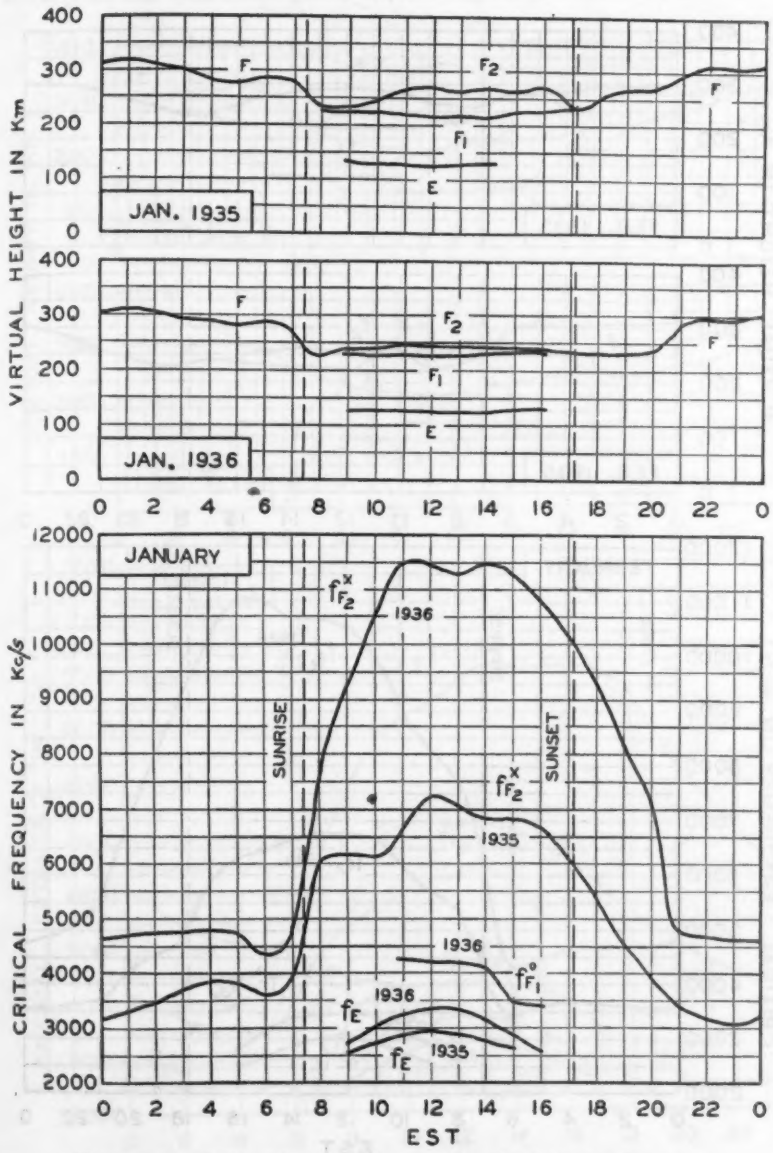

FIGURE 1.—*Critical frequencies and virtual heights for January.*
Curves represent hourly averages.

$f^0_{F_1}$=F_1-region critical frequency, in kilocycles per second, ordinary ray.

$f^z_{F_2}$=F_2-region critical frequency, in kilocycles per second, extraordinary ray.

f^z_F=night-F-region critical frequency in kilocycles per second, extraordinary ray.

EST=eastern standard time (=75° west meridian time).

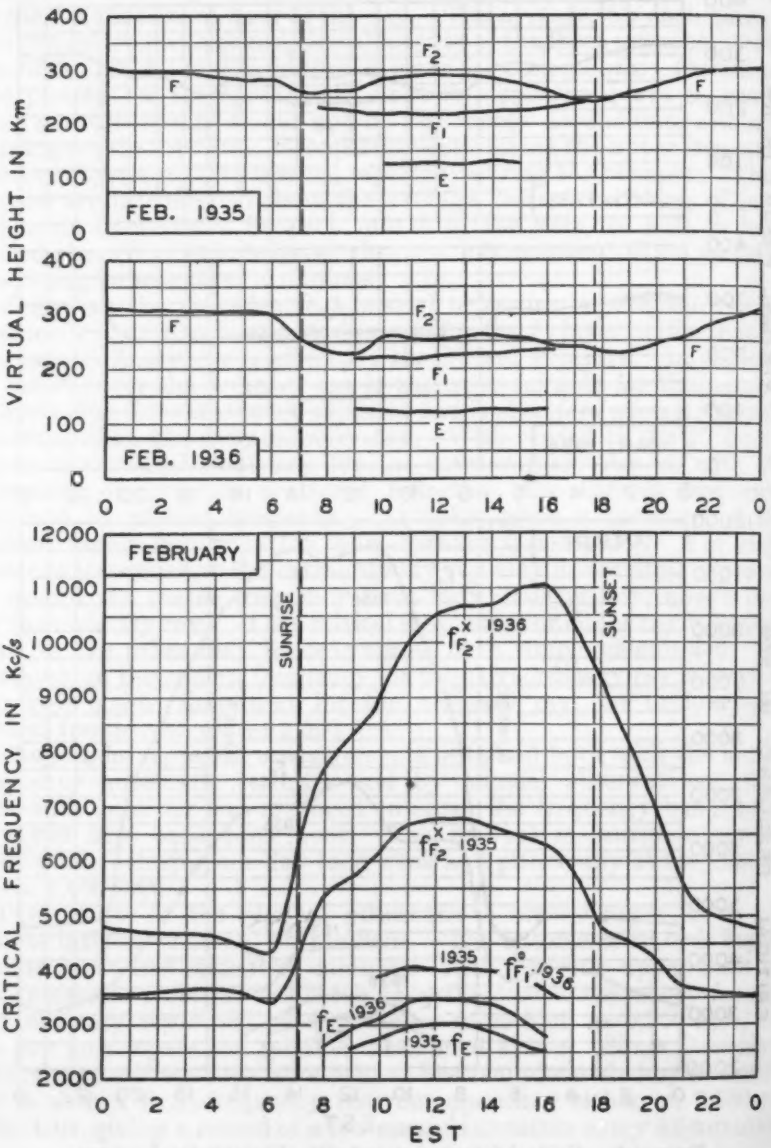

FIGURE 2.—*Critical frequencies and virtual heights for February.*
Curves represent hourly averages.

Figures 1 to 15, inclusive, give the hourly averages of critical frequencies and minimum virtual heights for the E, F_1, and F_2 regions of the ionosphere for each month of the year from May 1934 to December 1936. For a given month the several years are plotted on the same figure through September 1936. This arrangement makes it easy to see changes which have occurred from year to year. October to December 1936 were plotted separately because the scale already in use was inadequate for the higher critical frequencies.

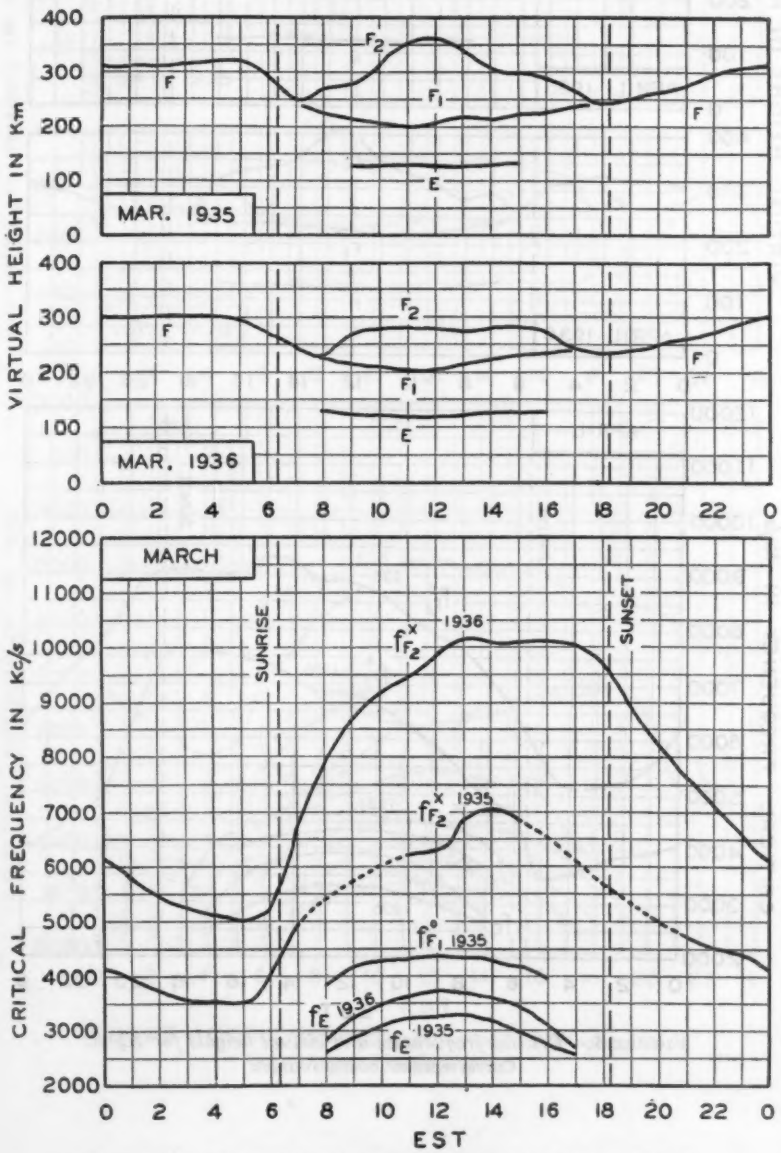

FIGURE 3.—*Critical frequencies and virtual heights for March.*
Curves represent hourly averages.

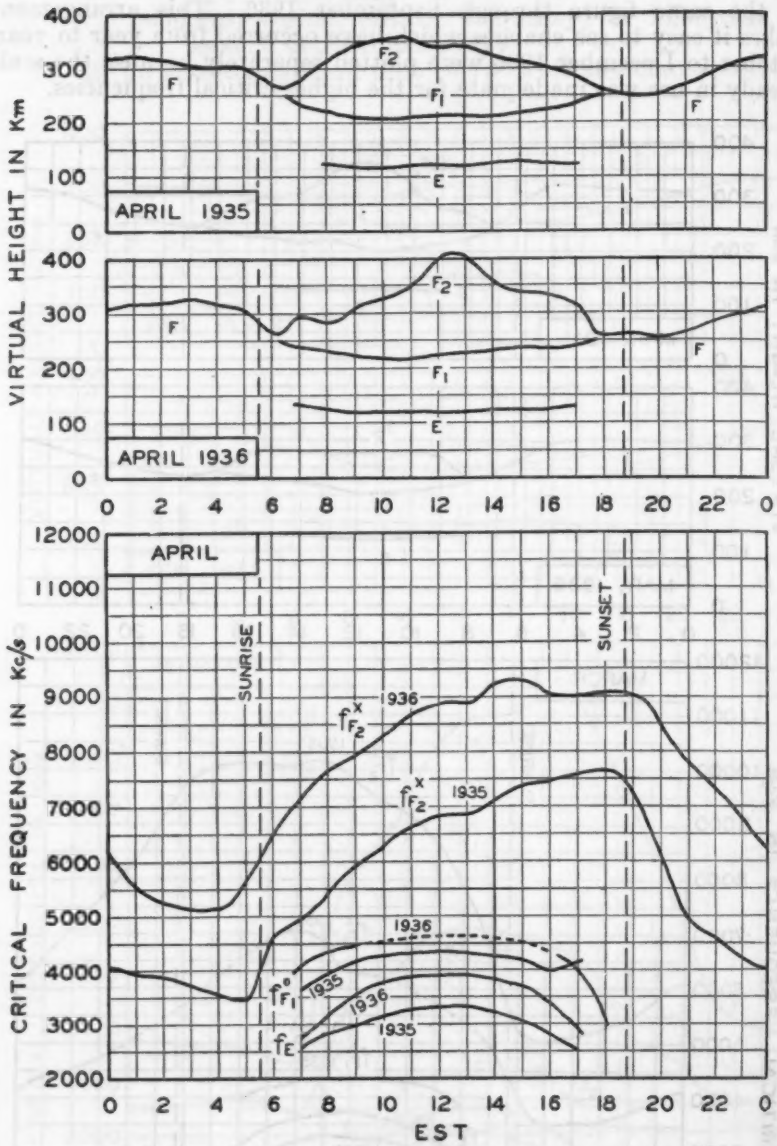

FIGURE 4.—*Critical frequencies and virtual heights for April.*
Curves represent hourly averages.

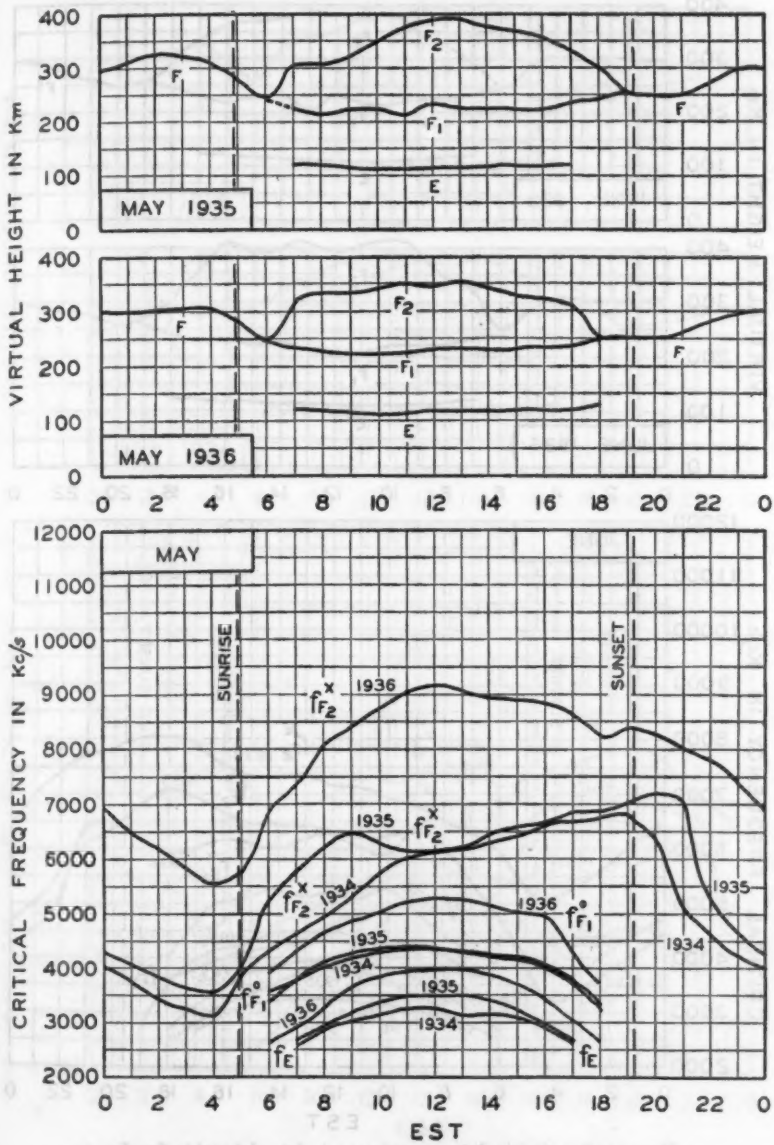

FIGURE 5.—*Critical frequencies and virtual heights for May.*
Curves represent hourly averages.

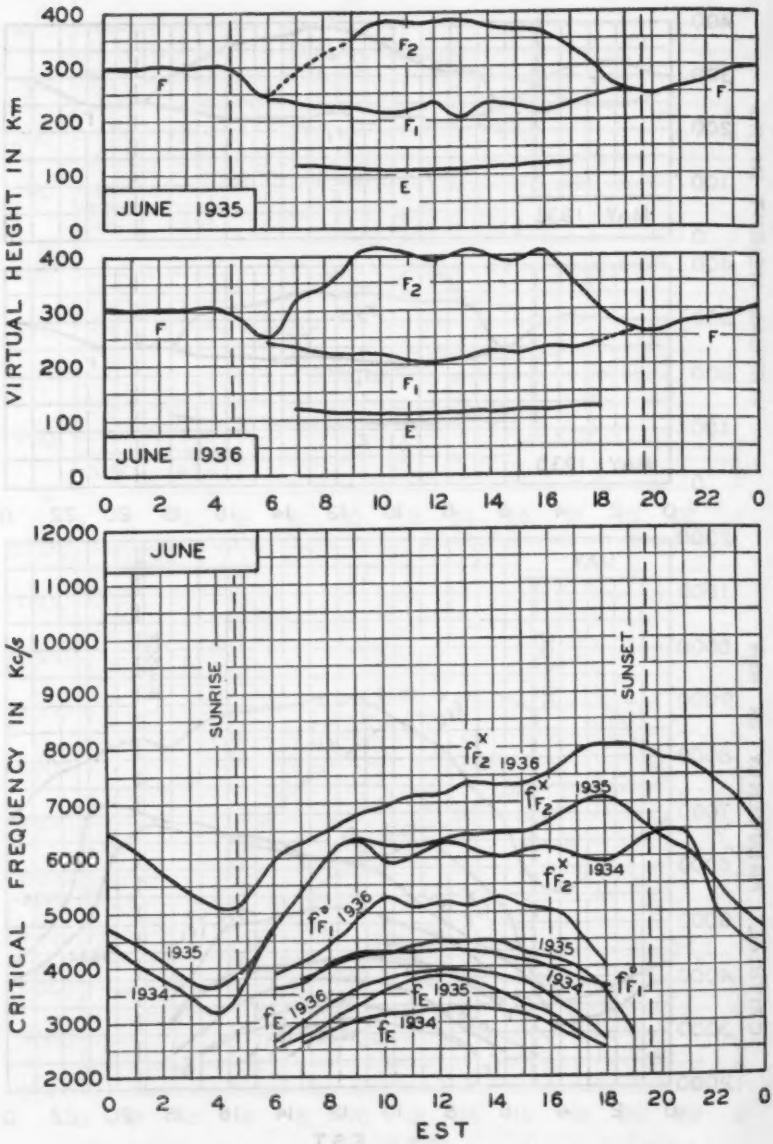

FIGURE 6.—*Critical frequencies and virtual heights for June.*
Curves represent hourly averages.

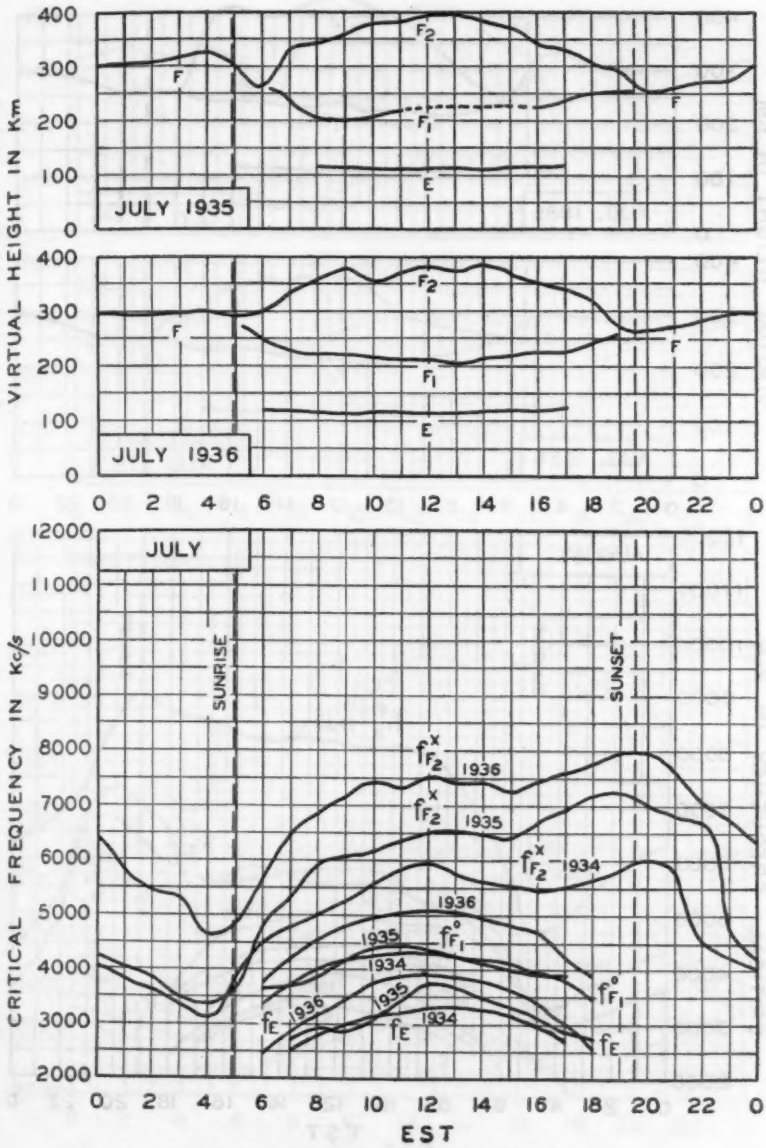

FIGURE 7.—*Critical frequencies and virtual heights for July.*
Curves represent hourly averages.

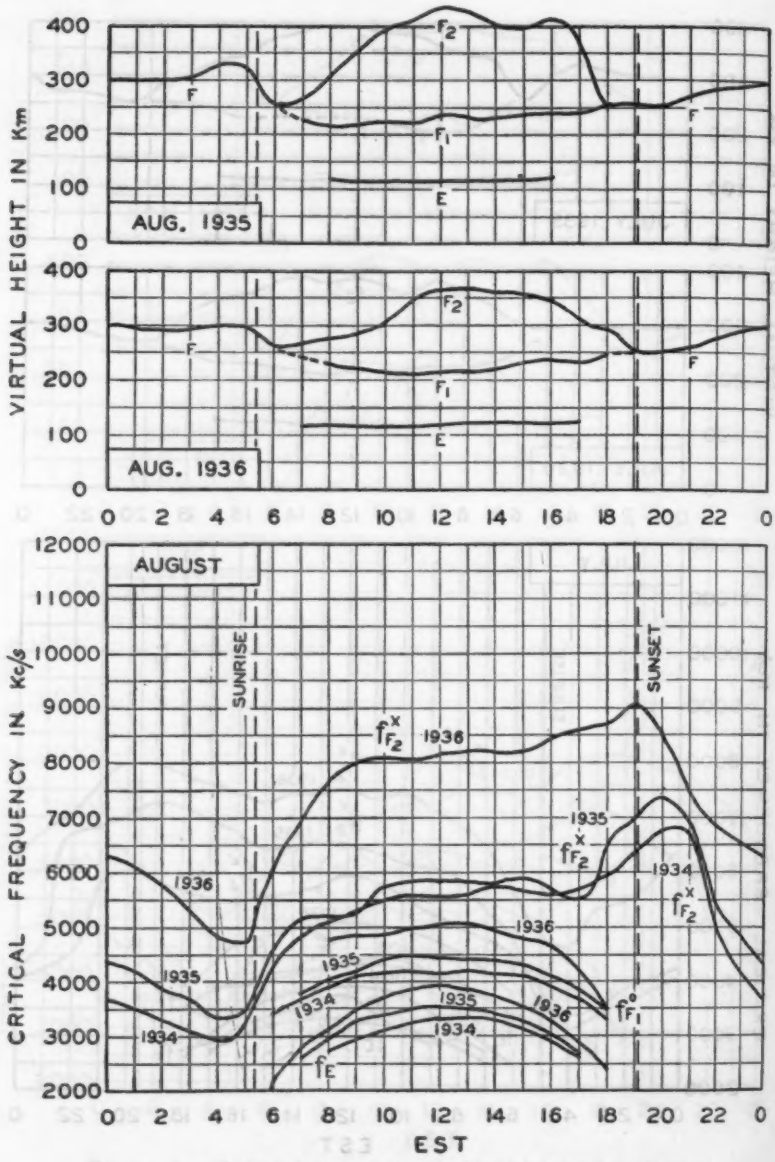

FIGURE 8.—*Critical frequencies and virtual heights for August.*
Curves represent hourly averages.

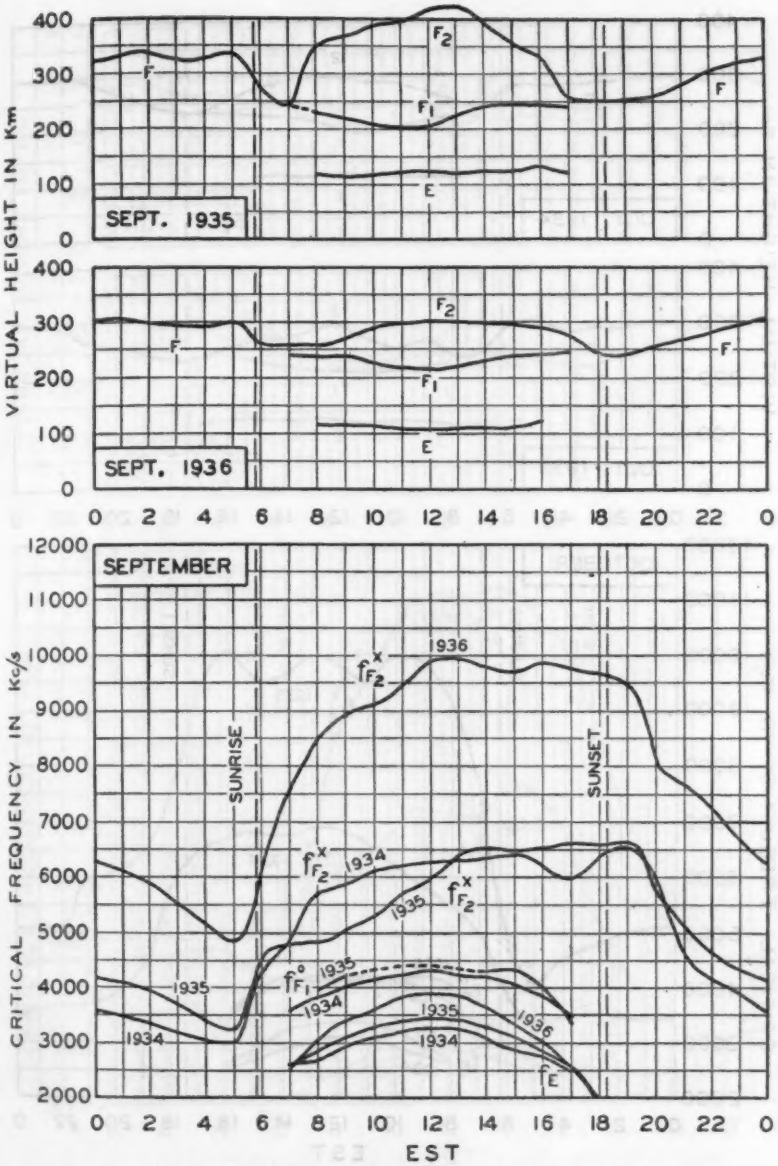

FIGURE 9.—*Critical frequencies and virtual heights for September.*
Curves represent hourly averages.

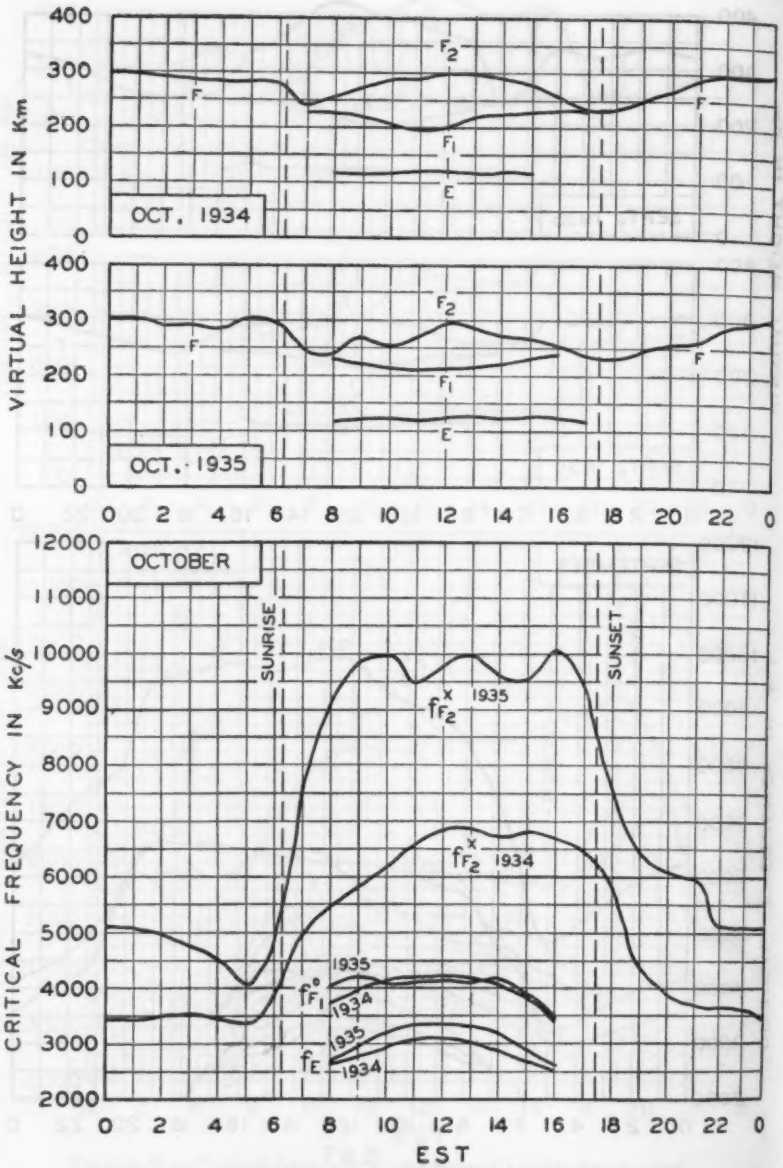

FIGURE 10.—*Critical frequencies and virtual heights for October.*
Curves represent hourly averages.

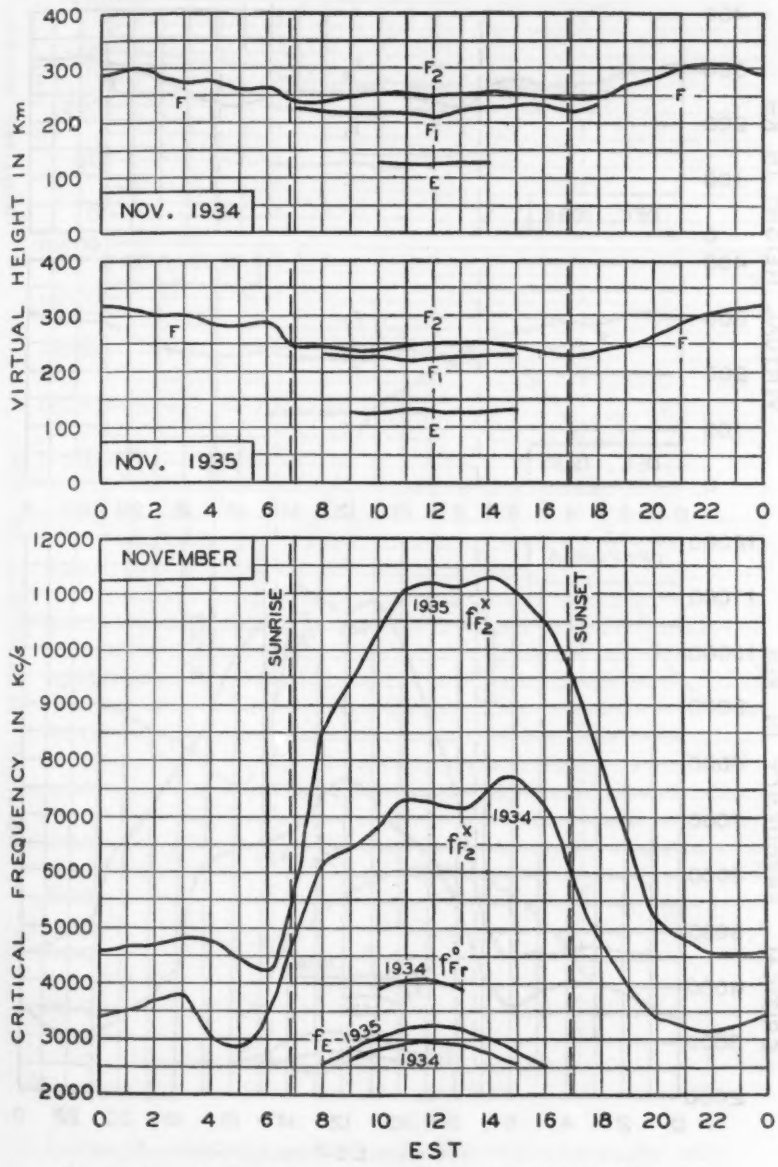

FIGURE 11.—*Critical frequencies and virtual heights for November.*
Curves represent hourly averages.

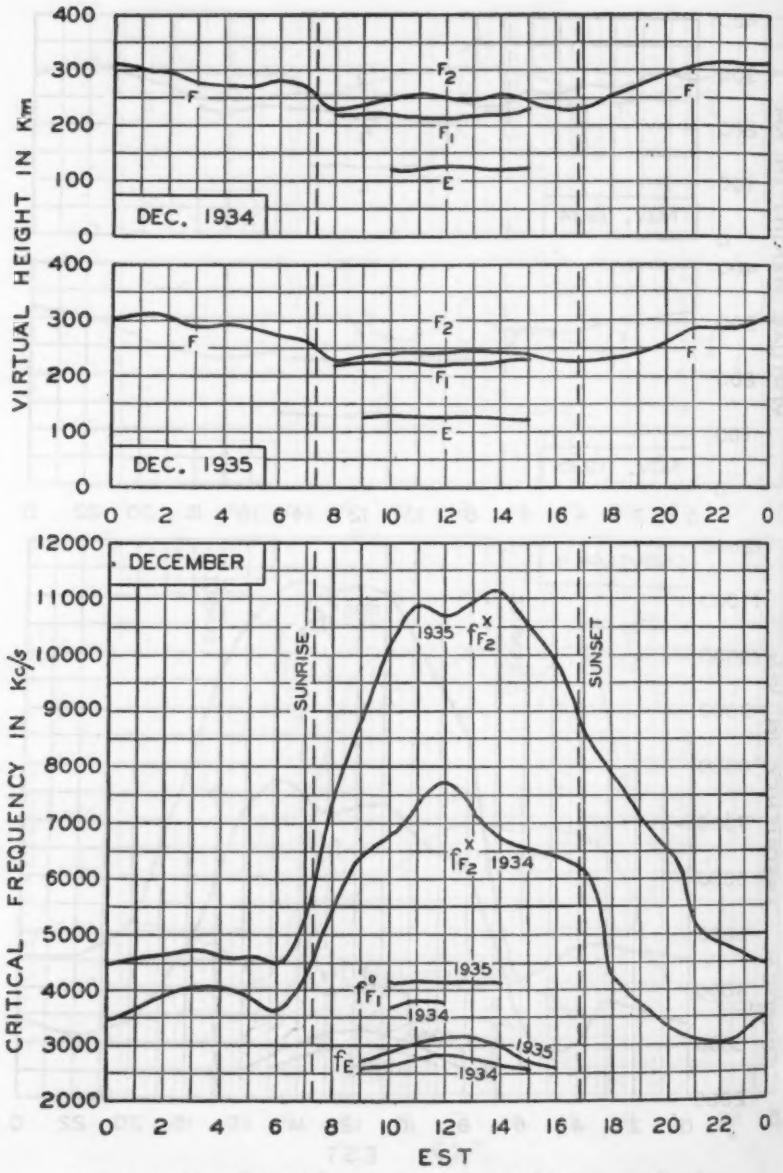

FIGURE 12. *Critical frequencies and virtual heights for December.*
Curves represent hourly averages.

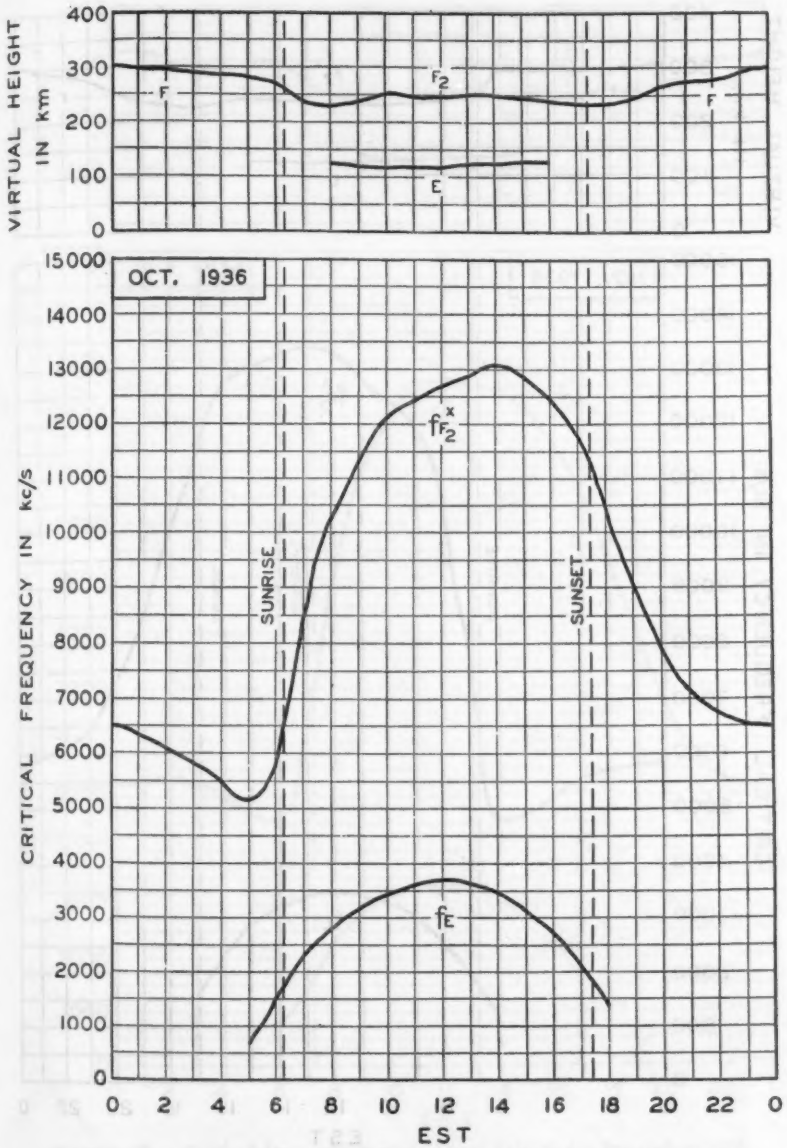

FIGURE 13.—*Critical frequencies and virtual heights for October 1936.*
Curves represent hourly averages.

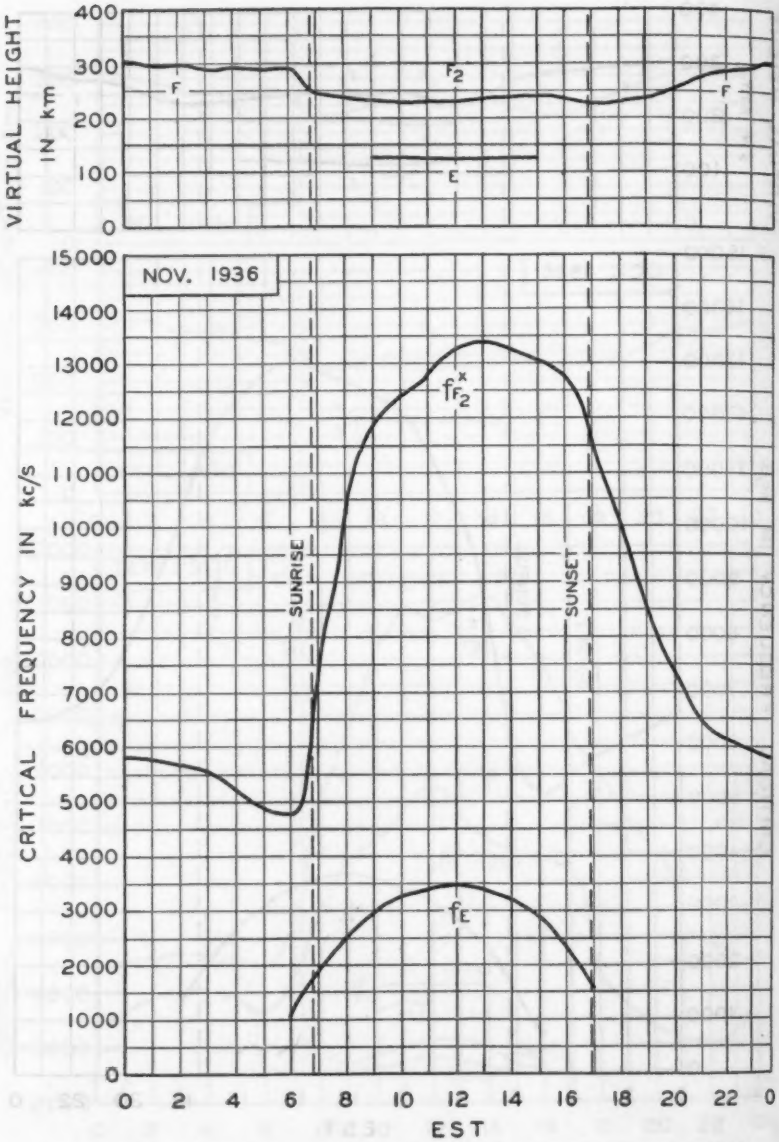

FIGURE 14.—*Critical frequencies and virtual heights for November 1936.*
Curves represent hourly averages.

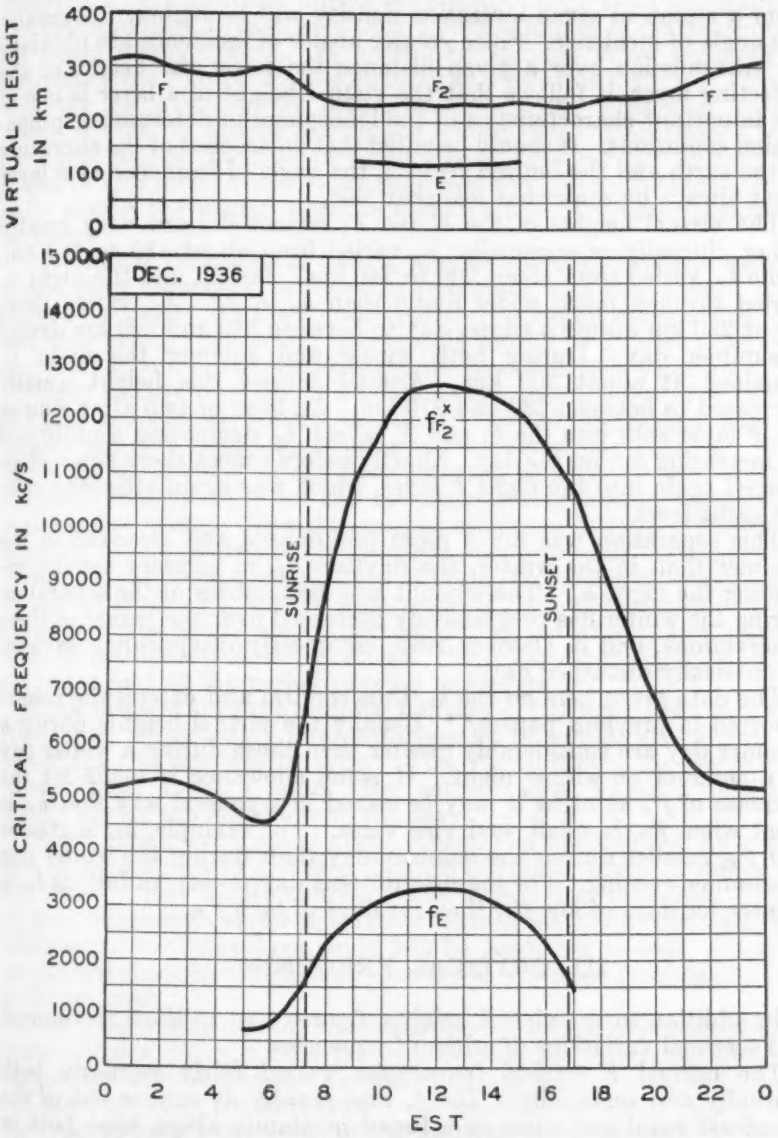

FIGURE 15.—*Critical frequencies and virtual heights for December 1936.*
Curves represent hourly averages.

II. VIRTUAL HEIGHTS

Referring to these figures, we shall consider first the virtual heights. In general, the maximum frequency of waves which may be returned from a region of given ionization density will be higher, the greater the angle of incidence. Since greater angles of incidence are obtained for transmission over a given distance the lower the height of the reflecting layer, it follows that the virtual height of a layer is one of the important characteristics of the ionosphere in determining propagation conditions. It should be noted that on account of the curvature of the earth and the ionized regions, the angle of incidence at a layer must always be somewhat less than 90°.

The virtual heights of the E and F_1 regions did not vary greatly either diurnally or seasonally; h_E varied from about 110 to 130 km, while h_{F_1} varied from about 200 to 240 km. The h_{F_2} and the night h_F varied through much wider limits than h_E or h_{F_1}. h_{F_2} varied from about 230 km during a winter day to between 350 and 500 km during a summer day. During both winter and summer the night h_F remained at about 300 km. Around sunrise this height usually decreased to between 230 and 270 km. An hour or two after sunrise the F layer split into the F_1 and F_2 layers, h_{F_1} decreasing slightly and h_{F_2} increasing during the day. Shortly before sunset these two regions merged again into the night F layer, which rose again after sunset to the night level.

This separation was much more pronounced and clear-cut in the summer than in the winter, the daytime h_{F_2} in summer usually exceeding the night h_F. The amount and distinctness of the separation during the winter has progressively decreased over the period of these observations, and in October 1936, completely disappeared, save on magnetically disturbed days.

The data given here on the h_{F_2} thus confirm and extend the results reported in previous papers.[3] [4] Usually the virtual heights during a summer day are considerably greater than those during a winter day or a summer or winter night. If some allowance is made for the decrease of $f^z{}_F$ at night it may be stated in a general way that h_{F_2} is great when $f^z{}_{F_2}$ is small, and vice versa. For example, h_{F_2} is greater and $f^z{}_{F_2}$ smaller during the summer day than during the winter day or summer evening. For the intermittent day-to-day variations h_{F_2} is greater for days of low $f^z{}_{F_2}$ than for days of high $f^z{}_{F_2}$.

III. CRITICAL FREQUENCIES

In addition to the virtual heights, figures 1 to 15 show the diurnal and seasonal variations of critical frequencies.

The normal E critical frequencies varied fairly regularly both diurnally and seasonally. The f_E rose rapidly at sunrise out of the broadcast band and came to a broad maximum about noon both in summer and in winter. The summer values were greater than the winter values. The diurnal variation of f_E was symmetrical about noon. Neglecting the sporadic E, the values at sunrise were about the same as those at sunset. Some observations made at night indi-

[3] E. O. Hulburt, *Theory of the ionosphere.* Terr. Mag. **40**, 193 (1935).
[4] E. B. Judson, *Comparison of data on the ionosphere, sunspots, and terrestrial magnetism.* J. Research NBS **17**, 323 (1936).

cated that the f_s at that time was usually found between 600 and 1,000 kc/s. There was a long time increase of f_s as well as of the other regions which will be discussed later.

The F_1 critical frequencies varied fairly regularly when they were observed, i. e., principally during the summer day. Both the ordinary and extraordinary F_1 rays were then normally found, the extraordinary ray being much weaker. F_1 critical frequencies never occurred at night since the F_1 layer lost its identity as a separate layer and merged with the F_2 layer shortly before sunset. They were also usually poorly defined or absent during the winter day. There was a long time year-to-year increase of f_{F_1} similar to that for f_s. During the period of this increase the f_{F_1} became less and less well defined, especially during the winter, until, in October 1936, it usually could not be found.

The diurnal variations of the $f^z{}_{F_1}$ may be classified into two general types: the winter type, centered in December, and the summer type, centered in June. In the winter type the $f^z{}_{F_1}$ began rising about one-half hour before sunrise and rose rapidly until 2 or 3 hours after sunrise, coming to a broad maximum centered about 1300 local time. It fell fairly rapidly from about 2 hours before until 3 hours after sunset and then more slowly during the night. The night decrease was not smooth but was broken up by plateaus and secondary maxima. The maximum at about 4 a. m., first observed in 1933 at the National Bureau of Standards, [5] [6] has become progressively less and less marked in successive winters since the sunspot minimum in 1933. The minimum for the 24 hours usually occurred about an hour before sunrise. Except for rare occasions, on days of magnetic storms the day-to-day variations in the $f^z{}_{F_1}$ curves were small. Thus the behavior of the ionosphere was nearly always regular during the winter, and, indeed, could be predicted over short periods. This was especially true during the latter part of the period covered in this paper.

In the summer type the morning increase in $f^z{}_{F_1}$ began about sunrise. It occurred considerably later with respect to sunrise and was much slower than in the winter type. The $f^z{}_{F_1}$ continued to rise in this manner until about 4 hours after sunrise, after which it rose less rapidly during the remainder of the day.

The maximum occurred at about sunset, and was followed by a very slow and more regular decrease through the night, until the minimum was reached just before sunrise. The day-to-day variations in the $f^z{}_{F_1}$ were in general greater in summer than in the winter time, and the behavior of the ionosphere could not be predicted as well, although the general shape of the diurnal curves was the same from day to day in the summer.

During the spring and fall the transition between winter and summer characteristics did not take place gradually, as would appear from the average curves, but the diurnal variation shifted erratically back and forth between the two types. In general, the whole day was of one type, although the value of $f^z{}_{F_1}$ differed widely on different days. The general shift in the average curves represents a relative predominance of winter or summer conditions during the month.

It may be seen from the graphs that the maximum $f^z{}_{F_2}$ for the year occurred during the winter day and a lesser maximum occurred near

[5] T. R. Gilliland. *Ionospheric investigations.* Nature (London) **134,** 379 (1934).
[6] T. R. Gilliland. *Multifrequency ionosphere recording and its significance,* J. Research NBS **14,** 283 (1935); Proc. Inst. Radio Engrs. **23,** 1076 (1935).

sunset in summer. Both maxima were fairly broad and indicated that a frequency near the maximum transmission frequency might be used for 8 or 9 hours during the day. This time centered at about 1300 local time during the winter and at about sunset during the summer.

IV. LONG-TIME EFFECTS

Since the sunspot minimum in the winter of 1933–34 the critical frequencies of the E, F_1, and F_2 regions have increased over a long period which is associated with the 11-year sunspot cycle. This long-time increase was superimposed on the seasonal variations and may be seen in figures 1 to 15. The largest and most striking long-time changes occurred in the $f^2_{F_2}$.

V. INTERPRETATION AND APPLICATIONS

The three principal properties of the ionosphere affecting sky-wave transmission are absorption, virtual height, and critical frequency.

Absorption.—The absorption of radio waves in the ionosphere determines the maximum distance and minimum frequency for practical high-frequency communication. The absorption varies in general with time of day, season, frequency and length of path. Absorption seems to take place mainly in the lower ionosphere, that is in the E layer or below. The absorption is greater during the summer day than during the winter day. It is greater for the lower high frequencies, that is, those frequencies which are close to or below the E critical frequency for a given distance. It is usually greater during the day than during the night, especially for these lower high frequencies. The evidence indicates that a higher frequency at large angles of incidence behaves, with respect to absorption, like a much lower frequency at small angles of incidence.

The effect of absorption at different frequencies is illustrated by field-intensity measurements of two transmitting stations about 600 km distant, one at 6,060 kc/s and the other at 9,570 kc/s. Measurements on the 6,060-kc transmission indicated day field intensities about 2 percent of the night field intensities. For this distance this frequency was below the E-critical frequency for several hours during the day. Similar measurements on the 9,570-kc station indicated day field intensities of approximately the same intensity as the night field intensities. For this distance this frequency was well above the E-critical frequency at all hours of the day. These two examples illustrate the advantage of using a transmission frequency well above f_x if $f^2_{F_2}$ is high enough to reflect transmissions at such frequencies.

Virtual height.—The virtual height is an important characteristic of an ionized layer for determining the maximum frequency for which the waves will be reflected from the layer. For a given transmission distance the angle of incidence at a layer will be greater the lower the layer. On account of the curvature of both the earth and the ionized layers, the maximum possible angle of incidence is also greater the lower the layer. Since the critical frequency for a given ionization density varies approximately as the secant of the angle of incidence, it follows that for a given ionization density and distance a lower layer can reflect waves of a higher frequency. It is thus apparent that even though the E-layer ionization density is lower than that of the F_1

layer, the former may frequently determine the maximum usable frequency. Because of the high f_s and low f_{F_1} during the summer day, this condition exists fairly regularly at that time. This condition also exists during days of severe magnetic disturbances when the $f^z{}_{F_1}$ is especially low and h_{F_1} is abnormally great in these latitudes. Sporadic E reflections frequently control long-distance transmissions both day and night. Good sporadic E reflections often provide intense signals at high frequencies and sometimes at ultrahigh frequencies. These reflections are very common during the summer but occur at irregular intervals. The irregularities are both geographical and temporal.

For frequencies near the critical frequency the virtual heights increase rather rapidly and are considerably greater than the minimum values shown in the graphs, but undergo similar diurnal and seasonal variations. Since this is so the virtual height diminishes as the angle of incidence increases for a given frequency and the angles of incidence for several paths cannot be calculated from a single virtual height. Therefore, a knowledge of the actual variation of the virtual height with frequency is necessary in order to calculate accurately the maximum usable frequency or the skip distance. In the interests of brevity the variations of virtual heights with frequency are not presented here, but typical examples of such variations may be found in many of the papers on the ionosphere.

The following tabulation gives a conservative estimate of the factors by which the normal-incidence critical frequency may be multiplied to obtain approximately the maximum usable frequency over long distances, 2,500 km or more.

Normal E layer	4½
Sporadic E	5
F_2 layer (winter day and summer sunset)	2½
F_2 layer (summer day)	2
F layer (summer and winter night)	2¼

Reception measurements indicate that these values may be modified by the slope of the land, near the transmitter or receiver, in the path of the wave. The reason for this is that the slope of the land affects the distribution of intensity of the energy transmitted or received in a given vertical plane, especially at low angles.

Critical frequency.—In contrast to the effect of absorption, the ionization density, measured by critical frequency, largely determines the minimum distance range and maximum frequency for practical high-frequency radio communication.

Because of the high $f^z{}_{F_1}$ and the low f_s during the winter day, the highest frequencies are transmitted by way of the F_2 layer at this time. During the summer day, however, $f^z{}_{F_1}$ is much lower and f_s is higher than in winter so that the band of frequencies which can penetrate the E layer and be returned by the F_2 layer is very small or nonexistent. This effect is increased for the reason that h_{F_1} is greater in summer than in winter. Hence most long and medium distance transmission during the summer is by way of the E layer. The frequent occurrence of sporadic E reflections during the summer, both by day and by night, increases the likelihood of such transmission. In general, it should be noted that the probability of E-layer transmission over long distances is greater than over short distances of a few hundred kilometers, other things being equal.

The F_2-layer is capable of reflecting higher frequencies during the winter day than at any other time. This condition exists for a period of 7 or 8 hours, centered at about 1300 local time at the place where the wave strikes the layer. The most favorable time for transmission to the west is thus later than for transmission to the east. In the summer, however, the F_2 layer can reflect higher frequencies for a period of 7 or 8 hours around sunset at the place where the wave strikes the layer than at any other hour of the day. The period of lowest f_F and consequent lowest maximum frequencies which can be reflected from the F layer occurs about an hour before sunrise, both summer and winter. Because of the slow decrease of f_F during the late summer evening, F transmission of higher frequencies is more likely then than during the late winter evening.

Normal E transmission will take place at the highest frequencies around noon local time. Sporadic E reflections are especially useful for transmission in the summer morning and evening.

The F_1 layer is normally useless for transmission save for short distances and for a very limited band of frequencies, and does not need to be considered from a transmission standpoint. The reason for this is that f_{F_1} is not sufficiently above f_E for a wave to penetrate the E layer and be reflected from the higher F_1 layer, at least at fairly large angles of incidence.

For single-reflection transmission the controlling portion of the ionosphere is halfway between the terminal points. For multireflection transmission, the ionosphere along the entire path, except for that portion within several hundred kilometers from the terminal points, must be considered.

From the critical frequency graphs of figures 1 to 15, the year-to-year ratios of useful transmission frequencies as well as the ratios of normal-incidence critical frequencies for each month may be obtained. The long-time increase is apparent for all the regions, and is believed to be associated with the 11-year sunspot cycle. When allowance is made for the seasonal variations, f_E and f_{F_1} are seen to have increased by a factor of about 1.3, during the period of these observations. During the same period the f_{F_2} increased by a factor of about 1.9. The effect of the general increase in critical frequencies is to raise the maximum usable frequencies proportionally and also to increase the absorption on the medium-high frequencies. This means that the most effective frequencies for transmission have increased along with the increase in sunspot activity and may be expected to continue to increase until the sunspot maximum is reached. The sunspot minimum was during the winter of 1933–34 and the next maximum is expected about 1939.

It should be emphasized that these results are averages and represent data taken systematically and over a long period of time at Washington, D. C. Reports [7] from Watheroo, Australia, and Huancayo, Peru, indicate that ionosphere conditions are different in the southern hemisphere. Much more comprehensive data will have to be obtained from other latitudes, especially from higher latitudes, before a world-wide picture of the ionosphere may be found. For purposes of transmission, however, the ionosphere may be considered

[7] L. V. Berkner, H. W. Wells, and S. L. Seaton. *Characteristics of the upper region of the ionosphere.* Terr. Mag. 41, 173. (1936).

as essentially uniform, at least over a range of latitude somewhat exceeding that of the United States.

It is believed that current information on ionosphere conditions is of sufficient interest to warrant publication of the future data monthly. It is planned to do this in the form given in figures 13 to 15, inclusive.

VI. TRANSMISSION IRREGULARITIES

Two types of transmission irregularities, which are not shown on the average curves, have been observed.

The first type has occurred during fairly severe magnetic storms when the $f^z{}_{F_1}$ has been observed to be lower, the h_{F_1} higher and absorption greater than normal during the night of and the day following the local magnetic disturbance.[8 9] During a period of such magnetic disturbances the maximum usable frequency was much less than during a magnetically quiet period. A second type of irregularity is the "fadeout," [10 11 12] a sudden wiping out of practically all high-frequency sky-wave transmission for periods of a few minutes to about an hour. This is caused by a sudden increase in absorption in the lower regions of the ionosphere—the E layer or below—owing to a sudden increase of ionization. This effect is accompanied by a sudden brief disturbance of the earth's magnetic field. The cause of these phenomena is a burst of radiation from a sudden solar eruption. No relation has been observed between this effect in the lower ionosphere and the magnetic storm effect in the higher ionosphere, as entirely different regions of the ionosphere are concerned.

VII. CONCLUSIONS

The general form of the diurnal and seasonal variations of the critical frequencies and virtual heights has recurred from year to year. The daytime critical frequencies of the E and F_1 regions were symmetrical about noon, reaching a diurnal maximum at noon and a seasonal maximum in midsummer. The diurnal maximum of $f^z{}_{F_1}$ occurred at about 1300 local time in the winter and at about sunset in the summer. The diurnal maximum in winter was much greater than in summer. The diurnal minimum in both winter and summer occurred about one hour before sunrise. The critical frequency decreased much more rapidly during the winter evening than during the summer evening.

In addition to the seasonal variations there has been a continuous long-time increase of critical frequencies associated with the 11-year sunspot cycle. It was pointed out that this effect increased the upper limit of useful transmission frequencies determined by penetration of the ionosphere and also increased the lower limit of useful transmission frequencies determined by absorption in the lower ionosphere.

Finally, for practical applications, it should be emphasized that the absorption, virtual heights, and critical frequencies of all portions of the ionosphere traversed by the waves must be considered in determining transmission conditions over a given path.

WASHINGTON, February 23, 1937.

[8] S. S. Kirby, T. R. Gilliland, E. B. Judson, and N. Smith. *The ionosphere, sunspots, and magnetic storms.* Phys. Rev. **48**, 849 (1935).
[9] S. S. Kirby, T. R. Gilliland, N. Smith, and S. E. Reymer. *The ionosphere, solar eclipse, and magnetic storm.* Phys. Rev. **50**, 258 (1936).
[10] J. H. Dellinger. *Confirmation of cosmic phenomenon,* Science **82**, 548 (1935).
[11] J. H. Dellinger. *High-frequency fadeouts continue.* QST **20**, 37 (1936).
[12] J. H. Dellinger. *Direct effects of particular solar eruptions on terrestrial phenomena.* Phys. Rev. **50**, 1129 (1936).

U. S. DEPARTMENT OF COMMERCE NATIONAL BUREAU OF STANDARD

RESEARCH PAPER RP1002

Part of Journal of Research of the National Bureau of Standards, Volume 18, June 1937

ACCELERATED WEATHERING TESTS OF MINERAL-SURFACED ASPHALT SHINGLES

By Hubert R. Snoke and Braxton E. Gallup

ABSTRACT

A method for testing mineral-surfaced asphalt-prepared roofing by accelerated weathering is described, and the results of tests by this method on 39 samples of standard-weight strip shingles, from eight manufacturers, are reported. All of the types of failure encountered in long outdoor exposures of these roofings have been produced in exposures of 7 months or less, the samples furnished by each manufacturer showing a characteristic behavior, largely independent of the granular surfacing materials used.

Except that the samples containing fine mineral filler in the asphalt coatings appear to be the most resistant to weathering, analyses of the samples under test (table 1), including fiber analyses of the felts and petrographic examination of the mineral fillers and fine surfacing materials, show no differences in composition sufficiently great to warrant the prediction of decided differences in their behavior to weathering.

The results of water absorption tests on unweathered samples and on samples exposed 1, 5, and 7 months to accelerated weathering are given. Accelerated blister, slide, and abrasion tests developed by the industry are briefly described, and the results of these tests on the samples in this investigation are reported.

CONTENTS

	Page
I. Introduction	670
II. Description of material and methods of manufacture	670
III. Test methods	671
1. Analytical methods	671
2. Heat tests	671
(a) Accelerated blister test	671
(b) Accelerated "slide" test	672
3. Abrasion tests	672
4. Accelerated weathering test	672
5. Water absorption tests	673
IV. Discussion of results	673
1. Analytical results	673
2. Heat tests	675
3. Abrasion tests	675
4. Accelerated weathering tests	677
(a) Color changes	677
(b) Blistering	677
(c) Pitting	678
(d) Loss of granules	678
(e) Cracking	679
(f) Warping	679
(g) Behavior of back coating	679
(h) Slippage	679
(i) Water absorption	679
V. Summary	680

138329—37——3

I. INTRODUCTION

Mineral-surfaced asphalt shingles are a comparatively recent development of the roofing industry, having come into general use within the past 25 years. When properly laid they have proved to be durable and, from the standpoint of cost, are particularly adapted to low-cost housing projects. Because they can be produced in practically any color or combination of colors and in a wide variety of patterns, they are satisfactory decorative roofing materials.

Federal specifications have been adopted for these shingles, in which are included requirements for the weight of the various constituents and for the total weight per unit area of the finished product.

The quality of the raw materials used and the process of manufacture are probably the greatest factors in determining the resistance to weathering of roofing of this type. With an industry that is developing as rapidly as this one, with raw materials and manufacturing processes constantly changing, and with a finished product that will last from 10 to 20 years, or longer, outdoor weathering tests are of no great value. By the time conclusive results are obtained by this method, the material under test is not representative of that then on the market.

This paper describes the results of an investigation made with funds furnished by the Works Progress Administration, for the benefit of the Federal agencies engaged in housing activities and associated with the Central Housing Committee. The purpose of the investigation was to study the effect of accelerated weathering tests on representative shingles now on the market. Analyses were made of all the samples in the test; also, they were subjected to accelerated blister, slide, and abrasion tests that have been developed by the industry. Test pieces similar to those used for the accelerated weathering test, also samples of whole shingles laid as on a roof, have been exposed outdoors for future reference.

As by-products of this investigation, the factors which govern the durability of these materials and the value of the accelerated weathering test for factory control in their manufacture are clearly shown.

II. DESCRIPTION OF MATERIAL AND METHODS OF MANUFACTURE

Mineral-surfaced asphalt shingles are manufactured on an organic felt base, made by pulping fibrous materials and converting the prepared pulp into a dry continuous sheet on a paper-making machine. Low-grade paper stock is used in the manufacture of these felts, the content of cotton rags seldom exceeding 70 percent and being in many cases less than 50 percent.[1]

The shingles are usually made by a continuous process. The felt enters the machine as a dry sheet, passing first into a saturator where it is thoroughly impregnated with a relatively soft asphalt, then around an air-cooled looping system, through the coating rolls, and, while the coatings are still hot, by the granule "feeders" and through press rolls to embed the granules firmly, and finally, through cooling rolls to the shingle cutter and packing machine.[2]

[1] See table 2.

[2] A detailed and illustrated description of the manufacture of asphalt-prepared roofing, and of many types of asphalt shingles, is given in Asphalts and Allied Substances, third edition, by Herbert Abraham, published by D. Van Nostrand Co., New York, N. Y.

Because of limited equipment for making accelerated weathering tests, only so-called standard-weight strip shingles, weighing approximately 90 pounds per 108 square feet of shingle surface, were included in the tests. The samples were restricted to those coated with the natural and artificial mineral surfacing granules in most common use and were taken from the regular stocks of eight of the larger manufacturers of these materials. Table 1 gives the numbers of the shingles and shows them grouped by manufacturers. Under "Color" in this table are the names of the granular surfacing materials furnished by the manufacturers, and under "Granule treatment", their statements as to what treatment, if any, was given the granules before they were embedded in the asphalt coatings. Also, under "Mineral matter", the column headed "Reported" gives the percentages of fine mineral filler each manufacturer states he has added to the coating asphalt.

III. TEST METHODS

1. ANALYTICAL METHODS

In general, the data presented in table 1, showing the composition of the shingles, were obtained by the methods outlined in Federal Specification SS–R–521, Roofing and Shingles; Mineral-Surfaced, Asphalt-Prepared,[3] except that the front and back coatings were examined separately. Petrographic methods were used to determine the nature of the granules and of the fine mineral fillers, all of the mineral matter passing a no. 70 U. S. Standard Sieve being arbitrarily classified as filler and expressed as the percentage of the total weight of the front and back coatings. No correction was made for the mineral surfacing material on the back coatings, or for the mineral matter passing a no. 70 sieve included in the granular surfacing materials. This explains the lack of agreement between the amount of filler found and that reported by the manufacturer.

In the petrographic examination of the mineral matter, that retained on a no. 70 sieve was assumed to be surfacing material, and that passing a no. 200 sieve the fine mineral filler. In each case only the constituent present in greatest quantity is reported.

The fiber analyses of the desaturated felts (table 2) were made by the method given in Federal Specification UU–P–31, Paper, General Specifications.[4] This method is also covered by ASTM Method D 272–34, Standard Methods of Analysis of Roofing Felt for Fiber Composition.[5]

2. HEAT TESTS

The percentage of volatile matter and the behavior at 80° C (table 3) were determined by the methods described in Federal Specification SS–R–521. The accelerated blister and slide tests were made, except for slight modifications, according to methods developed by H. W. Greider of the Philip Carey Co. These tests are briefly described as follows:

(a) ACCELERATED BLISTER TEST

Test pieces, 2½ by 6 inches, are immersed in a water bath at 125° F, for 1 hour; then removed and placed immediately, granule surface upward, in a rotating-shelf oven at 220° F for 1 hour. They are then

[3] Copies of Federal specifications mentioned in this paper may be obtained from the Superintendent of Documents, Government Printing Office, Washington, D. C., price 5 cents each, stamps not accepted.
[4] See footnote 3.
[5] Book of Standards, Am. Soc. Testing Materials, pt. II, p. 1162 (1936).

examined while still hot and before the blisters have had time to subside. In these tests samples showing not more than two blisters not exceeding 1/16 inch in diameter at base were rated "Good"; those with more than two and not more than eight blisters, none exceeding 1/8 inch in diameter at base, were rated "Fair"; and those with more than eight blisters, or with blisters greater than 1/8 inch in diameter at base, were rated "Poor." This test does not exactly duplicate the Greider test in that the latter employs a specially designed oven equipped with electric strip heaters radially arranged in the roof.

(b) ACCELERATED "SLIDE" TEST

Test pieces 2½ by 6 inches are suspended vertically in an oven at 220° F for 1 hour. The slippage of the coating and granular surfacing material is measured from the lower back edge of the test piece.

3. ABRASION TESTS

Wet and dry abrasion tests[6] to determine how well the granular surfacing materials are embedded in the asphalt coatings were made on all the samples, using the "Carey abrasion test apparatus" and the "Minnesota Mining rub test machine." Both of these instruments and the method of the tests are described elsewhere,[7] so that only a general statement of the principles involved in each test is necessary here. The Carey apparatus permits the roofing sample itself to provide the abrasive action by causing two pieces of roofing to abrade each other. The Minnesota Mining machine uses a standardized steel wire brush to abrade the roofing.

4. ACCELERATED WEATHERING TEST

It has been shown in a previous paper that asphalts behave similarly when exposed to accelerated and outdoor weathering tests.[8] In these, as in the previous tests, the purpose was to subject the samples to exaggerated conditions simulating outdoor exposure, in this case to continuous light and heat from a carbon-arc lamp, with intermittent water spray. The apparatus used is essentially the same as that described in previous papers[9] and needs only a brief description here.

The test pieces, cut 3 inches wide and as long as the short dimension of the shingle, i. e., 10 or 12½ inches, were placed in vertical slots around the inside of a metal cylinder encircling the arc lamp. The cylinders were 30 inches in diameter so that the exposed surface of each test piece was approximately 15 inches from the source of light. Each cylinder was equipped with a revolving mechanism geared to give one complete revolution in 20 minutes. The water spray was furnished by a perforated pipe in a fixed, vertical position about 2 inches from the test pieces, and connected with the city water supply through a reducing valve to insure constant pressure. The maximum temperature at the surface of the panels varied from 82° F on a cold day to 102° F on a hot day and was usually sufficient to dry the sur-

[6] The authors are indebted to Dr. H. W. Greider, of the Philip Carey Co., and Mr. L. A. Hatch, of the Minnesota Mining and Manufacturing Co., for making these tests.

[7] H. W. Greider and G. A. Fasold, *A comparision of abrasion test methods for embedding of granular mineral surfacing on asphalt roofing*, Proc. Am. Soc. Testing Materials, pt. I, p. 453 (1936).

[8] O. G. Strieter, BS J. Research 5, 247 (1930) RP197.

[9] Percy H. Walker and E. F. Hickson, BS J. Research 1, 1 (1928) RP1; O. G. Strieter, BS J. Research 5, 247 (1930) RP197.

faces of the panels, except for a small area at the bottom, before they returned to the water spray.

Three exposure units were in practically continuous operation for 7 months, a month in this case meaning 30 days of 24 hours each. All the lamps were adjusted to practically the same conditions at the start of the test, but to insure uniformity of treatment for all samples, a schedule was followed whereby panels were moved from one cylinder to another, and their ends reversed, at regular intervals.

Examinations were made weekly during the first month of the test, and thereafter once each month. One complete set of samples was removed after being exposed 1 month, another after 5 months, and the final set after 7 months. These three sets, with an original unweathered set, were used for the water absorption tests next described.

5. WATER ABSORPTION TESTS

These tests were made by immersing the samples described above, previously dried to constant weight, in water at room temperature for 24 hours; then removing them from the water, drying the surface moisture with a towel, and weighing.

IV. DISCUSSION OF RESULTS

1. ANALYTICAL RESULTS

The data presented in table 1 show that these materials are, in general, remarkably uniform in composition. Except that the samples furnished by manufacturer *H* (samples 35 to 39, inclusive) contain no fine mineral filler in the coating asphalt, and therefore have a correspondingly greater weight of bitumen per unit area, there are no differences in composition great enough to warrant the prediction of decided differences in the behavior of these materials to weathering.

All but 12 of the samples individually met the requirements of Federal Specification SS–R–521 in every respect. Samples 1, 18, 20, 22, and 26 fail to meet the requirement for weight of the desaturated felt (minimum 10.8 pounds per 108 square feet), samples 7, 13, 14, 16, 17, and 31 fail as regards percentage saturation of the felt (minimum 175%), and sample 26 as regards total weight of organic fibers and bitumen per 108 square feet (minimum 45 pounds). Since different sections of the sheet from which these shingles are cut may differ in composition, the average analyses of the materials supplied by each manufacturer are probably more representative of the material furnished by that manufacturer. On this basis only the material furnished by manufacturer *D* would fail to meet all the requirements of the specification, the average saturation of the felt (167%), being lower than the minimum specified (175%).

Federal Specification SS–R–521 contains no requirement for pliability of shingles. The pliability test used was the one required for mineral-surfaced roll roofing under the above specification and all but four samples, from a single manufacturer, passed the test.

The results of the fiber analysis of the felts, table 2, show practically the same constituents in all of the felts, with as much variation in composition between samples from the same manufacturer as between those from different manufacturers. In this table all of the constituents that were identified are listed. The percentages shown, however,

are in many cases little better than approximations, it being customary in analyses of this kind to report as a trace any constituent present in small amount. Where a constituent is present in considerable quantity the amount reported can be considered accurate within plus or minus 10 percent.

O. G. Strieter [10] found no significant difference in the resistance to outdoor weathering of asphalt-prepared roofing, which may be attributed to the kind of fiber or combination of fibers employed.

TABLE 2.—*Fiber analysis of felts*

Sample	Ground wood	Chemical wood	Jute	Hair	Wood	Rag	Silk	Rayon	Kapok
	Percent	*Percent*	*Percent*	*Percent*	*Percent*	*Percent*	*Percent*	*Percent*	*Percent*
1	16.9	8.3	11.8	0.8	2.3	53.5	1.6	4.5	0.3
2	10.9	9.4	13.9	.4	2.6	51.2	2.4	7.5	1.8
3	18.6	18.1	7.2	.4	2.5	45.6	3.0	3.4	0.2
4	12.4	5.9	15.8	.7	2.9	50.9	4.8	6.7	0
Average	14.7	10.4	12.2	.6	2.6	50.3	2.9	5.5	.6
5	17.8	8.2	10.2	.3	4.7	50.7	3.0	1.6	3.5
6	24.0	13.1	13.0	0	0.8	43.3	2.7	1.0	2.1
7	16.2	9.0	11.0	1.4	3.9	57.0	0.9	-------	-------
8	14.6	9.7	10.1	1.6	4.0	59.2	.6	-------	-------
Average	18.1	10.0	11.1	0.8	3.3	52.5	1.8	-------	-------
9	2.0	7.5	5.5	0.6	1.5	77.5	0.4	4.3	-------
10	1.5	17.0	6.6	1.8	0.5	65.6	3.8	3.1	-------
11	2.8	8.4	13.2	0.6	1.2	68.5	2.0	2.6	-------
12	4.4	13.7	8.3	.6	1.2	68.5	1.5	1.6	-------
Average	2.7	11.6	8.4	0.9	1.1	70.0	1.9	2.9	-------
13	6.2	9.2	10.2	1.5	7.1	59.3	3.3	2.5	0.6
14	15.8	12.7	8.6	1.7	2.7	54.3	2.0	2.2	-------
15	14.2	15.5	11.7	1.4	2.4	48.4	4.3	2.2	-------
16	17.1	14.0	16.9	1.4	2.4	40.8	5.8	1.6	-------
17	8.8	12.9	17.1	1.0	2.5	54.5	2.5	0.7	.2
Average	12.4	12.9	12.9	1.4	3.4	51.5	3.6	1.8	-------
18	18.8	13.3	4.6	-------	0.5	50.2	3.9	6.6	-------
19	22.7	16.2	15.1	0.7	.7	40.4	1.6	7.8	-------
20	20.4	16.3	12.8	-------	-------	33.4	0.5	6.7	-------
21	15.8	14.1	4.9	1.2	1.1	54.3	3.6	4.7	-------
22	18.5	19.3	4.1	0.6	0.3	48.8	0.5	7.3	-------
23	19.8	14.9	3.1	.6	.2	49.3	1.3	5.4	-------
24	20.7	18.1	7.0	1.2	.2	42.9	0.7	8.9	-------
Average	19.5	16.0	7.4	0.6	0.4	45.6	1.7	6.9	-------
25	11.2	14.0	14.9	0.1	1.5	55.4	0.7	1.9	-------
26	8.5	22.3	13.9	.6	1.6	46.2	1.6	4.6	-------
27	15.2	12.8	16.0	.5	0.1	52.9	0.2	2.0	-------
28	13.4	13.9	18.9	.4	1.1	47.3	.7	4.0	-------
29	10.2	10.7	11.8	.4	1.7	61.9	1.5	2.3	-------
30	5.4	8.1	10.9	.7	0.1	72.1	0.5	2.5	-------
Average	10.6	13.6	14.4	0.4	1.0	56.0	0.9	2.9	-------
31	17.3	5.3	6.9	0.3	3.6	65.8	0.4	0.5	-------
32	12.5	4.4	6.4	.2	3.2	57.1	4.2	6.2	0.7
33	15.1	8.6	10.8	-------	3.8	58.2	2.0	1.5	-------
34	10.6	5.5	4.2	.6	3.2	69.8	4.0	1.3	.4
Average	13.9	5.9	7.1	0.3	3.4	62.7	2.6	2.4	-------
35	5.2	18.3	8.8	-------	1.5	54.5	1.9	9.6	-------
36	7.5	15.3	13.3	-------	1.3	53.2	3.3	6.0	-------
37	7.9	20.4	6.2	0.5	-------	53.2	2.5	9.4	-------
38	9.1	13.4	10.6	.2	7.7	54.9	3.4	-------	-------
39	3.2	9.6	18.5	1.1	4.4	54.6	4.1	4.5	-------
Average	6.6	15.4	11.5	0.4	3.0	54.1	3.0	5.9	-------

[10] O. G. Strieter, J. Research NBS 16, 511 (1936) RP888.

MANUFAC

Sample	Color	Type of granules	Granule treatment			Weight	Weight	T
			Oiled	No oil	Resin-treated			
						lb/108 ft²	lb/108 ft²	
1	Natural green	Slate		×		89.2	10.4	
2	Silicated green	Black slate coated with green cement.	×			90.8	11.5	
3	Natural blue-black	Slate	×			91.0	11.8	
4	Natural red	do		×		90.8	11.5	
Average						90.4	11.3	

MANUFAC

5	Natural red	Slate	×			89.0	11.1	
6	Ceramic bright green	Quartz with fluxed green coating.			×	90.7	10.9	
7	Natural blue-black	Slate	×			90.0	12.7	
8	Kentucky green stone	Low order slate	×			89.3	11.0	
Average						89.7	11.4	

MANUFAC

9	Ceramic bright green	Quartz with fluxed green coating.	×			86.7	11.8	
10	Natural green	Slate			×	86.7	11.6	
11	Natural red	do	×			91.6	11.3	
12	Natural blue-black	do	×			92.8	11.6	
Average						89.4	11.6	

MANUFAC

13	Blue-black	Slate			×	89.4	11.2	
14	Natural red	do			×	94.6	11.0	
15	Ceramic bright red	Burned shale			×	87.6	11.5	
16	Ceramic bright green	Quartz with fluxed green coating.			×	102.4	10.9	
17	Natural green	Slate			×	83.8	11.4	
Average						88.8	11.3	

MANUFAC

18	Ceramic green	Quartz with fluxed green coating.	×			89.6	10.4	
19	do	do		×		94.8	10.9	
20	Cement coated brier green.	Gray slate with thin green coating.	×			88.5	9.9	
21	Natural red	Slate	×			92.3	10.8	
22	Burnt shale indian red	Burned shale		×		93.4	10.7	
23	Natural blue-black	Slate	×			91.5	11.5	
24	Natural green	do	×			91.5	10.9	
Average						91.7	10.7	

MANUFAC

25	Natural red	Slate	×			87.5	11.7	
26	Bright red silicate	Gray slate coated with unglazed red cement.	×			87.2	10.7	
27	Dura green silicate	Gray slate coated with unglazed green cement.	×			88.4	11.6	
28	Natural black	Slate	×			87.7	11.5	
29	Natural green	do	×			90.9	11.0	
30	Dura green ceramic	Quartz with fluxed green coating.	×			86.4	11.6	
Average						88.0	11.3	

MANUFAC

31	Natural blue-black	Slate	×			88.0	12.5	
32	Tile red	Burned shale	×			91.4	12.6	
33	Charmain green	Quartz with fluxed green coating.	×			87.6	11.5	
34	Natural red	Slate	×			88.1	11.3	
Average						88.8	11.9	

MANUFAC

35	Natural blue-black	Slate	×			89.5	12.4	
36	Natural red	do	×			88.0	12.4	
37	Jade green	Quartz with fluxed green coating.	×			97.0	11.0	
38	Natural green	Slate	×			91.3	11.1	
39	Tile red	Burned shale	×			87.5	12.5	
Average						90.7	11.9	

[a] Ground rock in which basic minerals predominate.

[b] Ground rock in wh

TABLE 1.—*Analytical results*

MANUFACTURER *A*. SIZE OF SAMPLES 10 BY 36 INCHES

Felt				Bituminous matter			Mineral matter						Ash	Pliability at 25° C
										Passing no. 70 sieve				
Weight	Thickness	Saturation	Ash	Top	Bottom	Saturant	Top	Bottom	Retained on no. 70 sieve	Reported	Determined	Type of filler passing no. 200 sieve		
lb/108 ft²	in.	%	%	lb/108 ft²	lb/108 ft²	lb/108 ft²	lb/108 ft²	lb/108 ft²	lb/108 ft²	%	%		lb/108 ft²	
10.4	0.049	192	9.8	18.9	0.9	20.0	36.8	0.7	28.9	35.0	32.9	Silicate rock [a]	40.9	Passed.
11.5	.056	198	10.4	12.2	1.2	22.7	40.0	.7	31.1	35.0	41.5	do	43.6	Do.
11.8	.053	191	9.4	14.0	1.0	22.5	39.6	.4	34.3	35.0	28.7	do	41.4	Do.
11.5	.054	185	10.5	16.1	1.0	21.0	38.6	.7	27.3	35.0	38.5	do	38.7	Do.
11.3	0.053	191	10.0	15.3	1.0	21.5	38.7	0.6	30.4	.....	35.4	.....	41.1	

MANUFACTURER *B*. SIZE OF SAMPLES 12½ BY 36 INCHES

11.1	0.057	205	9.1	17.6	1.1	22.8	34.7	0.5	29.6	30.4	26.0	Quartz	37.1	Passed.
10.9	.058	203	9.4	18.4	.8	22.6	36.3	.4	30.6	30.4	26.5	do	39.2	Do.
12.7	.060	171	12.5	17.6	1.1	21.9	36.7	.3	31.0	30.4	25.7	do	39.6	Do.
11.0	.052	178	8.6	18.6	1.1	19.7	36.9	.5	33.4	30.4	21.9	do	39.6	Do.
11.4	0.057	189	9.9	18.0	1.0	21.7	36.1	0.4	31.1	.....	25.0	.....	38.9	

MANUFACTURER *C*. SIZE OF SAMPLES 10 BY 36 INCHES

11.8	0.058	195	8.3	14.9	2.7	24.0	33.2	1.5	28.9	25.0	26.7	Dolomitic limestone	34.0	Passed.
11.6	.056	194	8.6	15.6	2.2	22.5	34.3	0.9	29.6	25.0	25.5	do	34.0	Do.
11.3	.052	188	9.1	15.9	2.1	21.3	38.9	1.2	34.2	25.0	26.5	do	38.3	Do.
11.6	.053	181	9.5	16.4	1.7	20.9	41.1	.7	34.2	25.0	30.4	do	39.7	Do.
11.6	0.055	189	8.9	15.7	2.2	22.2	36.9	1.1	31.7	.....	27.3	.....	36.5	

MANUFACTURER *D*. SIZE OF SAMPLES 10 BY 36 INCHES

11.2	0.051	160	8.3	19.3	4.0	17.9	31.9	2.6	22.2	25.3	35.6	Silicate rock, [a] also slate flour.	37.0	Passed.
11.0	.053	163	9.2	20.6	2.8	18.3	36.9	2.0	26.4	25.3	35.7	do	41.1	Do.
11.5	.054	177	9.3	18.5	2.3	20.6	33.3	2.0	25.8	25.3	33.2	Black slate flour	38.2	Do.
10.9	.052	157	9.3	21.3	4.1	17.1	41.1	3.6	29.0	25.3	39.7	Silicate rock [a]	50.2	Do.
11.4	.051	169	9.9	22.1	1.7	19.2	33.7	1.7	24.1	25.3	33.2	Black slate flour	49.8	Do.
11.3	0.052	167	9.2	20.1	2.7	19.0	33.9	2.1	24.6	.....	34.4	.....	41.5	

MANUFACTURER *E*. SIZE OF SAMPLES 12½ BY 36 INCHES

10.4	0.054	190	11.0	14.2	5.0	19.9	33.7	2.0	29.6	40.0	29.4	Black slate flour	41.8	Passed.
10.9	.051	186	11.4	15.3	5.5	20.9	36.8	2.3	31.2	40.0	30.8	do	43.6	Do.
9.9	.052	196	10.8	14.9	2.1	19.5	37.1	0.5	32.6	40.0	31.2	do	39.3	Do.
10.8	.053	193	13.0	15.4	5.3	21.1	33.2	2.2	31.6	40.0	27.9	do	39.0	Do.
10.7	.052	188	11.9	16.5	6.2	20.2	33.0	2.7	29.8	40.0	29.2	do	40.0	Do.
11.5	.052	199	13.7	16.4	1.8	23.0	36.2	0.7	29.4	40.0	29.3	do	43.2	Do.
10.9	.052	185	11.6	19.6	2.1	20.2	35.9	.8	29.1	40.0	30.5	do	38.1	Do.
10.7	0.052	191	11.9	16.1	4.0	20.7	35.1	1.6	30.5	.....	29.8	.....	40.7	

MANUFACTURER *F*. SIZE OF SAMPLES 12½ BY 40 INCHES

11.7	0.052	182	8.0	15.1	0.9	21.3	37.2	1.2	28.9	35.0	36.3	Ground quartz	40.7	Passed.
10.7	.051	188	7.8	12.6	.7	20.1	41.9	0.3	32.5	35.0	34.0	Silicate rock [b]	45.2	Do.
11.6	.053	196	10.4	11.0	.4	22.8	40.5	.6	34.0	35.0	42.2	Slate flour, etc	44.1	Do.
11.5	.053	195	7.9	12.6	.4	22.5	39.3	.9	32.5	35.0	34.7	Slate flour	42.0	Do.
11.0	.058	201	10.7	15.7	.9	22.1	38.6	.8	33.1	35.0	34.9	do	42.7	Do.
11.6	.064	175	12.2	12.8	.9	20.3	37.4	1.0	31.0	35.0	39.3	Silicate rock [b]	40.0	Do.
11.3	0.055	189	9.5	13.3	0.7	21.5	39.1	0.8	33.2	.....	36.9	.....	42.4	

MANUFACTURER *G*. SIZE OF SAMPLES 10 BY 36 INCHES

12.5	0.057	169	8.8	16.8	1.7	21.2	33.8	0.8	25.5	35.0	34.9	Dark slate flour [a]	37.0	Passed.
12.6	.060	195	10.7	16.9	1.8	24.6	34.5	.9	27.6	35.0	32.7	do	40.4	Do.
11.5	.055	183	8.7	16.8	2.3	21.0	34.0	1.0	27.3	35.0	31.4	do	37.5	Do.
11.3	.054	193	9.5	14.5	2.9	22.0	33.9	1.3	29.2	35.0	31.0	do	38.1	Do.
11.9	0.056	185	9.4	16.2	2.2	22.2	34.0	1.0	27.4	.....	32.5	.....	38.2	

MANUFACTURER *H*. SIZE OF SAMPLES 10 BY 36 INCHES

12.4	0.061	201	8.1	26.1	1.2	25.0	22.4	1.6	21.8	None	9.6	Dark slate flour	26.3	Failed.
12.4	.060	207	10.0	24.1	1.5	25.7	34.3	1.9	24.6	...do...	8.4	Pale slate flour	28.4	Passed.
11.0	.055	192	8.8	29.2	0.5	21.2	33.2	1.3	32.8	...do...	7.7	Carbonate, slate flour, etc.	37.7	Failed.
11.1	.055	205	9.3	33.3	.9	22.7	21.5	1.0	21.2	...do...	5.9	Pale slate flour	24.5	Do.
12.5	.059	202	10.3	25.8	1.0	25.3	22.0	1.2	21.1	...do...	9.3	Brick dust, pale slate flour, etc.	26.6	Do.
11.9	0.058	201	9.3	27.7	1.0	24.0	24.7	1.4	24.3	.....	8.2	.....	28.7	

[a] rock in which acid minerals predominate. [a] Small amount of ground asbestos present. [d] Not included in the average.

UNIV. OF MICH.

2. HEAT TESTS

All the samples met the requirements of Federal Specification SS–R–521 for volatile matter and heat test at 80° C (table 3). The results of the accelerated blister and slide tests reported in this table are discussed in connection with the results of the accelerated weathering test.

TABLE 3.—*Heat tests*

Sample	Volatile at 80° C[a]	Accelerated blister	Accelerated slippage	Sample	Volatile at 80° C[a]	Accelerated blister	Accelerated slippage
	Percent		*Inch*		*Percent*		*Inch*
1	0.12	Fair	1/16	20	0.08	Fair	1/8
2	.18	do	1/16	21	.07	Good	1/16
3	.17	Good	3/16	22	.05	do	1/8
4	.14	Fair	1/8	23	.08	Fair	3/16
				24	.05	Good	1/8
Average	0.15			Average	0.06		
5	0.12	Good	1/16				
6	.09	do	1/8	25	0.24	Good	1/16
7	.06	do	1/16	26	.18	do	1/16
8	.06	do	1/8	27	.18	Poor	1/16
				28	.18	Fair	1/16
Average	0.08			29	.17	do	1/8
				30	.18	Good	0
9	0.06	Poor	1/4				
10	.12	Good	1/8	Average	0.19		
11	.15	Fair	5/16				
12	.08	Good	1/16	31	0.12	Poor	1/16
				32	.09	Fair	1/16
Average	0.10			33	.06	Good	1/16
				34	.12	Fair	1/16
13	0.11	Good	1/8				
14	.11	do	1/8	Average	0.10		
15	.12	do	1/16				
16	.05	do	1/8	35	0.12	Fair	1/8
17	.18	do	1/4	36	.12	do	1/8
				37	.06	do	3/16
Average	0.11			38	.12	do	3/16
				39	.12	do	1/16
18	0.06	Good	1/8				
19	.05	do	1/8	Average	0.11		

[a]Behavior at 80° C—all samples satisfactory.

3. ABRASION TESTS

There is very little agreement of results, either between the wet and dry tests of the same method, or between the two abrasion test methods, when the loss of granules on all the samples from each manufacturer is averaged. However, there is a definite relationship between the various methods if the samples are grouped according to the kind of granules with which they are surfaced. That is, by the Philip Carey method, when the granule loss for all of the samples surfaced with the same kind of granules is averaged, they are placed in the following ascending order by both wet and dry tests; black slate, artificial red, green slate, red slate, and ceramic green. By the Minnesota Mining and Manufacturing Co. method, in both wet and dry tests, the order is: black slate, artificial red, ceramic green, green slate, and red slate.

These results indicate that initial adhesion of granules, as determined by abrasion methods, is mainly a function of the type of granule rather than of the asphalt coating or of the method of manufacture.

The loss of granules in the accelerated weathering test for the 5 and 7 months' exposures show very close agreement, that is, samples are rated in the same order by the 5 and 7 months' tests. The results of the accelerated weathering tests, however, are not in agreement with those of the abrasion tests. Apparently, the abrasion tests are of value in determining how well granules are embedded at the time of manufacture, but can not be used to predict how well they will adhere on exposure. More conclusive information on this subject could be obtained by making abrasion tests on samples that had been exposed to the accelerated weathering test for different periods of time.

TABLE 4.—*Loss of granules*

Sample	P. C. abrasion test		M. M. Co. abrasion test		Accelerated weathering loss in—	
	Dry	Wet	Dry	Wet	5 months	7 months
	lb/108 ft²	lb/108 ft²	lb/108 ft²	lb/108 ft²	lb/108 ft²	lb/108 ft²
1	3.08	5.14	0.74	3.32	6.50	9.59
2	2.63	6.05	.37	4.80	7.53	11.64
3	2.74	4.00	1.11	1.11	4.00	5.13
4	3.20	5.37	0.74	2.22	2.28	2.97
Average	2.91	5.14	0.74	2.86	5.08	7.33
5	2.51	3.65	1.48	3.32	2.09	3.14
6	3.43	4.45	2.58	2.95	0.76	1.62
7	1.83	2.85	0.74	1.11	1.52	3.43
8	1.48	1.48	0.74	1.11	1.04	2.38
Average	2.31	3.11	1.38	2.12	1.35	2.64
9	3.20	5.94	1.48	1.11	1.37	0.57
10	2.85	3.72	1.11	0.74	1.94	3.42
11	1.94	3.43	1.11	1.11	0.80	4.22
12	0.46	0.57	0.37	0.37	0.57	1.25
Average	2.11	3.41	1.02	0.83	1.17	2.36
13	4.23	4.23	1.11	1.11	4.67	0.24
14	3.08	5.71	1.48	1.85	4.22	6.16
15	3.08	3.88	1.48	2.22	1.03	1.48
16	4.34	4.80	1.11	1.11	0.91	2.62
17	4.45	6.96	5.54	5.91	6.84	9.36
Average	3.84	5.12	2.14	2.44	3.53	5.77
18	6.87	6.16	2.22	2.95	2.75	6.38
19	6.39	5.14	2.22	2.22	3.13	7.04
20	4.45	7.54	5.17	2.58	3.32	4.18
21	4.57	5.60	4.06	5.91	4.85	7.24
22	2.17	2.74	0.74	0.74	0.95	1.81
23	2.63	3.88	1.48	1.48	4.75	8.00
24	2.74	4.11	0.74	1.48	4.28	5.70
Average	4.26	5.02	2.38	2.48	3.43	5.76
25	2.51	4.11	0.74	1.11	2.38	4.38
26	4.34	6.17	1.11	3.32	1.33	2.66
27	4.80	7.88	1.48	4.43	0.95	2.00
28	1.14	1.83	0.37	0.74	1.23	2.09
29	3.31	4.57	1.11	1.48	4.08	5.33
30	3.88	4.45	1.11	0.74	0.85	2.28
Average	3.33	4.83	0.99	1.97	1.80	3.12
31	3.08	4.11	1.11	1.48	4.90	7.99
32	2.28	2.85	1.11	2.22	0.23	1.14
33	5.14	5.48	1.85	1.48	4.68	9.36
34	4.56	6.40	2.58	2.95	6.27	8.22
Average	3.76	4.71	1.66	2.03	4.02	6.68
35	2.63	4.91	1.11	1.48	5.82	9.47
36	4.00	5.71	2.22	3.32	4.56	6.62
37	4.11	7.08	0.74	2.95	3.08	6.73
38	2.40	4.22	1.11	1.85	5.48	7.76
39	2.17	2.51	0.37	0.74	1.37	2.85
Average	3.06	4.89	1.11	2.07	4.06	6.69

4. ACCELERATED WEATHERING TESTS

Figures 1 to 10, inclusive, are actual-size photographs of sections of the test pieces exposed 7 months to the accelerated test. The numbers on the photographs refer to the numbers of the samples listed in table 1. Examination of these photographs will show practically every type of failure found in asphalt prepared roofing that has been weathered outdoors, that is, fading, blistering, cracking of the surface coating, pitting, and loss of granules. No attempt has been made to rate generally the samples from the various manufacturers in the order of resistance to weathering or to establish a definite time ratio between accelerated and outdoor weathering.

In general, it can be said that the roofings of each manufacturer develop certain types of failure and retain commendable features peculiar to that particular brand. While there are certain similarities of behavior in the samples surfaced with the same granules but from different manufacturers, the most striking similarities are found when all of the samples from each manufacturer are considered without regard to the type of mineral surfacing used.

No detailed description of the behavior of each sample has been attempted. However, the types of failure found are here considered separately with reference to particular samples in which each is illustrated.

(a) COLOR CHANGES

The samples surfaced with oil- or resin-coated granules were the first to show color changes. In some cases this change appeared to be a slight fading, for example, the blue-black granules changed to a grayish-black with an accompanying change of texture which improved the appearance of the sample. In other cases, notably the ceramic red granules, the first change was an apparent color intensification. These changes are similar to those that take place in outdoor exposures and are caused by the destruction of the oil or resin coatings on the granules.

As the test proceeded, decided color changes similar to fading were noticed on all the samples, and were most evident on those surfaced with natural slate granules. Except for the blue-black granules, some of which became almost white, these color changes were described by several experienced observers as typical fading in severe outdoor exposures, and were so reported at the end of the test.

The fact that the continued wetting and drying of the surface of the samples would deposit salts that might be suspended or dissolved in the water, and the presence of a yellowish deposit, which partially obscures the color of the granules, render it impossible to make any definite statement as to the relation of color changes in the accelerated test and those obtained by outdoor exposures.

(b) BLISTERING

Blistering is probably the most frequent cause of complaint in roofing of this type and has been the subject of considerable study by the industry. In addition to giving the roofing an unsightly appearance, blisters physically weaken the asphalt coating; also, by exposing the coating to the effect of light and heat, they decrease its resistance to weathering.

The cause of blistering has been variously ascribed to moisture in the felt or coating asphalt, gases occluded in the coating or saturant, the type of asphalt, moisture in the granules, the kind of granules, faulty manufacturing practices, wetting of the material before application, etc. However, the presence of moisture in the sheet is probably the basic cause of most blisters.

In these tests some samples showed surface blisters after 24 hours of exposure, and at the end of 1 month practically all showed blisters. In general, these blisters increased in size for approximately 5 months, after which a noticeable subsidence was observed.

Figures 11, 12, and 13 show cross sections of typical kinds of blisters, each set of four samples showing the original unweathered material, and the same material after 1, 5, and 7 months in the accelerated weathering test. These sections show wide extremes, from scarcely detectable small blisters to large interconnecting ones.

Samples 30 and 34, figures 8 and 9, respectively, illustrate typical small individual blisters, and samples 9 to 12, inclusive, figure 3, large interconnecting ones.

In the accelerated blister tests, the blisters formed were of a different type than those in the accelerated weathering test, and they were always isolated and higher in relation to the diameter at the base, no doubt as the result of the higher temperature in the blister tests. In the weathering tests the blisters were relatively low and covered a larger area, in many cases several smaller blisters running together to form a series of connecting blisters. There is apparently no direct relationship in the formation of blisters by the two tests.

(c) PITTING

Pitting is closely related to blistering, being a further development in which the thin layer of asphalt surrounding the void has broken, either through the loss of a granule which penetrates the layer, or by the weathering of the thin layer of asphalt coating exposed by the formation of a blister. Pits or holes ranging from pin-point size to more than ¼ inch in diameter may be observed in figures 1 to 10. Samples showing small pits are illustrated by samples 1 and 2, figure 1, and sample 6, figure 2; large pits are shown by sample 35, figure 9, and samples 37, 38, and 39, figure 10. Samples from manufacturers *C* and *F* showed virtually no pits, while those from the other manufacturers had more and larger pits arranged as follows in increasing order of severity: *B, A, E, G, D, H.*

(d) LOSS OF GRANULES

The loss of granules by weight, on weathering, is greater for the natural slate granules than for the artificial granules (table 4). When this loss is averaged for all the samples surfaced with the same kind of granules, they are placed in the following ascending order: Ceramic red, ceramic green, natural red, black, and green slates.

From the standpoint of appearance, the position of the natural and artificial granules is reversed. The loss is less apparent for the natural slate granules because of their flat shape and scalelike overlapping. The artificial granules in most cases are practically equidimensional

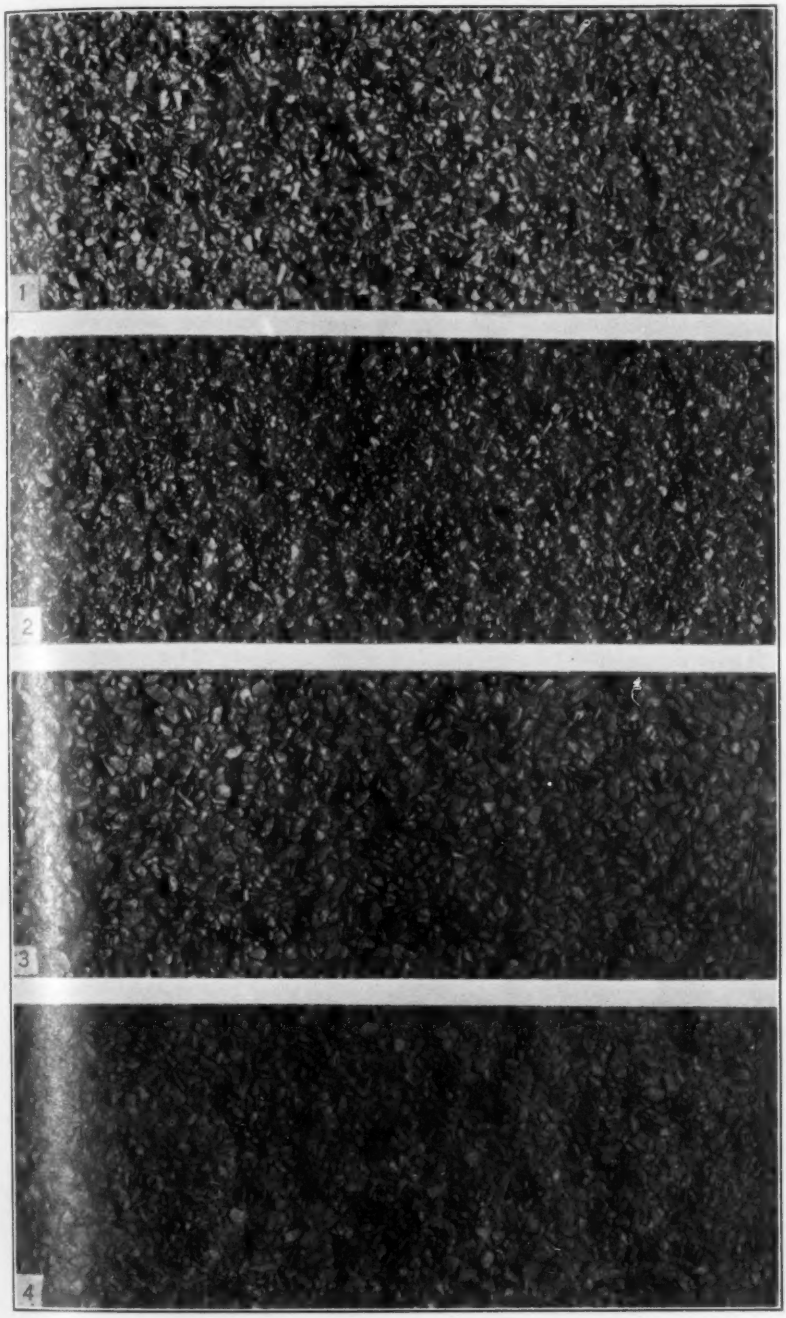

FIGURE 1.—*Exposed 7 months to accelerated weathering.*

Granular surfacing materials: 1, Natural green slate; 2, silicated green; 3, blue-black slate; 4, red slate.

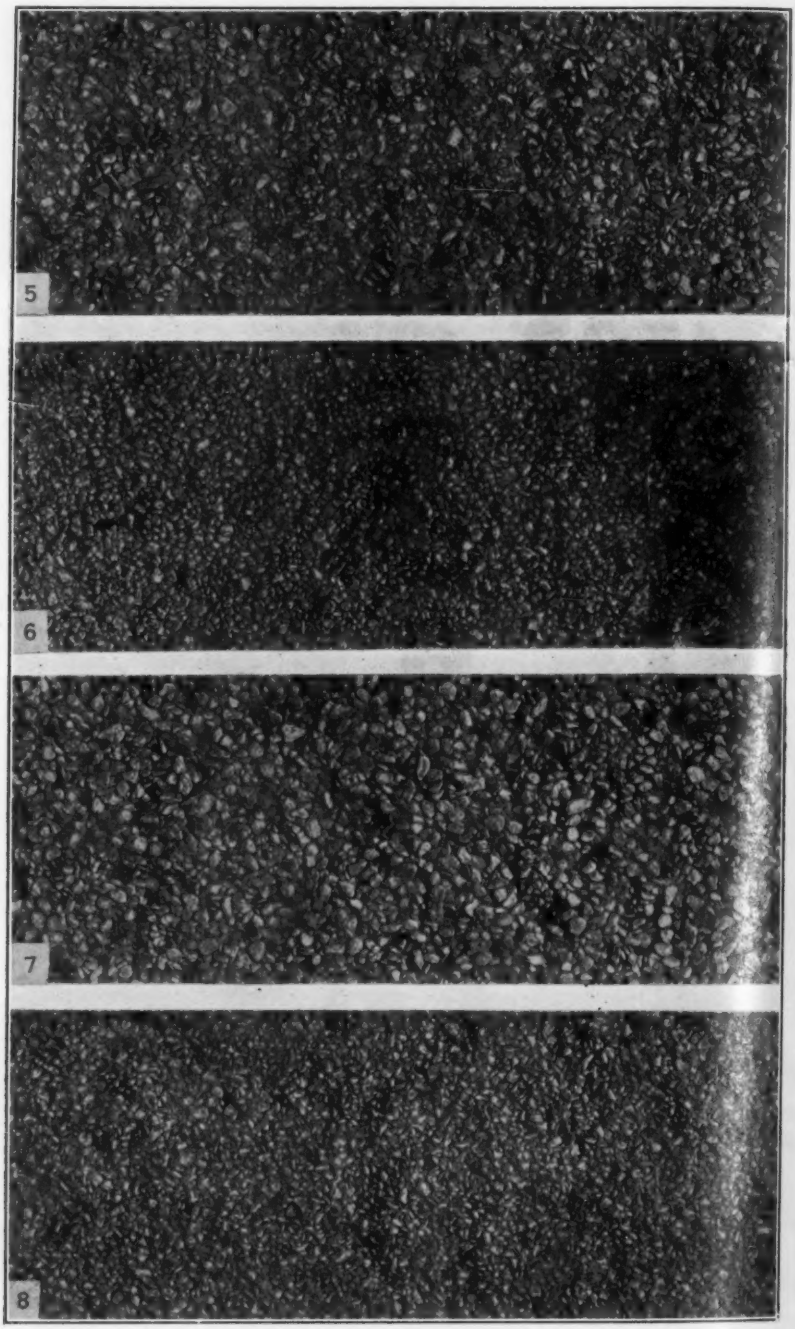

FIGURE 2.—*Exposed 7 months to accelerated weathering.*

Granular surfacing materials: 5, red slate; 6, ceramic green; 7, blue-black slate; 8, Kentucky greenstone.

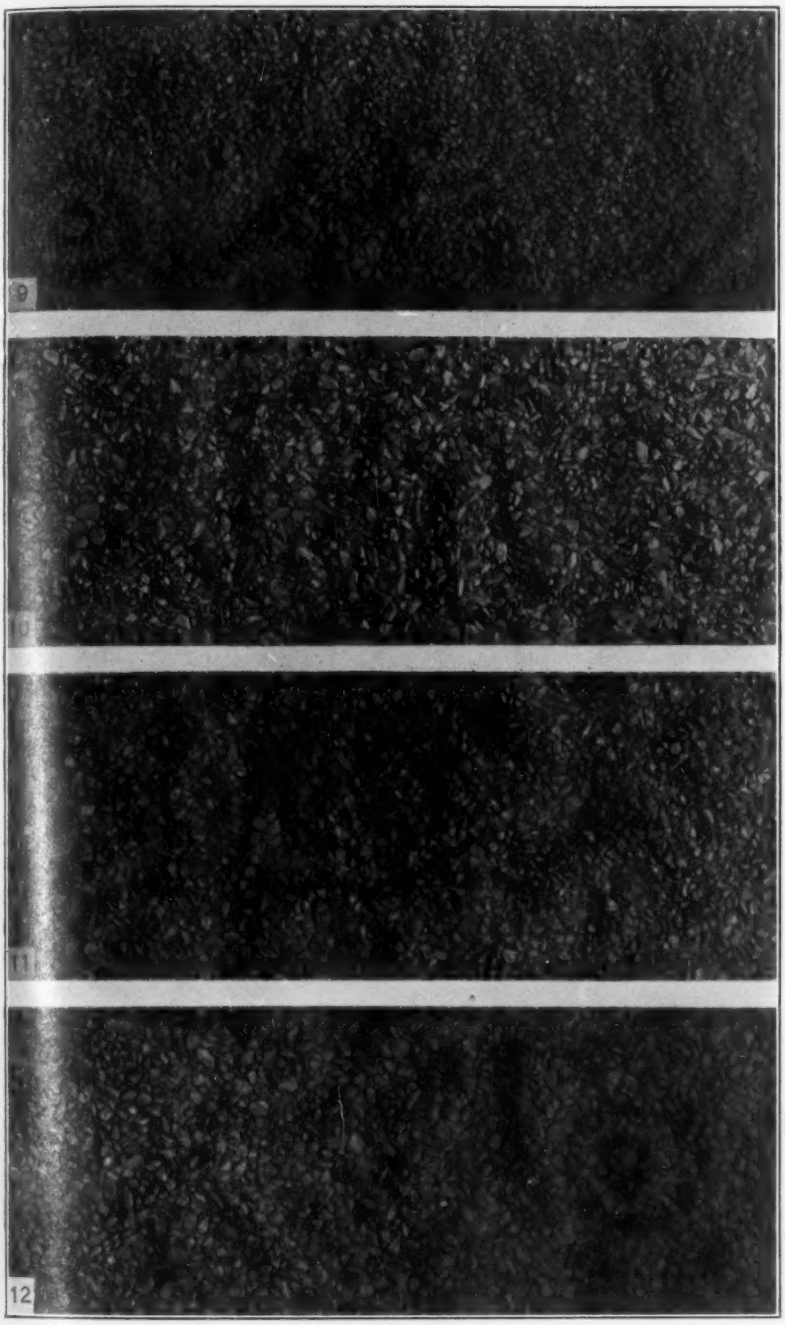

FIGURE 3.—*Exposed 7 months to accelerated weathering.*

Granular surfacing materials: 9, ceramic green; 10, green slate; 11, red slate; 12, blue-black slate.

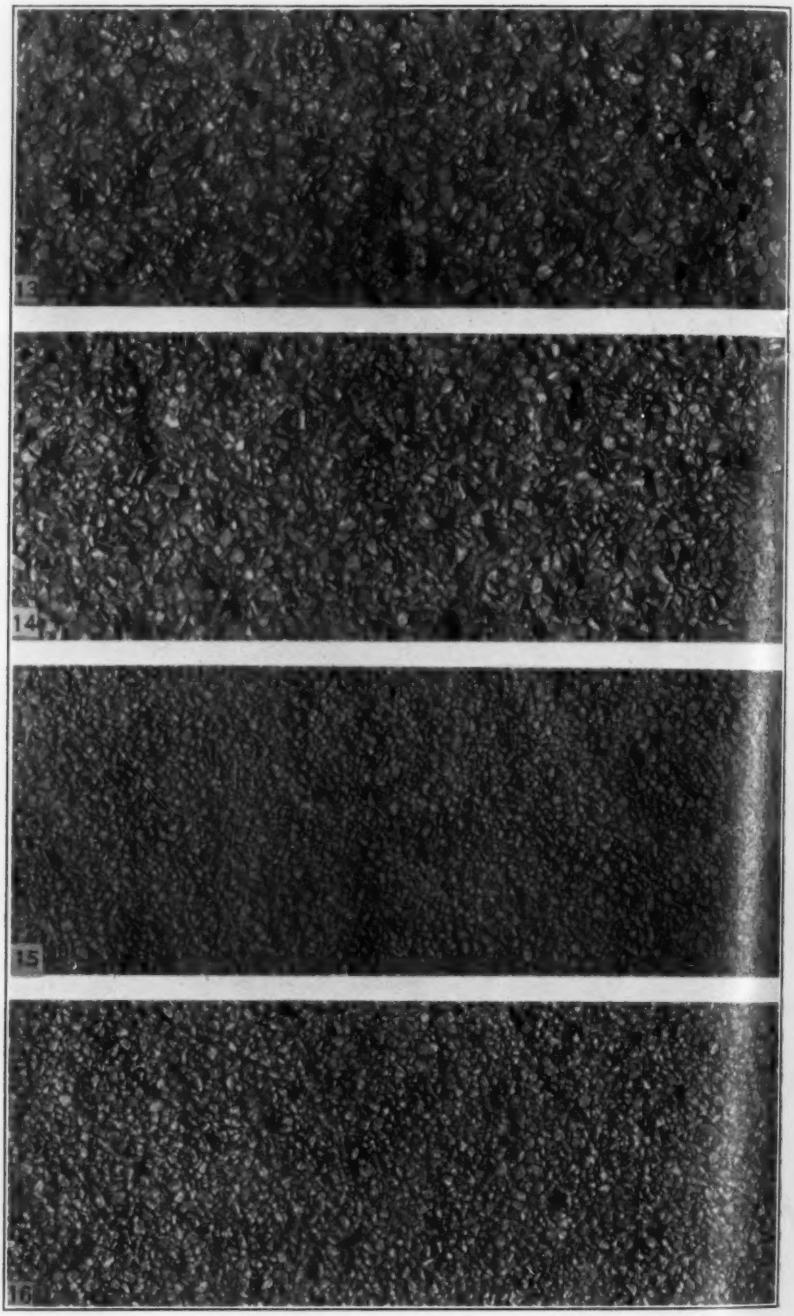

FIGURE 4.—*Exposed 7 months to accelerated weathering.*

Granular surfacing materials: 13, blue-black slate; 14, red slate; 15, ceramic red; 16, ceramic green.

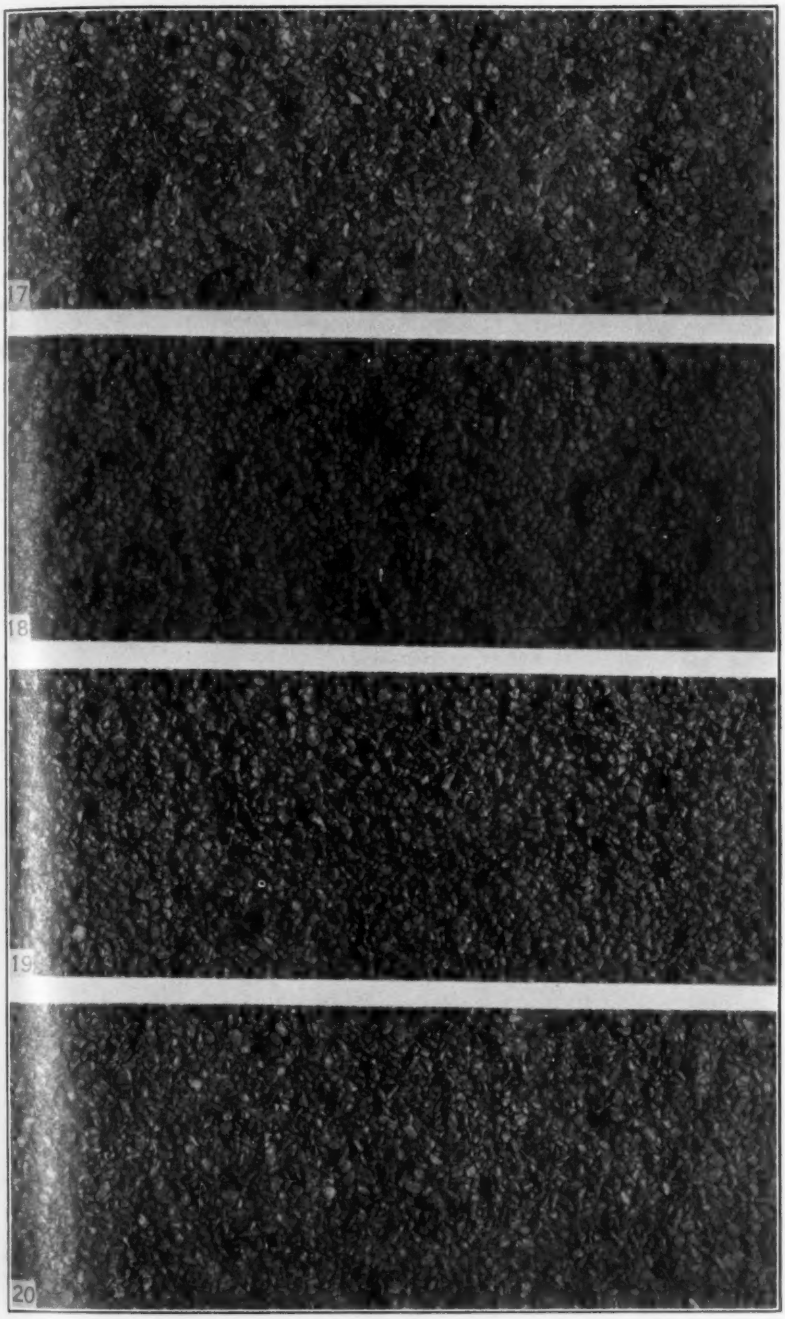

FIGURE 5.—*Exposed 7 months to accelerated weathering.*

Granular surfacing materials: 17, natural green slate; 18, ceramic red; 19, ceramic green; 20, cement-coated brier green.

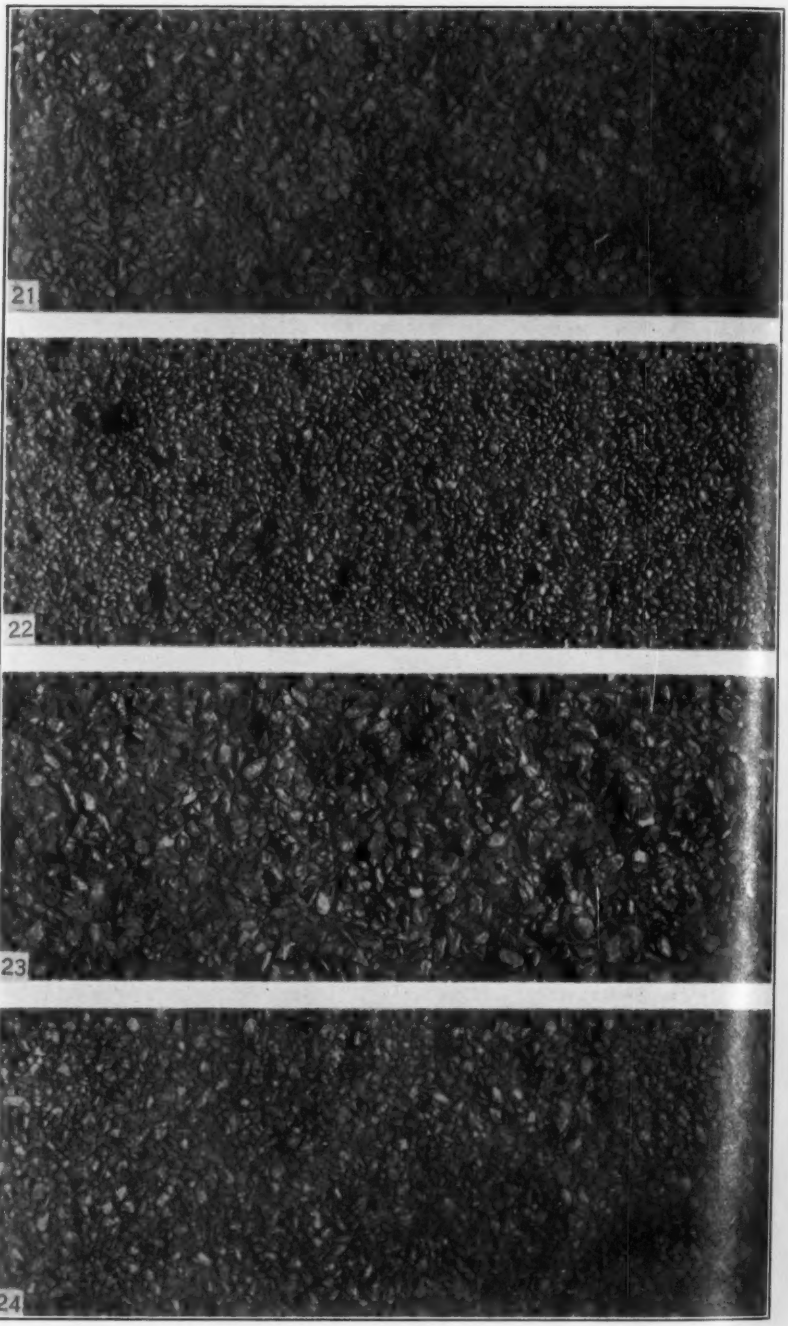

FIGURE 6.—*Exposed 7 months to accelerated weathering.*

Granular surfacing materials: 21, red slate; 22, burnt shale, indian red; 23, blue-black slate; 24, natural green slate.

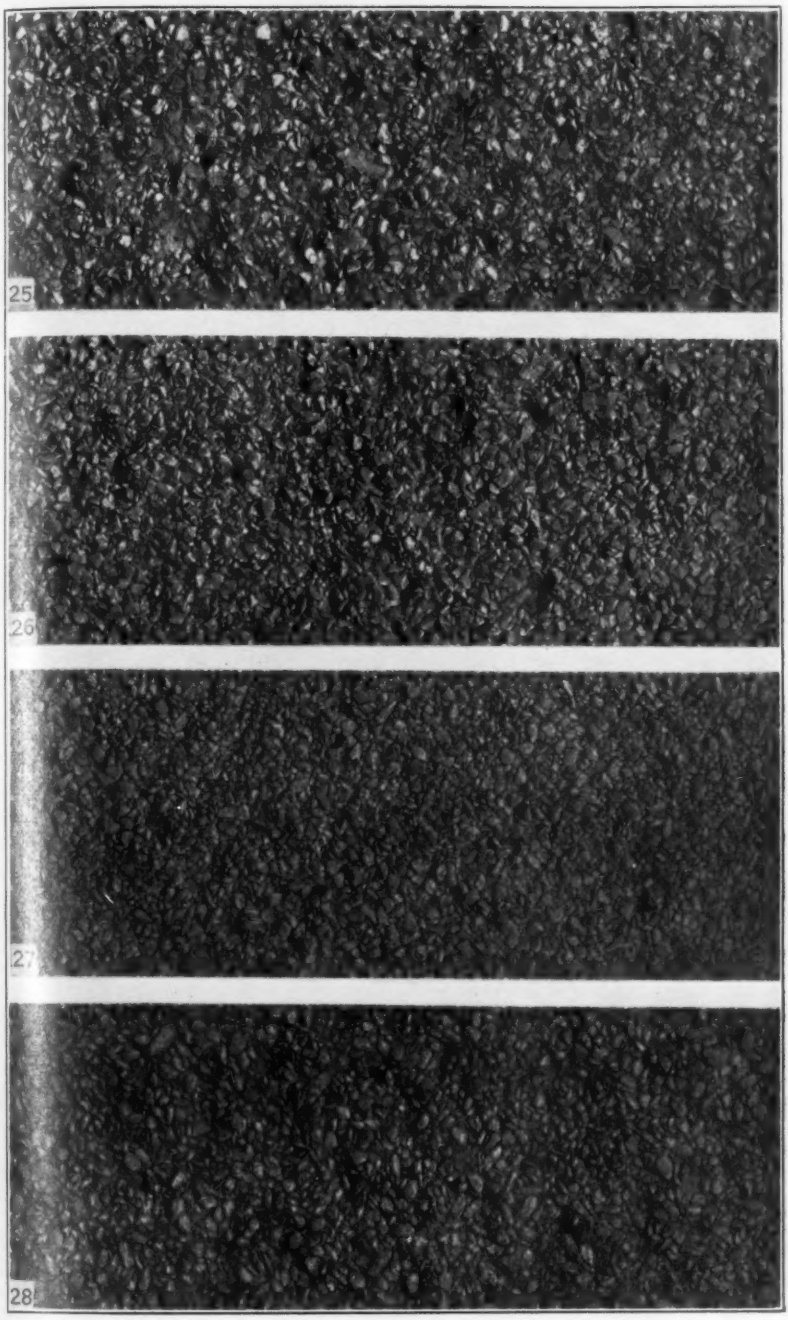

FIGURE 7.—*Exposed 7 months to accelerated weathering.*

Granular surfacing materials: 25, red slate; 26, silicated red: 27, silicated green; 28, black slate.

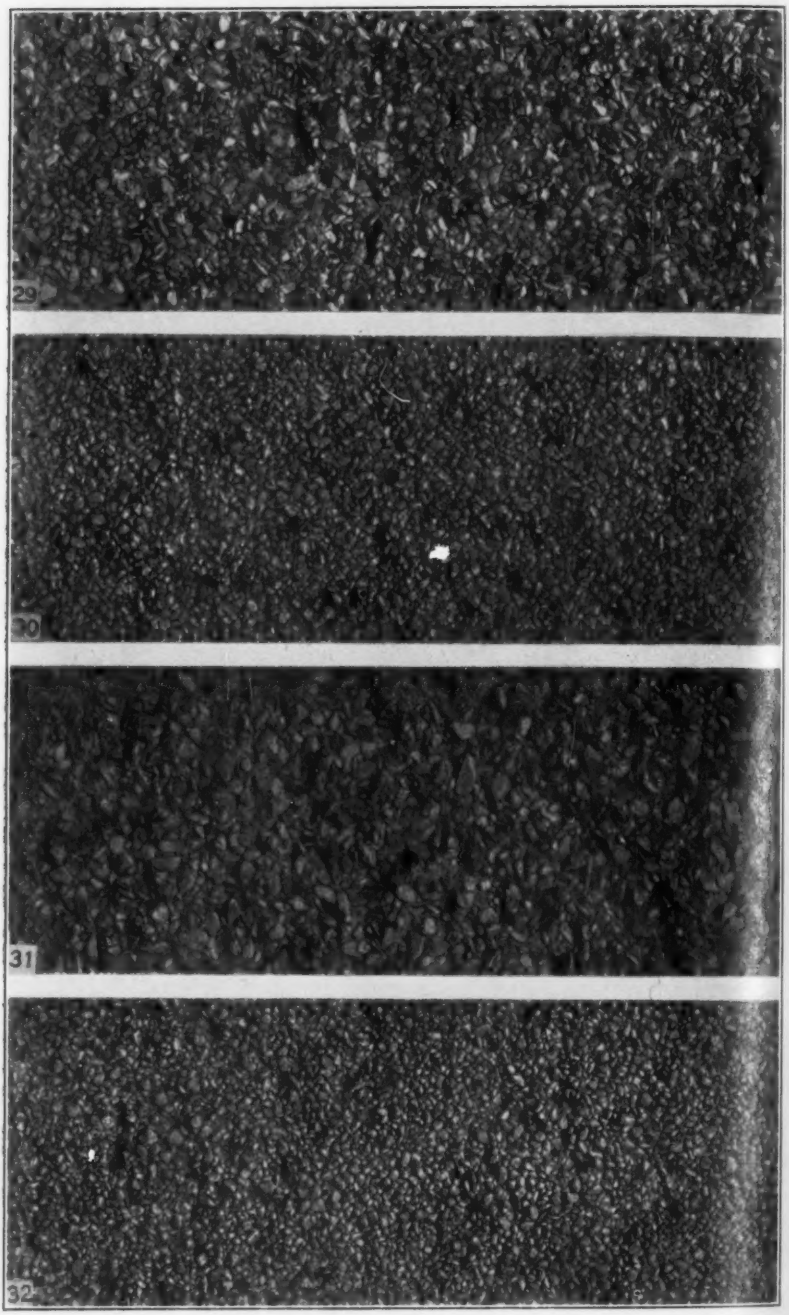

FIGURE 8.—*Exposed 7 months to accelerated weathering.*

Granular surfacing materials: 29, natural green slate; 30, ceramic green; 31, blue-black slate; 32, tile red.

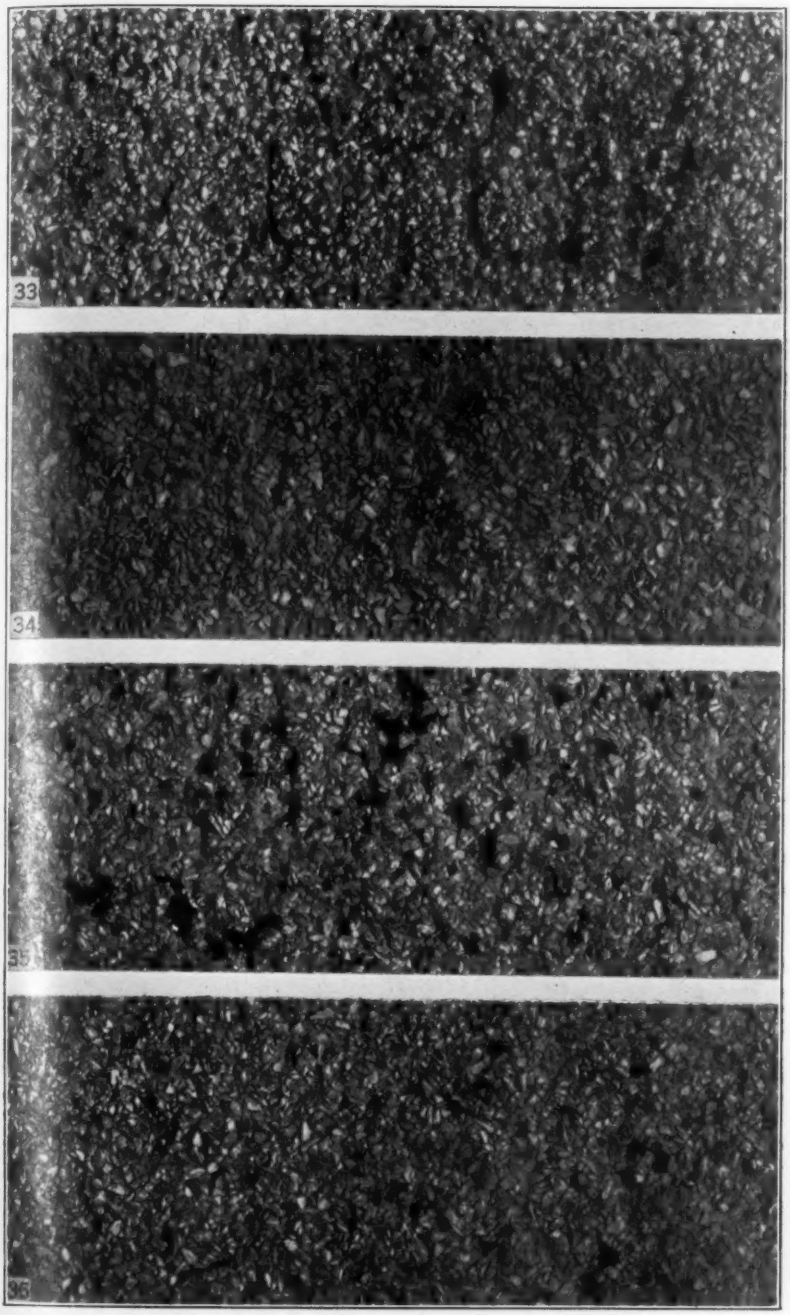

FIGURE 9.—*Exposed 7 months to accelerated weathering.*

Granular surfacing materials: 33, ceramic green; 34, red slate; 35, blue-black slate; 36, red slate.

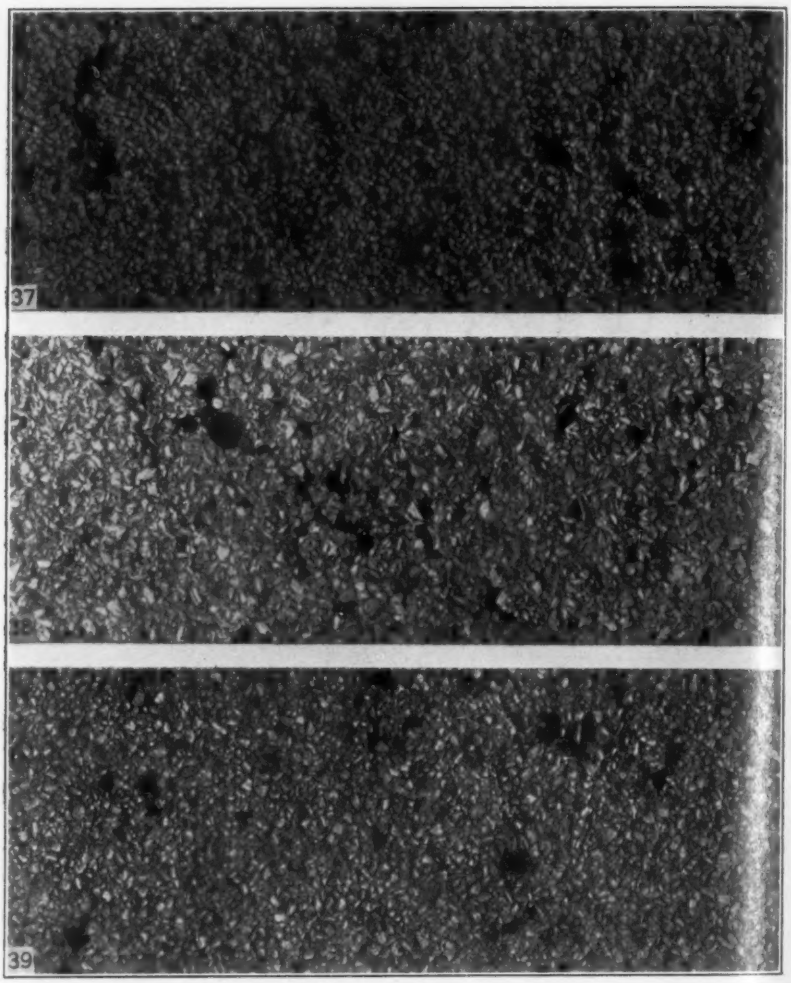

FIGURE 10.—*Exposed 7 months to accelerated weathering.*

Granular surfacing materials: 37, ceramic green; 38, natural green slate; 39, tile red.

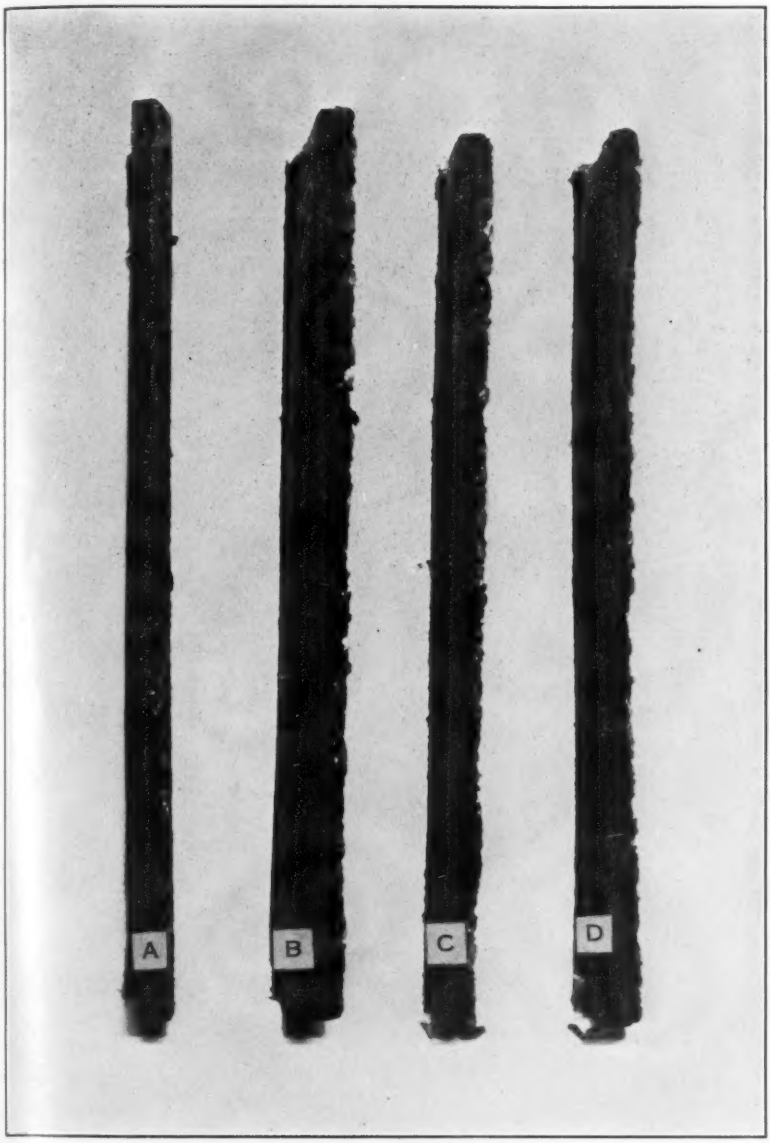

FIGURE 11.—*Cross sections of asphalt shingle test pieces* $\times 1\frac{1}{2}$ *(slight blistering).*

A. Original unweathered material.
B. Exposed 1 month to accelerated weathering.
C. Exposed 5 months to accelerated weathering.
D. Exposed 7 months to accelerated weathering.

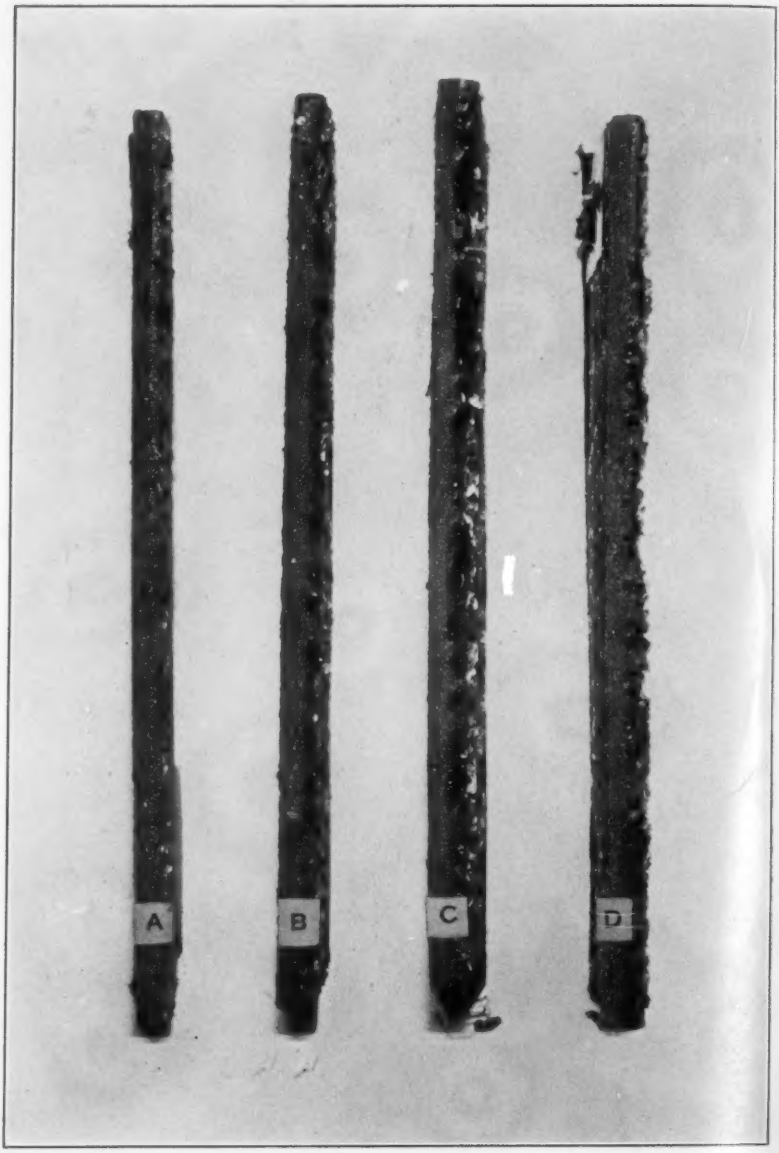

FIGURE 12.—*Cross sections of asphalt shingle test pieces* ×1½ (*medium blistering*).

A. Original unweathered material.
B. Exposed 1 month to accelerated weathering.
C. Exposed 5 months to accelerated weathering.
D. Exposed 7 months to accelerated weatherihg.

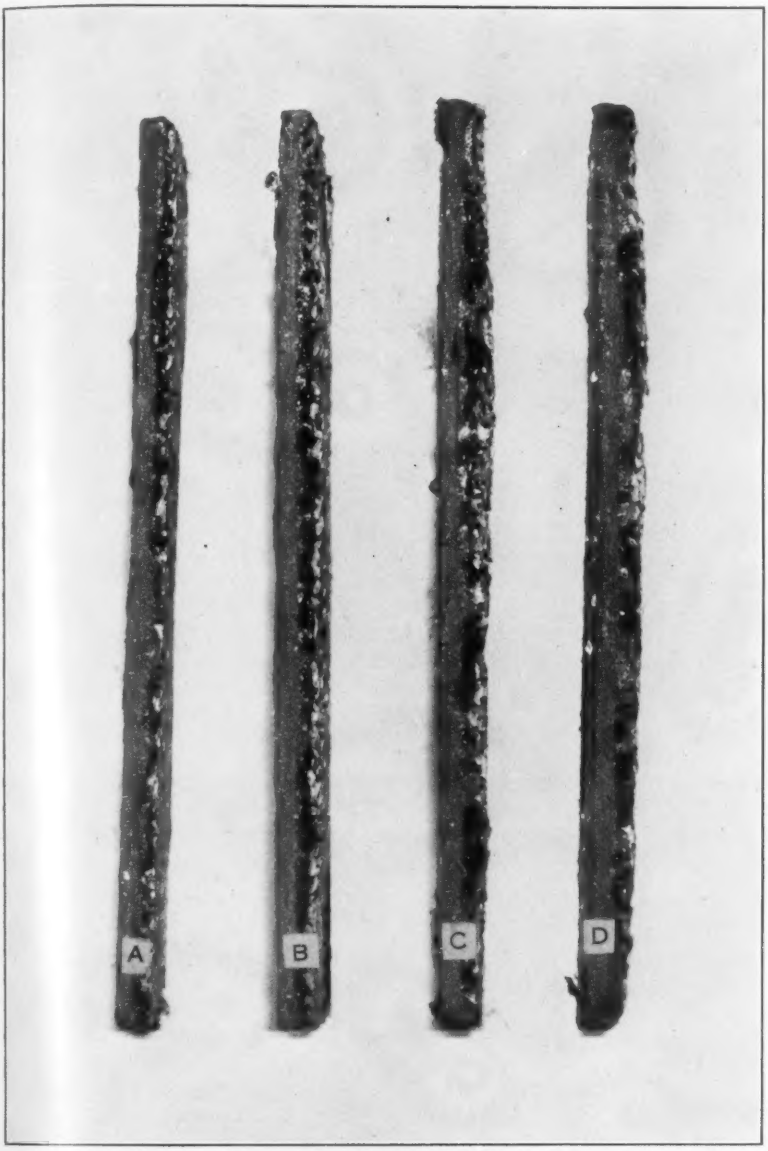

FIGURE 13.—*Cross sections of asphalt shingle test pieces* $\times 1\frac{1}{2}$ *(severe blistering).*

A. Original unweathered material.
B. Exposed 1 month to accelerated weathering.
C. Exposed 5 months to accelerated weathering.
D. Exposed 7 months to accelerated weathering.

UNIV. OF MICH.

and consequently do not overlap. With a few exceptions all samples showed good adhesion of granules. Those which appear noticeably poor in this respect are: Sample 13, figure 4; samples 18 and 19, figure 5; sample 33, figure 9; and sample 37, figure 10.

No general comparison could be made between the various kinds of granule treatments since most of the samples were surfaced with oil-treated granules. Samples 18 and 19 offer the only direct comparison between oiled and unoiled granules, other factors being the same. In this case no appreciable difference was noted.

(e) CRACKING

This defect, which is probably one of the most serious, occurred in relatively few samples. In the most severe cases, the surface coating has large cracks extending as much as 2 inches in length and down to the felt. Cracks of this type are illustrated in samples 36, 17, 13, 38, and 33 in the order of severity. Samples 16 and 22 illustrate slight cracking. The remaining samples show little or no cracking.

(f) WARPING

After about 1 month in the accelerated weathering test, some samples showed a decided tendency to warp or curl. When laid on a flat surface with the granular surfacing upwards, at the end of the test, the most extreme cases showed the center of the panel raised ½ inch, the maximum distortion permitted by the slots used to hold the samples. Samples 31 to 39, inclusive, from manufacturers *G* and *H*, were distorted most. Samples 25 to 30, from manufacturer *F*, showed slight distortion. All other samples remained practically flat.

(g) BEHAVIOR OF BACK COATING

The back coatings of all the samples from manufacturer *G* showed bleeding in spots. The back coatings of those from manufacturer *E* bled uniformly and blistered severely; and those of all other samples were practically unaffected or showed very slight bleeding.

(h) SLIPPAGE

The front asphalt coatings of all samples from manufacturer *C* show a slippage of approximately ¼ inch at the end of the test. This group of samples exhibited the greatest average slide in the accelerated slide test (table 3), which showed a possible relationship between the two tests. Samples from other manufacturers showed no slippage of the coating.

(i) WATER ABSORPTION

Water absorption (table 5) naturally increases with the extent of weathering, and is apparently influenced more by the materials used and the process of manufacture than by the type of granule, since, in general, where low average water absorption is shown for the samples from a particular manufacturer, all of the samples, regardless of the surfacing material, are low.

TABLE 5.—*Water absorption*

Sample	Original	Exposure for—			Sample	Original	Exposure for—		
		1 month	5 months	7 months			1 month	5 months	7 months
	lb/108 ft²	lb/108 ft²	lb/108 ft²	lb/108 ft²		lb/108 ft²	lb/108 ft²	lb/108 ft²	lb/108 ft²
1	1.94	2.05	2.74	3.42	18	1.43	1.62	2.19	3.33
2	2.28	2.74	3.08	3.88	19	1.52	2.10	2.00	3.33
3	2.05	1.82	2.05	2.85	20	1.14	1.71	2.00	2.76
4	1.94	2.05	2.28	3.54	21	1.14	1.33	2.19	2.76
					22	1.14	1.62	2.85	3.42
Average	2.05	2.16	2.54	3.42	23	0.86	1.62	2.19	2.10
					24	1.52	1.62	2.00	2.95
5	1.52	1.62	2.57	2.47					
6	1.71	1.71	2.57	2.47	Average	1.25	1.66	2.20	2.95
7	1.81	3.05	2.28	2.47					
8	0.86	1.43	2.76	2.47	25	2.19	2.76	2.57	2.76
					26	2.19	2.19	3.05	2.76
Average	1.47	1.95	2.54	2.47	27	2.29	2.48	2.76	3.24
					28	1.71	1.90	2.38	2.19
9	1.37	1.60	2.17	2.97	29	1.81	2.29	2.95	3.42
10	1.14	1.14	3.72	4.68	30	1.43	1.62	2.19	2.38
11	1.25	1.60	2.51	3.54					
12	0.80	1.25	3.31	3.20	Average	1.94	2.21	2.65	2.79
Average	1.14	1.40	2.93	3.60	31	1.48	1.94	2.62	6.85
					32	1.71	2.28	2.74	3.88
13	1.48	0.91	1.94	4.45	33	1.37	1.71	2.17	5.25
14	1.94	2.28	3.31	5.82	34	1.60	1.71	2.85	6.05
15	2.17	2.28	2.85	4.33					
16	2.05	2.40	2.85	4.22	Average	1.54	1.91	2.59	5.51
17	1.83	2.28	3.31	4.22					
					35	1.37	1.71	2.05	2.85
Average	1.89	2.03	2.85	4.61	36	1.60	1.82	2.51	3.20
					37	1.71	2.28	3.08	4.57
					38	1.37	2.05	2.85	4.45
					39	2.40	2.74	4.45	7.42
					Average	1.69	2.12	2.99	4.50

V. SUMMARY

1. Of 39 samples of mineral-surfaced asphalt strip shingles from 8 manufacturers, 12 failed to meet the composition requirements of Federal Specification SS–R–521. Averaging the analyses of shingles from each manufacturer, those from only one manufacturer failed to meet the requirements. Except that the shingles submitted by one manufacturer contained no fine mineral filler in the asphalt coatings, and that those from another were low in percentage saturation of the felt, the samples were remarkably uniform in composition, and showed no differences sufficiently great to warrant the prediction of decided differences in their behavior to weathering.

2. All of the types of failure encountered in long outdoor exposures of these roofings under the most severe conditions can be produced in a relatively short time by accelerated weathering. The samples from each manufacturer exhibit a characteristic behavior which is largely independent of the type of granular surfacing materials used, which indicates that the types of asphalt used and the manufacturing process largely influence the behavior to weathering, if large variations in the proportions by weight of the several constituents in the finished roofing are excluded.

3. In these tests the samples which contained fine mineral filler in the asphalt coatings (not required in the Federal specification) withstood weathering best. In general, noncompliance with the re-

quirements of the Federal specification was not evidenced in the results of these tests.

4. Mechanical abrasion tests are of value to determine adhesion of granules at the time of manufacture and should be of value for factory control. Apparently these tests can not be used to predict how well granules will adhere on exposure to the weather.

The authors express appreciation to O. G. Strieter, Research Associate at the National Bureau of Standards, representing the Asphalt Shingle and Roofing Institute, for many helpful suggestions, and to the members of the Manufacturing and Industrial Research Committee of the Asphalt Shingle and Roofing Institute, who furnished the shingles used in this investigation, and who have at all times shown a cooperative interest in this work; also to the following members of the Bureau staff: C. P. Saylor for the petrographic examination of the mineral surfacing and filler materials, and M. L. Rollins and T. M. Plitt for the fiber analyses of the desaturated felts.

WASHINGTON, April 8, 1937.

quirements of the Federal specification was not evidenced in the results of these tests.

4. Mechanical abrasion tests are of value to determine adhesion of granules at the time of manufacture and should be of value for factory control. Apparently these tests can not be used to predict how well granules will adhere on exposure to the weather.

The author expresses appreciation to O. G. Strieter, Research Associate at the National Bureau of Standards, representing the Asphalt Shingle and Roofing Institute, for many helpful suggestions, and to the members of the Manufacturing and Industrial Research Committee of the Asphalt Shingle and Roofing Institute, who furnished the shingles used in this investigation, and who have at all times shown a very active interest in the work; also to the following members of the Bureau staff: C. P. Saylor for the petrographic examination of the mineral surfacing and filler materials, and M. L. Rollins and T. M. Hunt for the fiber analyses of the unsaturated felts.

Washington, April 8, 1937.

U. S. DEPARTMENT OF COMMERCE NATIONAL BUREAU OF STANDARDS

RESEARCH PAPER RP1003

Part of Journal of Research of the National Bureau of Standards, Volume 18, June 1937

COMPRESSIBILITY OF FUSED-QUARTZ GLASS AT ATMOSPHERIC PRESSURE

By Walter B. Emerson

ABSTRACT

The compressibility of fused-quartz glass was determined with sufficient accuracy to establish the required corrections for change of length with change of pressure of the fused-quartz glass étalons used in a Fabry-Perot interferometer to evaluate the indices of refraction of air for converting standards of wave length in air to their value in vacuo. Compressibility determinations were made for the same changes of pressure that were used for index measurements; namely, from vacuum to atmospheric pressures.

Determination of the compressibility of fused-quartz glass was made by interferometric comparison of the relative change in length of end gages of fused quartz and stainless steel.

Values for the compressibility of both fused quartz and stainless steel were also determined by a direct method which depended upon the relative change in length of a closed tube and a solid gage of the same material. By this method the compressibilities of fused quartz and of a stainless steel were determined independently, thereby eliminating the existing uncertainty as to the compressibility of steel at atmospheric pressure obtained by extrapolation from much higher pressures and eliminating, also, the necessity for comparison of materials with great difference in thermal expansivity.

Relative values for fused quartz and stainless steel were also derived from comparative changes in length with pressure of tubes and gages of dissimilar materials.

The measurements gave the following values for longitudinal compressibility at 1 atmosphere pressure:

For fused-quartz glass $9.9\times10^{-7}\pm5\times10^{-8}$ per atmosphere.

For a sample of stainless steel $\leqslant3.1\times10^{-7}$ per atmosphere.

CONTENTS

	Page
I. Introduction	684
1. Compressibility of separator involved in index of air determinations	684
2. Required accuracy of index determinations and of compressibility corrections	684
3. Materials for separators	685
4. Status of values for compressibility; purpose of this investigation	686
II. Methods for determining compressibility	686
1. Method 1.—Comparison of two gages of unlike materials	686
2. Method 2.—Comparison of a closed tube and gage of the same material	687
3. Method 3.—Comparison of a tube and gage of unlike materials	690

CONTENTS—Continued

	Page
III. Apparatus	690
1. Gages, tubes, and interferometer plates	690
(a) End gages, tube, and plates of fused quartz	690
(b) End gages and tube of steel; plates of fused quartz	691
2. Temperature-control apparatus	691
3. Air pump	692
4. Interferometric measuring apparatus	692
IV. Experimental procedure and results	693
1. Preliminary measurements	693
(a) Comparison of two fused-quartz gages	693
(b) Comparison of a fused-quartz gage with steel gages	694
(c) Effect of change of pressure upon temperatures within the chamber	694
(d) Cooling curves of steel gages	694
(e) Time required to establish thermal equilibrium within the constant-temperature chamber	695
2. Final measurements	696
(a) Method 2.—Comparison of a closed tube and gage of the same material	696
(1) Fused-quartz tube and fused-quartz gage	696
(2) Steel tube and steel gage	701
(b) Method 3.—Comparison of a tube and gage of unlike materials	701
(1) Fused-quartz tube and steel gage	701
(2) Steel tube and fused-quartz gage	704
(c) Method 1.—Comparison of two gages of unlike materials	704
V. Summary of results	708
VI. Discussion of results	709
VII. Conclusion	711

I. INTRODUCTION

1. COMPRESSIBILITY OF SEPARATOR INVOLVED IN INDEX OF AIR DETERMINATIONS

Experimental procedure in the evaluation of the index of refraction of air by the Fabry-Perot interferometric method necessitates the determination of order of interference between surfaces of interferometer plates in air and in vacuum.

$$\text{Refractive index of air, } n, = \frac{\text{number of waves in thickness } (t) \text{ of air}}{\text{number of waves in thickness } (t) \text{ of vacuum}}$$

The distance between these surfaces is fixed by a separator of material, such as brass, steel, invar, or fused quartz. It is evident from the above relationship that any change in length of the separator during observations will affect, directly, the determined index value. Such change in length will be caused by change in pressure from vacuum to air pressure. This compressibility effect was recognized by Meggers and Peters,[1] but for lack of reliable data, they made no corresponding corrections to their results. The required accuracy of index values determines the degree of accuracy to which this compressibility correction must be known.

2. REQUIRED ACCURACY OF INDEX DETERMINATIONS AND OF COMPRESSIBILITY CORRECTIONS

Correlation of length determinations made by interferometric methods in a vacuum with those at atmospheric pressure, at which

[1] W. F. Meggers and C. G. Peters, *Measurement of the refractive index of air for wave lengths from 2218 to 9000 A.* Bul. BS **14**, 723 (1918–1919) S327.

our standard wave length is defined, requires an exact knowledge of the ratio of wave lengths of radiations in vacuum to their wave lengths in air; i. e., of the refractive indices of air. Wave lengths of many secondary standard radiations which were determined by comparison with the wave length of the primary standard red radiation of cadmium at atmospheric pressure are in agreement to within 1 or 2 units in the eighth significant figure. To transfer these air values to vacuum values with equal certainty requires that $(n-1)$ be known to 1×10^{-8}. Such accurate index determinations have not been made—present uncertainties are in the seventh decimal place. An index error of 1×10^{-7} results in an error of 1 part per 10 million in vacuum wave lengths and consequently in lengths transferred to air values from vacuum measurements. To satisfy the demands of the metrologist, an accuracy of 1 part per 10 million, or 0.1μ per meter, should be attained.

Conversely, the atomic physicist demands a correspondingly accurate knowledge of the refractive index in the determination of optical dispersion for transference of his observations in air to basic vacuum values.

Measurement of indices with a certainty of 1×10^{-7} requires that the compressibility correction of the interferometer étalon be known to one-half this value, 5×10^{-8}.

3. MATERIALS FOR SEPARATORS

Change in length of separators may be caused (1) by a change in pressure or (2) by a change of temperature during observations. Change in length with pressure, or compressibility, is a definite property of a material and, for a known pressure change, no error in index determinations should arise from this source, provided that its compressibility correction be known to the required accuracy. Change in length with temperature depends upon the thermal expansivity of the separator material. Fused quartz with an expansivity of 5×10^{-7}, as contrasted with 120×10^{-7} for steel, is less affected by temperature change than other commonly used materials, with the exception of Invar. For the accuracy required in index determinations, error of length measurement should not exceed 0.005μ per decimeter of étalon, and this tolerance, in terms of temperature change, is equivalent to 0.1° C for fused quartz and 0.005° C for steel. Thus, the use of separators of low thermal expansivity eliminates the necessity for precision measurements of small differences in temperatures of 0.005° C. With these separators, errors in index determinations resulting from changes in length with the small temperature differences encountered under carefully controlled temperature conditions can be made negligible. End gages of fused quartz have been made (method to be described by C. G. Peters and E. L. Robinson in a future NBS publication) with such perfection of planeness and parallelism of end surfaces that, when used as separators in a Fabry-Perot interferometer, measurable interference over a path of 250 mm resulted. Such separators of various lengths have been used for recent index of air determinations at this Bureau.

138829—37——4

4. STATUS OF VALUES FOR COMPRESSIBILITY; PURPOSE OF THIS INVESTIGATION

Since change of index with pressure and compressibility are simultaneous effects under the conditions of measurement, the relative effect of each is not readily determinable. Very few data are available upon which to base this compressibility correction when using metals, practically none are available for fused quartz, and those which are available were determined for pressures of many atmospheres. Question arises as to the exactness of such values when extrapolated to pressures in the range of 0 to 1 atmosphere. Available data give the longitudinal compressibility of some steel specimens as 2.0×10^{-7}, and any error in this value is transferred directly as an error to index values. Since indices are required to 1×10^{-7}, the compressiblity corrections must be applied for steel separators and, likewise, for separators of fused quartz, which has a greater compressibility than that of steel.

Previous determinations of the compressibility of fused quartz proved disappointingly meager; consequently, this investigation was inaugurated with the hope that the compressibility of fused quartz might be determined with the accuracy of 5×10^{-8} required for index of air measurements.

II. METHODS FOR DETERMINING COMPRESSIBILITY

Determination of the compressibility of fused-quartz glass was made by interferometric comparison of the relative change in length with pressure of end gages of fused quartz and stainless steel. Values for the compressibility of both fused quartz and stainless steel were determined by a direct method which depends upon the relative change in length of a closed tube and a solid gage of the same material. Relative values for fused quartz and steel were also derived from comparative changes in length with pressure of a tube of either of these materials and a gage of the other material.

1. METHOD 1.—COMPARISON OF TWO GAGES OF UNLIKE MATERIALS

Published values for compressibility of steel at pressures from 2,000 to 12,000 atmospheres give a straight line ($P-\Delta V$) relationship.[3] The accepted value for volume compressibility of soft steel is 6.0×10^{-7} per megabar, which is equivalent to a longitudinal compressibility of 2.0×10^{-7} per atmosphere. For fused quartz (fused silica glass) Adams, Williamson, and Johnston found an increasing compressibility for decreasing pressure. Their extrapolated value for atmospheric pressure is equivalent to a longitudinal compressibility of 10.1×10^{-7} per atmosphere. The value for steel appears fairly well established, whereas that for fused quartz was considered somewhat questionable by its publishers.

By measuring the relative change in length with pressure of steel and fused quartz, and using the established value for steel, the com-

[3] Adams, Williamson, and Johnston, J. Am. Chem. Soc. 41, 12-42 (1919).

pressibility of fused quartz can be determined by sufficiently accurate measurements. For such determinations, two end gages of approximately equal length, one of fused quartz and the other of steel, were placed side by side in wringing contact with the plane surface of flat *B*, figure 1. The relative change in length of the gages from atmospheric to vacuum pressure was determined by the shift of fringes resulting from interference of light waves between the upper surfaces of the gages and the lower surface of interferometer plate *T*, which was supported by the longer gage and inclined at a slight angle to give straight fringes of optimum measurable width.

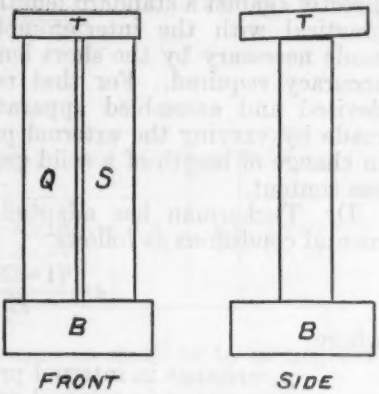

FIGURE 1.—*Assembly of plates and gages for comparison of the compressibility of fused quartz and steel.*

Using the measured length differences for a pressure change of 1 atmosphere and the accepted value for the longitudinal compressibility of steel, the longitudinal compressibility of fused quartz will be

$$C_Q = \frac{\Delta L}{L} + C_S$$

where

C_Q=coefficient of longitudinal compressibility of fused quartz.
C_S=coefficient of longitudinal compressibility of steel.
ΔL=measured relative change in length of the gages.
L=length of the gages.

Preliminary tests indicated that the most precise control of temperature conditions was necessary to attain the desired accuracy. Measurements by this method gave values of sufficient merit to verify the reliability of the method next described.

2. METHOD 2.—COMPARISON OF A CLOSED TUBE AND GAGE OF THE SAME MATERIAL

The interesting fact that the compression modulus is the only elastic constant of an isotropic material which affects the longitudinal strain of a long, closed circular cylinder under a difference of internal and external hydrostatic pressure was implicit in the equations given by Lamé [3] as early as 1852, but apparently Mallock [4] was the first to realize the possibility of using it to measure the compression modulus. Dr. L. B. Tuckerman, of this Bureau, called attention to this work and suggested that a modification of Mallock's method could be used to determine the change of length of either fused quartz or steel with changing pressure, directly. This eliminates the existing uncertainty as to the value computed for the compressibility of steel at atmospheric pressure by extrapolation from much higher pressures, and eliminates, also, the uncertainty resulting from comparison of materials with different thermal expansivities.

[3] G. Lamé, Leçons sur la Théorie mathématique de l'Élasticité des Corps solides, 2d ed., p. 188–190, Gauthier-Villars, Paris (1866).
[4] A. Mallock, *On a direct method of measuring the coefficient of volume elasticity of metals.* Proc. Roy. Soc. (London) 74, 50–52 (1904–05). See also footnote 5.

Since Mallock used atmospheric pressure outside his tubes and varied the internal pressure, he could measure the change of length directly against a standard length at constant pressure. This was not practical with the interferometric method here used, which was made necessary by the short lengths of the gages and tubes and the accuracy required. For that reason, C. G. Peters, of this Bureau, devised and assembled apparatus with which measurements were made by varying the external pressure and measuring the difference in change of length of a solid gage and a sealed tube with a constant gas content.

Dr. Tuckerman has adapted Lamé's equations to these experimental conditions as follows:

$$e=\frac{(1-2\sigma)}{E}\ \frac{(\rho^2 p_i-p_0)}{1-\rho^2} \tag{1}$$

where

p_i=change in internal pressure.
p_0=change in external pressure.
e=change in longitudinal strain.
ρ=ratio of internal to external diameter.
E=Young's modulus.
σ=Poisson's ratio.

The quantity $(1-2\sigma)/E$ is the longitudinal compressibility C, which, for isotropic materials, is $\frac{1}{3}k$, where k is the modulus of cubic compressibility. If the material exhibits transversely symmetrical anisotropy,[5] E and σ are the elastic constants pertaining to purely axial stress. That formula 1 applies to this case as well as to the isotropic case has been verified by Dr. Tuckerman from an extension of Lamé's theory.

If a small hole is bored in the cylinder, $p_i=p_0$ at all times. This gives for an isotropic material $e=-Cp_0=-Cp_i$, as it should be for uniform hydrostatic pressure. If the cylinder is filled with a fluid with a modulus of cubic compressibility k' and sealed and then maintained at a constant temperature

$$p_i=-\frac{k'\Delta V}{V}=\frac{1}{1-\rho^2}\frac{k'}{k}[\rho^2 p_i-p_0+A(p_i-p_0)] \tag{2}$$

$$A=\frac{2(1+\sigma)}{3(1-2\sigma)}$$

σ=Poisson's ratio.

V=volume of inclosed fluid.

Solving for p_i gives

$$p_i=\frac{\alpha}{1-(1-\alpha)\rho^2}p_0 \tag{3}$$

$$\text{where } \alpha=\frac{(1+A)\frac{k'}{k}}{1+A\frac{k'}{k}} \tag{3'}$$

[5] A. E. H. Love, The Mathematical Theory of Elasticity, 4th ed., p. 160-161. (Cambridge Univ. Press, 1927.)

Substituting for p_t in eq 1 gives

$$e=-C\frac{p_0}{1-(1-\alpha)\rho^2} \tag{4}$$

Approximate values are

	k	σ	A	α
Steel	1.5×10^{12}	0.3	2	2×10^{-6}
Fused quartz	3.5×10^{11}	.15	1	6×10^{-6}
Gas at atmospheric pressure	1.1×10^{6}			

From eq 3′, α with a gas filling becomes so small as to be negligible and for all practical purposes

$$e=-C\frac{p_0}{1-\rho^2} \tag{5}$$

for $\rho^2=0.5$, which is the condition of equal areas of horizontal sections of the hole and of the material of the tube

$$e=-2Cp_0$$

For this special case, the change in length with pressure will be twice that of a solid bar of the same material.

For a transversely anisotropic material, the expression for α, eq 3′, is different, but α is still negligible compared to 1; consequently, the result in eq 5 is the same.

These formulas are theoretically accurate only for a finite portion of an infinitely long cylinder. If, however, the end closure of the cylinder is made very rigid, the end effects can be neglected.

For making the measurements a fused-quartz tube was wrung to base plate B, figure 2. Interferometer plate T was wrung to the top of the tube, thereby closing it. A solid fused-quartz gage was wrung on B, beside the tube. A slight slope to the ends of the latter gave proper width to the fringes between T and the gage. Measurements were made of the shifts of the fringes on the gage relative to a reference mark on T.

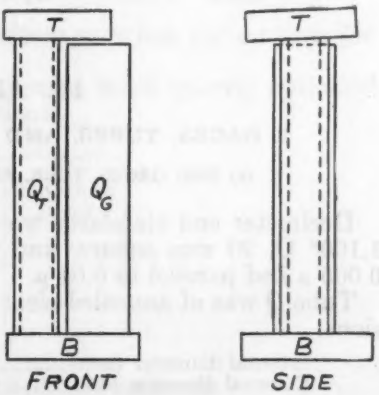

FIGURE 2.—*Assembly of fused-quartz tube and plates.*

There was no noticeable distortion of the fringes during the shift. This showed that the end plates were sufficiently rigid and the end effects could safely be neglected.

For a tube and gage of equal length, of identical material, and maintained at constant temperature, the coefficient of longitudinal compressibility for a change of external pressure of 1 atmosphere is

$$C_Q=\frac{\Delta L}{L\left[\frac{1}{1-\rho^2}-1\right]}$$

In a similar way the longitudinal compressibility of the steel gage and tube was determined.

3. METHOD 3.—COMPARISON OF A TUBE AND GAGE OF UNLIKE MATERIALS

For a closed tube the change in length with pressure is $1/(1-\rho^2)$ times that of a solid gage, with no corresponding increase in uncertainties of measurements of length or temperature. Consequently, by comparing the change in length of a tube of a material with unknown compressibility and a gage of another material of known compressibility, the derived compressibility of the former should be more accurate than values determined by method 1.

For a fused-quartz tube and a steel gage of equal length, maintained at constant temperature, the coefficient of longitudinal compressibility for a pressure change of 1 atmosphere will be

$$C_Q=\frac{\Delta L+C_sL}{\left(\frac{1}{1-\rho^2}\right)L}$$

By the use of a steel tube and a fused-quartz gage and, by using the value of C_Q found by method 3, the longitudinal compressibility of steel will be

$$C_s=\frac{C_QL-\Delta L}{\left(\frac{1}{1-\rho^2}\right)L}$$

III. APPARATUS

1. GAGES, TUBES, AND INTERFEROMETER PLATES

(a) END GAGES, TUBE, AND PLATES OF FUSED QUARTZ

Decimeter end standards were of clear fused quartz, annealed at 1,100° C, 20 mm square, and with end surfaces polished plane to 0.005 μ and parallel to 0.01 μ.

Tube Q was of annealed clear fused quartz of the following dimensions:

Internal diameter (mm)	10.848
External diameter (mm)	15.454
ρ^2	0.4927
Average length at 20° C (mm)	100.43
Slope (mm)	0.002

Its length was made slightly greater than 100 mm to permit wringing and substitution of gages beside it. The ends of the tube were polished plane, with no indications of rounding at the edges.

End plates for the tube were of annealed fused quartz, optically polished plane to 0.01 μ and of dimensions:

Plate	Diameter (mm)	Thickness (mm)
B	46	10
T	38	10

(b) END GAGES AND TUBE OF STEEL; PLATES OF FUSED QUARTZ

In addition to two steel decimeter Johansson gage blocks, stainless-steel end gages 20 mm square and 100.0000 mm long at 20° C were available. The following are known properties of this steel:

Analysis (%)---------- 0.32 C; 0.28 Mn; 0.02 P; 0.03 S; 0.35 Si; 0.03 Cu; 0.07 Ni; and 13.9 Cr.
Heat treatment---------- Heated to 950° C, quenched in oil, and drawn at 600° C.
Scleroscope hardness---------- 55.
Coefficient of thermal expansion--- 10.2×10^{-6}.

End surfaces of the gages were fine-lapped plane and parallel to 0.02 μ. Faintly perceptible lap marks were partially removed by polishing lightly with rouge. A 1-mm hole, drilled perpendicularly from a side to the center of a gage, permitted insertion of a thermocouple junction.

A tube of identical material and with the same heat-treatment was made to dimensions:

Internal diameter (mm)----------	15.8750
External diameter (mm)----------	22.4506
ρ^3----------	0.5000
Average length at 20° C (mm)----------	100.17824
Slope (mm)----------	0.002

The planeness and polish of its end surfaces were less perfect than for the quartz-glass tube.

End plates for this tube were of annealed fused quartz, optically polished plane to 0.01 μ and of dimensions:

Plate	Diameter (mm)	Thickness (mm)
B	57	21
T	40	10

2. TEMPERATURE-CONTROL APPARATUS

The temperature-control apparatus was that used by Souder and Peters.[6] Their constant-temperature chamber, however, was replaced

[6] *An investigation of the physical properties of dental materials.* Dental Cosmos, p. 9 (March 1920).

with a brass container 270 mm long, 67 mm in diameter, and of 1 mm thickness. Figure 3 shows this chamber with the gages in position for measurement. *W* is a plane-parallel glass window sealed in place with wax. A survey of the stirred, thermostated bath surrounding the chamber showed no temperature variation greater than 0.01° C with careful adjustment of heating and cooling. Temperature of the bath was measured by means of an exceptionally rapid standard mercury thermometer of 0 to 30° C range, subdivided into 0.1° C intervals. The rulings on this thermometer were narrow and well defined. With the temperature of the bath so adjusted that the top of the mercury column was in line with a ruling, a change of 0.005° C could be detected when viewed telescopically. An increase of room temperature of 2° C above that of the bath raised the temperature within the chamber 0.01° C. This increase remained constant so long as the relative difference between the bath and room was maintained. Temperature differences between bath and chamber were measured with a single-junction copper-constantan thermocouple, one junction of which was against the thermometer bulb, while the other was either placed against the side of a quartz-glass gage or inserted to the center of a steel gage. Potential differences were measured by means of a potentiometer-galvanometer combination with a sensitivity of 2.4 mm per microvolt.

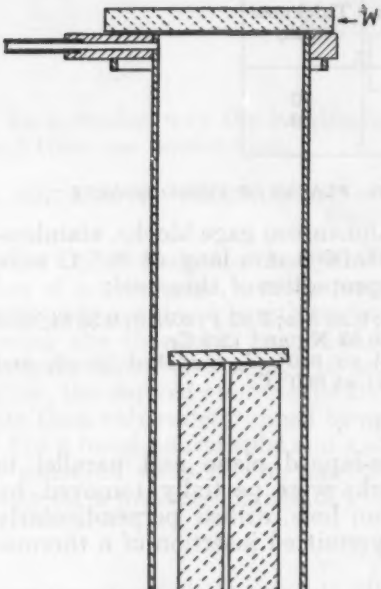

FIGURE 3.—*Constant-temperature chamber, with gages in position for measurement.*

3. AIR PUMP

By the use of a rotary air pump, pressure within the chamber was held below 0.5 mm, as indicated by a vacuum discharge tube.

4. INTERFEROMETRIC MEASURING APPARATUS

Relative changes and differences in length of tubes and gages were measured with a Pulfrich [7] viewing instrument. A helium lamp incorporated within the Pulfrich served as a source of illumination and a direct-vision prism within the instrument separated the fringe patterns due to helium radiations of different wave lengths. For measurement of fringe shifts, the yellow radiation only was used; for measurement of length differences of tubes and gages, the following radiations were used:

[7] Pulfrich, Z. Instrumentenk. 18, 261 (1898).

Radiation	Wave length (A)
Red	6678.149
Yellow	5875.618
Green	5015.675
Blue	4471.477

IV. EXPERIMENTAL PROCEDURE AND RESULTS

1. PRELIMINARY MEASUREMENTS

(a) COMPARISON OF TWO FUSED-QUARTZ GAGES

Preliminary comparisons were made with fused-quartz decimeter end gages 3 and 6 wrung side by side on a fused-quartz flat.[8] An interferometer plate of the same material formed a wedge with the top surfaces of the gages to give straight fringes of 2 mm width across the gage surfaces. The gages were placed within the chamber, controlled at 20° C, which was then sealed and evacuated. After the fringes had become stationary, readings were taken by means of the Pulfrich of the position of a fringe on gage 6 relative to an opposite one on gage 3. Air was then admitted and the magnitude and direction of the fringe shift were noted. This procedure was repeated for fringes located at various places on the gages. Results gave no difference in compressibility greater than 3.5×10^{-8} and gave a mean difference for the two quartz gages of zero. Table 1 summarizes the results of the determinations.

TABLE 1.—*Comparison of the compressibility of two fused-quartz gages*

Reference fringe number	Relative change in length of gages 6 and 3		Equivalent difference in longitudinal compressibility	Direction of pressure change
	Fringe	*μ*		
1	+0.012	+0.0035	$+3.5\times10^{-8}$	Vacuum to air.
2	−.008	−.0023	−2.3	Vacuum to air.
3	+.008	+.0023	+2.3	Vacuum to air.
4	−.010	−.0029	−2.9	Air to vacuum.
4	−.002	−.0006	−0.6	Vacuum to air.

Mean difference in compressibility of gages 3 and 6=0.0×10^{-8}.

[8] The method of wringing was, first, to clean the surfaces with alcohol and absorbent cotton. Next, the surfaces were covered with a thin film of grease by thoroughly rubbing with a cloth freshly impregnated with petroleum jelly. This film was reduced in thickness by vigorous rubbing and polishing with clean cotton until no trace of film was visible by reflected light. That edge of the gage to be measured was next brought gently into contact with the plate and the gage then allowed to grip in its desired position. Contact was indicated by a black appearance at the edge of the gage which gradually spread over its entire surface, provided the surfaces were thoroughly clean except for the minute film of grease. Rubbing had a tendency to attract small floating particles from the air to the surface. The presence of these was detected by the resulting colored or grayish appearance around the particles in the field of black contact. If particles were found to be present, the surfaces had to be separated and the process of wringing was then repeated until adherence was satisfactory. The separation is successfully effected by several hours immersion in water. It is believed, by this method of wringing surfaces of the perfection of those used, that the force of adherence was greater than 200 lb/in². Experience over a period of years in the comparison of standard end gages indicates that the separation was less than 0.005μ. Separations of this magnitude were found by other observers. (See F. H. Rolt, *Gages and fine measurements* 1, 164, 1929.)

(b) COMPARISON OF A FUSED-QUARTZ GAGE WITH STEEL GAGES

In the same manner, a fused-quartz gage was compared with a stainless-steel decimeter gage and with two Johansson decimeter steel gage blocks. Initial determinations gave consistent results of somewhat greater magnitude than expected. These observations were made from 5 to 15 minutes after a change of pressure, when the fringe position appeared constant. This apparent constancy was misleading, however, for readings delayed an hour gave less shift for the same change of pressure. This was ascribed to a change in temperature of the gages.

(c) EFFECT OF CHANGE OF PRESSURE UPON TEMPERATURES WITHIN THE CHAMBER

Temperature measurements with differential thermocouples between the water bath and the center of the chamber and the center of the stainless-steel gage indicated that a change of pressure of 1 atmosphere caused measured changes of 25° C within the chamber. The change as measured was less than the actual initial effect owing to the lag of couple and galvanometer and to a rapid transfer of heat to the surroundings. Twenty minutes were required for the temperature of the air within the chamber and for the bath to attain an approximate equalization of 0.01° C. In the meantime, the temperature of the steel gage was appreciably affected. After 9 minutes the temperature of the gage differed from that of the bath by 0.10° C. The maximum difference was estimated to be 0.14° C.

(d) COOLING CURVES OF STEEL GAGES

To investigate further the thermal relations between bath and gage under the conditions of measurement, cooling curves were taken for:

1. A steel gage wrung to a fused-quartz base plate (in air).
2. A steel gage wrung to a fused-quartz base plate (in vacuum).
3. A steel gage with a fused-quartz gage beside it (in air).
4. A steel gage with a fused-quartz gage beside it (in vacuum).

Rate of cooling was determined by temperature measurements with a thermocouple between the bath and the center of the steel gage at intervals from the time they were equal at an initial temperature until they were again equal after lowering the bath 1° C. Variation in the time required to control the bath at the lower temperature confused early measurements; consequently, the curves (fig. 4) are given for a 0.75° C change, for which temperature difference thermal equilibrium had become established. Table 2 gives approximate values taken from the curves, supplemented by end values obtained during actual compressibility determinations.

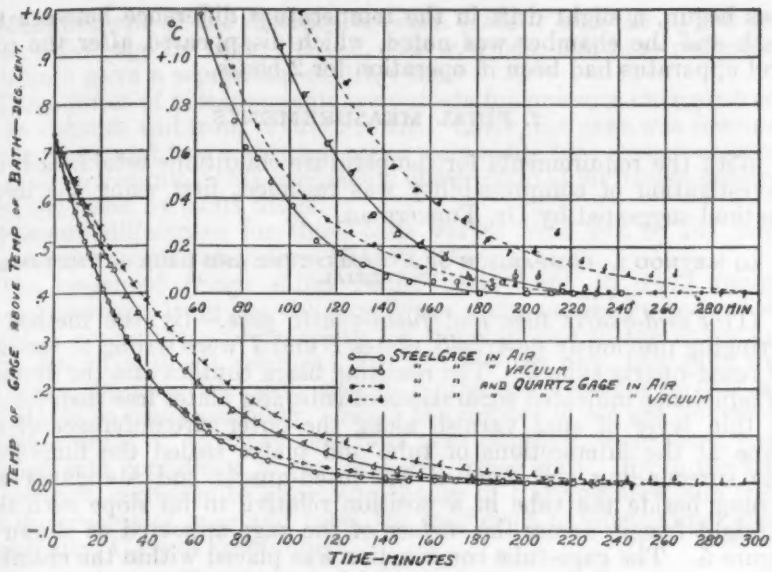

FIGURE 4.—*Cooling curves of a steel gage.*

TABLE 2.—*Time required for cooling a steel gage*

Difference in temperature of bath and gage (temperature of bath greater than temperature of gage)			Approximate time required for change			
			Steel gage alone in—		Steel and quartz gages side by side in—	
Difference		Total change	Air	Vacuum	Air	Vacuum
Initial	Final					
°C	°C	°C	min	min	min	min
0.75	0.20	0.55	45	65	45	75
.20	.02	.18	70	90	90	115
.02	±.005	.02±0.005	65	70	75	75
Total time to change from Δ=0.75° to Δ=±0.005°			180	225	210	265
Total time to change from Δ=0.20° to Δ=±0.005°			135	160	165	190

For the conditions of the compressibility experiments in which the change in temperature of the gage was 0.14° C, measurements for the steel-fused quartz combination should be delayed at least 2½ hours for air and 3 hours for vacuum after a change of pressure.

(c) TIME REQUIRED TO ESTABLISH THERMAL EQUILIBRIUM WITHIN THE CONSTANT-TEMPERATURE CHAMBER

Another effect investigated was the time required to establish thermal equilibrium within the constant-temperature chamber itself. In practice, the desired temperature was often 2 or 3° different from the overnight temperature of the apparatus. After control

was begun, a slight drift in the temperature difference between the bath and the chamber was noted, which disappeared after the control apparatus had been in operation for 2 hours.

2. FINAL MEASUREMENTS

With the requirements for temperature conditions established, the investigation of compressibility was resumed, first using the direct method suggested by Dr. Tuckerman.

(a) METHOD 2.—COMPARISON OF A CLOSED TUBE AND GAGE OF THE SAME MATERIAL

(1) *Fused-quartz tube and fused-quartz gage.*—By the method of wringing previously described, plates B and T were wrung to the ends of fused-quartz tube Q. The resulting black contact and the firmness of adherence indicated separations of tube and plates less than 0.005μ. A thin layer of spar varnish along the outer circumference of the tube at the intersections of tube and plates sealed the films from the surrounding air. One of the fused-quartz end standards was wrung beside the tube in a position relative to its slope such that straight fringes across the surface of the gage appeared as shown in figure 5. The gage-tube combination was placed within the chamber, which was controlled at the temperature found in the morning. Window W was sealed to the top of the chamber. A stopcock in the line to the pump was opened to the room.

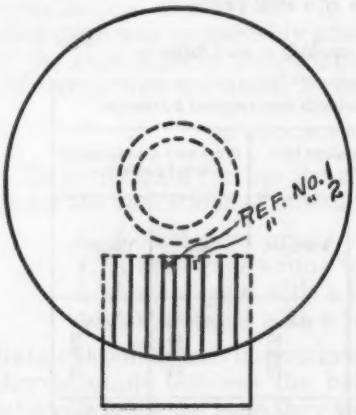

FIGURE 5.—*Appearance of the fringes and position of reference marks for the gage-tube combination.*

After temperature equilibrium had become established, in all cases at least 2 hours later, the position of a definite fringe of helium yellow was measured relative to a reference mark on plate T, by means of the Pulfrich. Usually 8 to 10 individual measurements were made for each position of a fringe. The maximum variation from the mean was 0.005 fringe. (This exactness of setting was due to the high degree of planeness of surfaces and to the tendency of an observer to establish a definite, repeatable criterion for the center of gravity of a fringe.) Barometric pressure and bath temperature were recorded.

Upon completion of these measurements, the stopcock was closed to the air; the pump was started and continued in operation until all measurements in vacuo were completed. The direction of fringe shift was noted. The vacuum discharge tube indicated a pressure less than 0.5 mm. Since the materials in this case were identical and of low thermal expansivity, little time was required to reach a stable condition. Readings made 30 to 210 minutes after a change of pressure gave no differences ascribable to temperature. In several instances, air was again admitted to the chamber and remeasurement of the fringe position was made.

Measurement of the distance between plate T and the upper surface of the gage by using the red, yellow, green, and blue radiations of helium gave a separation of 0.434 mm.

Three series of measurements were made for pressure changes from air to vacuum and from vacuum to air. Later, the gage was rewrung to the plate, and two additional series were made for pressure changes from air to vacuum. Measurements of two individual fringes differed from the mean by 0.003 fringe.

Pressure differences for these tests varied from 742 to 761 mm; gage temperatures varied from 20 to 24° C.

The measured fringe shifts varied from 0.065 to 0.077 fringe. These, however, were not the true fringe shifts caused by compressibility; a correction was necessary for the shift due to the change of wave length with air density. For a 0.434-mm gap, this shift was six times the measured shift and in a direction opposite to that attributable to compressibility. Since the indices of air are known to a higher order of accuracy than was here required, corrections were applied with confidence to the measured fringe shift. From the true fringe shift, corrected to a pressure change of 1 atmosphere, and from the dimensions of gage and tube, the coefficient of longitudinal compressibility, C_q, was determined.

$$\text{True shift}=\Delta_q=\left(\frac{p_0}{1-\rho^2}\right)C_qL_T-p_0L_gC_q$$

For $p_0=1$ atmosphere, and $\rho^2=0.4927$

$$C_q=\frac{\Delta}{1.9713L_T-L_g}$$

where $\Delta=$true shift for a pressure change of 1 atmosphere.

Table 3 gives a summary of the measurements of the compressibility of quartz by this method. Extreme values were $C_q=9.7\times10^{-7}$ to $C_q=10.1^{-7}$ with a mean value $C_q=9.9\times10^{-7}$ per atmosphere.

TABLE 3.—*Compressibility determinations using a tube and gage of the same material*

ΔP=measured p_0. $\Delta L(\tau,a)$=measured difference in length, $L\tau$, of tube and length, La, of gage. $\Delta\lambda$=change in wave length with pressure.

Temperature	ΔP	Measured shift		$\Delta L(\tau,a)$	Index at measured temperature and pressure	Order in vacuum (for λ=5877.243 A)	Shift resulting from $\Delta\lambda$	Total relative change in length of tube and gage at measured temperature					Coefficient of longitudinal compressibility	Time elapsed before observations were made
								For ΔP	For 760 mm					
		Air-vacuum	Vacuum-air					Air-vacuum and vacuum-air	Air-vacuum and vacuum-air	Air-vacuum	Vacuum-air	True shift (Δ)		
								FUSED-QUARTZ TUBE AND FUSED-QUARTZ GAGE						
°C	mm	*Fringe*	*Fringe*	μ	$(n-1)\times 10^7$		*Fringe*	*Fringe*	*Fringe*	μ	μ	μ		
23.0	742.7	------	0.065	434.96	2631	1480.2	0.389	0.324	0.332	------	0.0975	------	------	(Temperature constant 180 minutes before first observation.)
		0.068	------					.321	.328	0.0964	------	------	------	60 minutes after vacuum observation—temperature constant.
		------	.065					.324	.332	------	.0975	------	------	60 minutes after air observation—temperature constant.
														70 minutes after vacuum observation—temperature constant.
Mean	------	------	------	------	------	------	------	------	------	0.0964	0.0975	0.0970	9.90×10^{-7}	
24.1	751.3	0.071	------	433.79	2651	1476.2	0.391	0.320	0.324	0.0952	------	------	------	(120 minutes before first observation.)
		------	0.071					.320	.324	------	0.0952	------	------	60 minutes after air observation.
		.073	------					.318	.322	.0946	------	------	------	60 minutes after vacuum observation.
		------	.073					.318	.322	------	.0946	------	------	30 minutes after air observation.
														30 minutes after vacuum observation.
Mean	------	------	------	------	------	------	------	------	------	0.0949	0.0949	0.0949	9.69	
								Rewrung Quartz Gage						
22.0	761.2	0.065	------	434.96	2705	1480.2	0.400	0.335	0.334	0.0981	------	------	------	(120 minutes before first observation; 60 minutes after air observation; 60 minutes after vacuum observation.
		------	0.064					.336	.335	------	0.0984	------	------	
Mean	------	------	------	------	------	------	------	------	------	0.0981	0.0984	0.0983	10.03	

Rewrung Quartz Gage

20.0	743.0	[a]0.067 [b].064	------ ------	435.0− 435.0+	2659	1480.2	0.394	0.327 .330	0.334 .338	0.0981 .0993	------ ------	------ ------	------ ------	210 minutes before first observation; 210 minutes after air observation.
Mean	------	------	------	------	------	------	------	------	------	0.0987	------	0.0987	10.07	
20.0	751.9	[a]0.077 [b].072	------ ------	435.0− 435.0+	2691	1480.2	0.398	0.321 .326	0.324 .330	0.0952 .0970	------ ------	------ ------	------ ------	130 minutes before first observation; 80 minutes after air observation.
Mean	------	------	------	------	------	------	------	------	------	0.0961	------	0.0961	9.81	
Mean	------	------	------	------	------	------	------	------	------	------	------	------	$C_Q=9.9\times10^{-7}$	

STEEL TUBE AND STEEL GAGE

23.55	758.2	------ 0.053 ------ .054	0.063 ------ .052 ------	178.21	2681	606.4	0.163	0.100 .110 .111 .109	0.100 .110 .111 .109	------ 0.0323 ------ .0320	0.0294 ------ .0326 ------	------ ------ ------ ------	------ ------ ------ ------	70 minutes after vacuum observation—until Δr is constant. 67 minutes after air observation—until Δr is constant. 53 minutes after vacuum observation—until Δr is constant. 35 minutes after air observation—until Δr is constant.
Mean	------	------	------	------	------	------	------	------	------	0.0322	0.0310	0.0316	3.15×10^{-7}	
22.6	761.5	------ 0.049 ------ .047	0.064 ------ .057 ------ .052	178.21	2701	606.4	.164	0.100 .115 .107 .117 .112	0.100 .115 .107 .117 .112	------ 0.0338 ------ .0344 ------	0.0294 ------ .0314 ------ .0329	------ ------ ------ ------ ------	------ ------ ------ ------ ------	70 minutes after vacuum observation—until Δr is constant. 70 minutes after air observation—until Δr is constant. 60 minutes after vacuum observation—until Δr is constant. 65 minutes after air observation—until Δr is constant. 70 minutes after vacuum observation—until Δr is constant.
Mean	------	------	------	------	------	------	------	------	------	0.0341	0.0312	0.0327	3.26	

See footnotes at end of table.

TABLE 3.—*Compressibility determinations using a tube and gage of the same material*—Continued

Temperature	ΔP	Measured shift: Air-vacuum	Measured shift: Vacuum-air	$\Delta L(\tau,\sigma)$	Index at measured temperature and pressure	Order in vacuum (for λ=5877.243 A)	Shift resulting from $\Delta\lambda$	Total relative change in length of tube and gage at measured temperature: For ΔP: Air-vacuum and vacuum-air	For 760 mm: Air-vacuum and vacuum-air	For 760 mm: Air-vacuum	For 760 mm: Vacuum-air	For 760 mm: True shift (Δ)	Coefficient of longitudinal compressibility	Time elapsed before observations were made
						Rewrung Steel Gage								
°C	mm	*Fringe*	*Fringe*	μ	$(n=1)\times 10^7$		*Fringe*	*Fringe*	*Fringe*	μ	μ	μ		
20.0	747.5	[a] 0.073 [d] .071	-------	178.24	2675	606.5	0.162	0.089 .091	0.091 .093	0.0267 .0273	-------	-------	-------	$\Delta\tau$ constant 130 minutes before first observation; $\Delta\tau$ constant 130 minutes after air observation.
Mean	-------	-------	-------	-------	-------	-------	-------	-------	-------	0.0270	-------	0.0270	2.69	
19.4	747.2	[a] 0.050 [d] .054	-------	178.24	2679	606.5	0.163	0.113 .109	0.115 .111	0.0338 .0326	-------	-------	-------	$\Delta\tau$ constant 180 minutes before first observation; $\Delta\tau$ constant 160 minutes after air observation.
Mean	-------	-------	-------	-------	-------	-------	-------	-------	-------	0.0332	-------	0.0332	3.31	
Mean	-------	-------	-------	-------	-------	-------	-------	-------	-------	-------	-------	-------	$C_3=3.1\times10^{-7}$	

[a]=measured shift of first fringe. [b]=measured shift of second fringe. [c]=measured shift from first reference mark. [d]=measured shift from second reference mark.

(2) *Steel tube and steel gage.*—Plates B and T were wrung to the ends of the steel tube previously described. In this case the black contact did not extend to the outer circumference of the tube. This was attributed to a lack of sufficient planeness and polish of the ends of the tube. A slight "rounding off" at its edges was observed. In sealing the separations between surfaces, the spar varnish had a tendency to creep between the tube and the plates. The effect of this will be discussed later. Steel end gage 2 was wrung beside the tube on plate B.

One junction of a copper-constantan thermocouple was inserted in the hole of the gage in contact with the metal at its center; the other junction was in contact with the bulb of the bath thermometer.

Two series of observations were made with an initial wringing of gage 2 for air-vacuum and vacuum-air pressure changes after thermocouple measurements indicated that bath and gage temperatures were constant. The fringe shifts from vacuum to air were greater than those from air to vacuum by 0.004 and 0.010 fringe, respectively, for the two series. Since the temperature of the tube and of the gage may not have become equalized during the short intervals of 35 to 70 minutes between change-overs, the mean value for the two conditions was used. Later, with a rewringing of gage 2, two series of observations were made for air-vacuum pressure changes with delays of 130 and 160 minutes between readings. Fringe shifts were measured relative to two reference marks.

The measured separation of gage and plate was 0.1782 mm. For this separation, the correction attributable to the change of wave length with air density was three times the measured shift and opposite in direction to the compressibility shift.

For this steel tube-gage combination, the coefficient of longitudinal compressibility for $p_0=1$ atmosphere and $\rho^2=0.5$ was

$$C_S=\frac{\Delta}{2L_T-L_G}$$

Measurements and results for these determinations are given in table 3. The value $C_S=2.7\times10^{-7}$ appears somewhat at variance with those of other series. At the time of measurement, series 3 and 4 were considered equally good; consequently, it must be included, thus giving a maximum spread from the mean value of 0.4×10^{-7}.

The mean of all series was

$$C_S=3.1\times10^{-7} \text{ per atmosphere}$$

(b) METHOD 3.—COMPARISON OF A TUBE AND GAGE OF UNLIKE MATERIALS

(1) *Fused-quartz tube and steel gage.*—Steel gage 2 was next wrung beside the fused-quartz tube. Two series of comparative compressibility determinations were made; the first included vacuum-air and air-vacuum changes; the second was for vacuum-air only. In each series sufficient time was allowed before and after the change-over for thermal conditions to become constant.

The coefficient of longitudinal compressibility of quartz glass was derived from the equation

$$C_Q=\frac{\Delta+L_GC_S}{1.9713L_T}$$

Measurements and results are given in table 4. Using value $C_S=3.1\times10^{-7}$ found by method 2, values for C_Q were 10.2×10^{-7} and 10.0×10^{-7} for the two series or a mean value

$$C_Q=10.1\times10^{-7} \text{ per atmosphere}$$

By substitution of $C_Q=9.9\times10^{-7}$ as found by method 2, in the equation

$$C_S=\frac{1.9713L_TC_Q-\Delta}{L_G},$$

the mean value of the coefficient of steel required by these measurements was

$$C_S=2.7\times10^{-7} \text{ per atmosphere}$$

It must be appreciated that this latter substitution is not particularly desirable. The change in length of the tube with pressure is twice that of a solid gage, whereas the uncertainties attributable to temperature and fringe measurements remain the same for tube and gage. Furthermore, any error in the coefficient of compressibility of the tube results in double that error for the determined coefficient of the gage.

TABLE 4.—*Compressibility determinations using a tube and gage of unlike materials*

Temperature	ΔP	Measured shift: Air-vacuum	Measured shift: Vacuum-air	ΔL_{TG}	Index at measured temperature and pressure	Order in vacuum (for λ = 5877.243 A)	Shift resulting from $\Delta\lambda$	Total relative change in length of tube and gage at measured temperature: For ΔP: Air-vacuum and vacuum-air	For 760 mm: Air-vacuum and vacuum-air	For 760 mm: Air vacuum-	For 760 mm: Vacuum-air	For 760 mm: True shift (Δ)	Coefficient of longitudinal compressibility: Tube vs. gage	Coefficient of longitudinal compressibility: Gage vs. tube (Note: errors > by this method)	Time elapsed before observations were made
FUSED-QUARTZ TUBE AND STEEL GAGE															
°C	mm	*Fringe*	*Fringe*	μ	$(n-1)\times10^7$		*Fringe*	*Fringe*	*Fringe*	μ	μ	μ	(Use $C_S=3.1\times10^{-7}$)	(Use $C_Q=9.9\times10^{-7}$)	
22.9	760.7	{------ 0.183	0.186 ------	}431.79	2695	1469.4	0.396	{0.582 .579	0.581 .578	------ 0.1701	0.1707 ------	}0.1704	10.17×10^{-7}	2.56×10^{-7}	130 minutes before first vacuum observation; 190 minutes before air observation; 120 minutes before second vacuum observation.
23.0	760.3	------	.174	431.69	2693	1469.0	.396	.570	.570	------	.1675	.1675	10.03	2.85	230 minutes before vacuum observation; 190 minutes before air observation.
Mean	------	------	------	------	------	------	------	------	------	------	------	------	$C_Q=10.1\times10^{-7}$	$C_S=2.7\times10^{-7}$	
STEEL TUBE AND FUSED-QUARTZ GAGE															
													(Use $C_Q=9.9\times10^{-7}$)	(Use $C_S=3.1\times10^{-7}$)	
25.0	754.1	{0.285 ------	------ 0.333	}182.43	2653	620.8	0.165	{0.120 .168	0.121 .169	0.0355 ------	------ 0.0496	}0.0426	2.82×10^{-7}	10.47×10^{-7}	160 minutes before first air observation; 170 minutes before vacuum observation; 110 minutes before second air observation.
23.0	751.3	{.250 ------	------ .318	}180.49	2661	614.2	.163	{.087 .155	.088 .157	.0259 ------	------ .0461	}.0360	3.14	9.81	150 minutes before first air observation; 170 minutes before vacuum observation; 130 minutes before second air observation.
23.5	744.0	.280	------	180.98	2631	615.9	.162	.118	.121	.0355	------	.035	3.17	9.76	240 minutes before air observation; 180 minutes before vacuum observation.
Mean	------	------	------	------	------	------	------	------	------	------	------	------	$C_S=3.0\times10^{-7}$	$C_Q=10.0\times10^{-7}$	

(2) *Steel tube and fused-quartz gage.*—Three series of measurements were made with a fused-quartz gage wrung beside the steel tube. Observations were made in two series for vacuum-air and air-vacuum pressure changes. Fringe shifts for the two conditions differed by 0.048 and 0.068 fringe, respectively. In view of the fact that no difference for these two conditions had been observed previously, it was believed that sufficient time had not elapsed before measurements were made. Temperature measurements were made at the surface of the gage. Since the elapsed time was about the same for the two conditions, their mean value would approximate the true value. In the third series, for which an air-vacuum change only was made, the calorimeter was regulated 240 minutes before initial readings were taken; 180 minutes elapsed after the pressure change before final measurements were made. The result differed from the mean of the first two series by 0.013 fringe.

By substitution of $C_q=9.9\times10^{-7}$ (the value determined by method 2), values for the coefficient of longitudinal compressibility for steel were derived from:

$$C_s=\frac{L_qC_q-\Delta}{2L_T}$$

Measurements and results are given in table 4. The derived values varied from 2.8×10^{-7} to 3.2×10^{-7} with a mean value

$$C_s=3.0\times10^{-7} \text{ per atmosphere}$$

By the less accurate method of derivation of the compressibility of the gage from an assumed compressibility of the tube, and by substituting $C_s=3.1\times10^{-7}$ in the equation:

$$C_q=\frac{\Delta+2L_TC_s}{L_q}$$

the derived mean value of C_q was

$$C_q=10.0\times10^{-7} \text{ per atmosphere}$$

(c) METHOD 1.—COMPARISON OF TWO GAGES OF UNLIKE MATERIALS

To verify the relative results for fused quartz and steel which were determined by the closed-tube methods, final comparative determinations were made with gages of fused quartz and steel wrung, side by side, on a fused-quartz plate.

Black contact resulted from the wringing of the fused-quartz standard with a correspondingly great adherence. The adherence of the steel gage with its lapped and slightly polished surface was appreciably less. One junction of the thermocouple was in contact with the metal at the center of the steel gage; the other junction was in contact with the bulb of the bath thermometer. The wedge between the surfaces of the gages and the interferometer plate was produced by a cotton fiber as a separator. It was found, however, that change of pressure caused a slight tilting of the plate which affected the fringe position. To overcome this difficulty, two pieces of gold leaf 1.5 mm square were placed in adjacent corners of the quartz-glass gage and pressed between the surfaces of the gage and

plate to give the required fringe width. A slight shift of the fringes with pressure was noted, which did not affect the relative measurement of the fringes, however, since no tilting of the fringes was detected. Room temperature was held constant throughout a series of observations. Readings were delayed until the temperature difference between bath and gage had remained constant for 2 hours. Actual procedure was as follows:

The chamber was evacuated at 8:30 a.m. and brought to the required temperature. Differential temperature measurements were begun at 10:10 a.m. and continued until fringe measurements were made at 12:50 p.m. Air was admitted to the chamber at 1:00 p.m., which resulted in a slight increase in the temperature of the gage. To hasten equilibrium, the temperature of the bath was reduced 0.1° C for 20 minutes. Couple readings were begun at 1:30 p.m. and continued until fringe measurements and barometric readings were recorded at 3:40 p.m. Table 5 shows the constancy of the thermal conditions.

TABLE 5.—*Relative temperature of bath and gage for determination of* $C_Q - C_S$

Temperature differences at intervals before observations were made			
Before vacuum observations		Before air observations	
Time	Gage temp. above bath temp.	Time	Gage temp. above bath temp.
	°C		°C
10:10 a.m.	+0.005	1:00 p.m.[b]	
20	.013	30	+0.038
30	.013	40	.030
40	.015	50	.025
50	.020		
		2:00 p.m.	.030
11:00 a.m.	.025	10	.030
10	.030	20	.030
20	.030	30	.025
30	.025	40	.025
40	.025	50	.025
50	.022		
		3:00 p.m.	.030
12:00 noon	.020	10	.025
10 p.m.	.020	20	.025
20	.022	30	.030
30	.025	40 to 4 p.m.[c]	.025
40	.025		
50 to 1 p.m.[a]	.025		

[a] Readings made for vacuum.
[b] Air admitted and temperature of bath lowered 0.1° C for 20 minutes.
[c] Readings made for air.

Four series of measurements were made for pressure changes from air to vacuum and one series for a change from vacuum to air. Measurements were made on two adjacent fringes on the steel relative to two opposite fringes on the fused quartz. Differences between measurements of the two fringes were negligible, except for one series in which a difference of 0.038 fringe indicated that the observer may have changed his criterion for estimating the center of the fringe. In this case the mean value was used. Correction to fringe shift because of change of wave length with air density was negligible for the small difference in length of the gages.

Determinations (see table 6) for the five series varied from $C_Q - C_S = 5.6 \times 10^{-7}$ to 7.3×10^{-7}. The mean difference was

$$C_Q - C_S = 6.6 \times 10^{-7}$$

Value $C_Q - C_S = 5.6 \times 10^{-7}$ for series 4 appears somewhat out of line with the other determinations. This low value could have resulted either from a slight tilting of the fringes, which escaped detection, or from an increase of the gage temperature of 0.01° C. Omission of this result would increase the mean value to $C_Q - C_S = 6.9 \times 10^{-7}$.

These measured differences of the coefficients of compressibility agree favorably with the difference $C_Q - C_S = 9.9 \times 10^{-7} - 3.1 \times 10^{-7} = 6.8 \times 10^{-7}$, which was derived from direct compressibility determinations.

TABLE 6.—*Measured differences in compressibility of fused-quartz and steel gages*

Temperature	ΔP	Measured shift		$\Delta L_{(g,s)}$[a]	Index at measured temperature and pressure	Order in vacuum (for λ = 5877.243 A)	Shift resulting from $\Delta\lambda$	Total relative change in length of gages at measured temperature				Difference of coefficients $C_q - C_s$	Time elapsed before observations were made
								For ΔP	For 760 mm				
		Air-vacuum	Vacuum-air					Air-vacuum and vacuum-air	Air-vacuum and vacuum-air	Air-vacuum	Vacuum-air		
°C	mm	*Fringe*	*Fringe*	μ	$(n-1)\times10^7$		*Fringe*	*Fringe*	*Fringe*	μ	μ		
18.50	749.5	[b] 0.212											240 minutes before air observations; 180 minutes before vacuum observations.
		[c] .218											
Mean		0.215		1.41	2696	4.8	0.001	0.216	0.219	0.0643		6.4×10^{-7}	
19.25	754.6	[b] 0.223											Constant 135 minutes before air observations; waited 165 minutes, constant 110 minutes before vacuum observations.
		[c] .222											
Mean		0.223		0.49	2708	1.7	0.000	0.223	0.225	0.0661		6.6	
18.80	751.8	[b] 0.262											Waited 150 minutes, constant 80 minutes before air observations; waited 280 minutes, constant 240 minutes before vacuum observations.
		[c] .224											
Mean		0.243		0.94	2702	3.2	0.001	0.244	0.247	0.0726		7.3	
19.50	757.6	[b] 0.189											Waited 260 minutes, constant 240 minutes before air observations; waited 260 minutes, constant 120 minutes before vacuum observations.
		[c] .189											
Mean		0.189		0.25	2715	0.8	0.000	0.189	0.190	0.0558		5.6	
19.00	745.4		[a] 0.238										Waited 260 minutes, constant 170 minutes before vacuum observations; waited 160 minutes, constant 120 minutes before air observations.
			[b] .238										
Mean			0.238	0.73	2677	2.5	0.001	0.239	0.244		0.0717	7.2	
Mean												6.6×10^{-7}	

[a] $\Delta L_{g,s}$ = measured difference in length of gages. [b] Measured shift of first fringe. [c] Measured shift of second fringe.

V. SUMMARY OF RESULTS

The values for all of the compressibility determinations are summarized in table 7. By the direct method of determination (columns 1 and 2), in which identical materials were used and in which temperature uncertainties least affected the results, maximum differences of individual determinations were 4×10^{-8} for fused quartz and 6×10^{-8} for steel; maximum variations from mean values were 2×10^{-8} and 4×10^{-8}, respectively. The coefficients of longitudinal compressibilities determined by this method were

$$C_Q=9.9\times10^{-7} \text{ per atmosphere.}$$
$$C_S=3.1\times10^{-7} \text{ per atmosphere; or}$$
$$C_Q-C_S=6.8\times10^{-7}.$$

The difference of coefficients (column 3) determined by comparison of a fused-quartz gage and a steel gage was $C_Q-C_S=6.6\times10^{-7}$ per atmosphere. This determination is in good agreement with the difference derived by the direct method.

Substitution of the above values for C_Q and C_S in the comparative determinations by methods 1 and 3 (columns 4 to 9) gave consistent agreement for derived values. This agreement extended to those determinations (columns 6 and 9) in which experimental uncertainties had greatest effect upon results. Maximum variation of the mean of any comparative determination from the values of C_Q and C_S, which were determined directly, was 2×10^{-8} for fused quartz and 4×10^{-8} for steel.

TABLE 7.—*Summary of compressibility determinations for fused quartz and steel*

Compressibility	Method 2.—Direct		Method 1.—Comparison of gages of dissimilar materials			Method 3.—Comparison of tube and gage of dissimilar materials			
			Steel gage and quartz gage			Steel tube and quartz gage		Quartz tube and steel gage	
	Steel tube and steel gage	Quartz tube and quartz gage	Measured	Computed from column 3 values		[a] Assume $C_S=3.1\times10^{-7}$	Assume $C_Q=9.9\times10^{-7}$	Assume $C_S=3.1\times10^{-7}$	[a] Assume $C_Q=9.9\times10^{-7}$
				Assume $C_S=3.1\times10^{-7}$	Assume $C_Q=9.9\times10^{-7}$				
	1	2	3	4	5	6	7	8	9
C_S	3.2×10^{-7}				3.5×10^{-7}				
	3.3				3.3		2.8×10^{-7}		
	2.7				2.6		3.1		2.6×10^{-7}
	3.3				[b] 4.3		3.2		2.8+
					2.7				
Mean	3.1×10^{-7}				3.3×10^{-7}		3.0×10^{-7}		2.7×10^{-7}
C_Q		9.9×10^{-7}		9.5×10^{-7}					
		9.7		9.7					
		10.0		10.4		10.5×10^{-7}			
		10.1		[b] 8.7		9.8		10.2×10^{-7}	
		9.8		10.3		9.8		10.0	
Mean		9.9×10^{-7}		9.7×10^{-7}		10.0×10^{-7}		10.1×10^{-7}	
C_Q-C_S			6.4×10^{-7}						
			6.6						
			7.3						
			*5.6						
			7.2						
Mean			6.6×10^{-7}						

[a] Uncertainties should be greater by this method of determination.
[b] Values resulting from *, column 3.

VI. DISCUSSION OF RESULTS

The determined value, $C_Q = 9.9 \times 10^{-7}$, agrees with that of Adams, Williamson, and Johnston, extrapolated to atmospheric pressure from pressures of 2,000 to 10,000 atmospheres, whereas the determined value $C_S = 3.1 \times 10^{-7}$, is 50 percent greater than any measured values we have been able to locate on ferrous alloys ranging from 0.03 percent of other elements through ordinary low- and high-carbon steels, both annealed and quenched, and including a "stainless iron" containing about 16 percent of chromium and about 8 percent of nickel. These values are partly from published reports[9] [10] [11] [12] and partly from unpublished data of Dr. L. H. Adams, which he was kind enough to supply. Since all these values are based upon measurements made at pressures of many atmospheres, it is conceivable that determinations at lower pressures might show a divergence from the straight line relationship for steel. By extrapolation of their curves, Adams, Williamson, and Johnston derived compressibilities 2 to 22 percent greater at 1 atmosphere than at 10,000 atmospheres for certain materials. It is also possible, in view of the known fact that Young's modulus of high-alloy steels may differ by 20 percent from the value of plain carbon steels, that the compressibility of the 14-percent chromium steel used in this investigation may actually be considerably higher at all pressures than that for carbon steels. The 14-percent chromium steel was chosen because it is particularly free from changes of dimension during heat-treatment. This quality is generally associated with good isotropy of the material after heat treatment but the marked anisotropy of a heat-treated chrome-vanadium steel cylinder reported by Bridgman raised the question of possible anisotropy in the steel gage and tube. However, metallographic examination of sections of the steel in both the longitudinal and transverse directions gave no evidence of selective orientation of the crystals. In any case, the analysis of section II of this paper shows that no error would arise from the possibility of transverse anisotropy, as long as the axial elastic constants of the tube and the gage were identical. This seems a reasonable presumption, since both were given identical heat-treatment.

The only other suspected source of appreciable error in the work is that due to faulty wringing. For the fused-quartz tube and gages, no separation of surfaces was of sufficient magnitude to affect results. The wringing of the steel gage and of the steel tube was less satisfactory. Any error from this source would result in a greater change of length between plate and gage surfaces for a change of pressure than that due to compressibility. Furthermore there were two wrung surfaces between the tube and plates, and each had an area of contact of only half the external cross-sectional area of the tube, so that the manner of use of the tube would increase any error due to compression of wrung surfaces. The total movement in any case would appear attributable to compressibility and the results of comparative measurements of steel and fused quartz would be high C_S values.

It was originally intended to assume $C_S = 2.0 \times 10^{-7}$, the value cited in the literature, and from this value, to derive C_Q from comparative

[9] Bridgman, Proc. Am. Acad. Arts Sci. 58, 169–174, (1923).
[10] Adams, Williamson, and Johnston, J. Am. Chem. Soc. 41, 12–42 (1919).
[11] Grüneisen, Ann. Physik 33, 1239 (1910).
[12] Richards, J. Am. Chem. Soc. 37, 1643 (1915).

measurements. Substitution of this value in all comparative determinations of tubes and gages gives less consistent agreements of C_Q values (table 8, column 2) than does the use of $C_S=3.1\times10^{-7}$ (column 1) which was derived by direct measurement. To duplicate the latter agreement with an assigned value $C_S=2.0\times10^{-7}$ (column 3), would require an added change of length attributable to change of distance between surfaces of 0.022 μ (0.075 fringe) for the steel tube and 0.011 μ (0.038 fringe) for the steel gage at all times and for all wringings of the steel gage. Probability of this accidental relationship of errors of wringing or of an exceptionally high C_S for this stainless steel is vitiated to some extent by the result of direct comparison of the stainless-steel gage with the two Johansson steel gages used in the preliminary investigation. This comparison gave a somewhat greater compressibility for the Johansson gages which fall definitely into the class of plain-carbon steels for which the longitudinal compressibility is 2.0×10^{-7} at high pressures. If the correction for the wringing of the stainless-steel gage is negligible, no correction for an error in wringing of the steel tube may be applied which will bring the results of all measurements into the excellent agreement of column 1 without added assumptions which at present appear unwarranted. The measurements, therefore, seem to indicate that the compressibilities of steels in general are considerably greater in the range from 0 to 1 atmosphere pressure than at the higher pressures of many atmospheres at which they have previously been measured. Further measurements would be necessary to establish this definitely.

TABLE 8.—*C_Q values from comparative determinations; with and without assumed corrections for wringing*

Tubes and gages compared	Coefficient of longitudinal compressibility, C_Q		
	(Assuming $C_S=3.1\times10^{-7}$). No correction for wringing	(Assuming $C_S=2.0\times10^{-7}$)	
		No correction for wringing	Corrections for wringing: Steel tube=.022 μ Steel gage=.011 μ
	(1)	(2)	(3)
Quartz gage and steel gage	9.7×10^{-7}	8.6×10^{-7}	9.7×10^{-7}
Quartz tube and steel gage	10.1	9.6	10.1
Steel tube and quartz gage	10.0	7.8	10.0
Mean	9.9×10^{-7}	8.7×10^{-7}	9.9×10^{-7}
Quartz tube and quartz gage by direct comparison, $C_Q=9.9\times10^{-7}$			

With polished steel surfaces of the required planeness to avoid uncertainties here encountered, it is believed that the methods used in this investigation are sufficiently accurate to establish C_S. Greater accuracy of both C_S and C_Q determinations may be attained by increasing the length of specimens and by decreasing wall thicknesses of tubes to the minimum required for wringing. Combination of data resulting from measurements with new apparatus, which permits extension of determinations to 10 atmospheres, with those from meas-

urements of the same material at high pressures by the method of Adams, Williamson, and Johnston, would more definitely establish the $(P-\Delta V)$ relationship from 0 to 12,000 atmospheres.

VII. CONCLUSIONS

Fused-quartz glass.—The longitudinal compressibility of clear, annealed fused quartz for a pressure of 1 atmosphere was determined to be 9.9×10^{-7}, or

$$C_Q=9.9\times10^{-7}\pm5\times10^{-8} \text{ per atmosphere.}$$

Equivalent values are

Coefficient of longitudinal compressibility per megabar.... 9.8×10^{-7}.
Bulk compressibility per megabar, k..... 2.94×10^{-6}.

Steel.—The longitudinal compressibility of a heat-treated 14-percent chromium steel for a pressure of 1 atmosphere was determined to be 3.1×10^{-7} or

$$C_S=3.1\times10^{-7} \text{ per atmosphere.}$$

Equivalent values are

Coefficient of longitudinal compressibility per megabar.... 3.1×10^{-7}.
Bulk compressibility per megabar, k..... 9.3×10^{-7}.

For the reasons discussed in section VI, no limit of accuracy can be assigned to these values for steel.

The author expresses his appreciation to F. C. Roop for assistance in revising the manuscript and in checking the validity of the application of the formulas used.

WASHINGTON, February 20, 1937.

U. S. Department of Commerce National Bureau of Standards

RESEARCH PAPER RP1004

Part of Journal of Research of the National Bureau of Standards, Volume 18, June 1937

BEHAVIOR OF LEATHER IN THE OXYGEN BOMB

By Joseph R. Kanagy

ABSTRACT

The effect on leather of exposure in the oxygen bomb under various conditions was studied. The conditions varied were pressure of oxygen, temperature in the bomb, duration of exposure, and the moisture content and pH of the leathers. A comparison is given between natural aging and accelerated aging in the bomb. An explanation based on the probable structures of quebracho and chestnut tannins is suggested for the difference in stability of the two types of leather. Comparative values of stability to exposure were obtained for leathers tanned with chestnut, quebracho, chrome, and a commercial leather tanned with a blend of vegetable tannins.

CONTENTS

		Page
I.	Introduction	713
II.	Materials and methods	714
III.	Experimental results	715
	1. Effect of varying the oxygen pressure in the bomb	715
	2. Effect of varying the temperature of the bomb	716
	3. Effect of duration of exposure in the bomb	716
	4. Effect of varying the moisture contents of the leathers	716
	5. Effect of varying the pH of the leathers	717
	6. Comparative rates of the evolution of carbon dioxide from chestnut and quebracho leathers	718
IV.	Discussion	718
V.	Summary	722
VI.	References	722

I. INTRODUCTION

A study of the effect of oxygen on leather is important because the vegetable tannins which may constitute up to 50 percent of the weight of a finished leather are easily oxidized. J. Jany [1][1] measured the amount of oxygen absorbed at atmospheric pressure by tanning materials and found that the amount absorbed increased with an increase in pH. He also found that pyrogallol absorbed more oxygen than phenol, this fact supporting the theory that the oxidation depends upon the number of hydroxyl groups. E. W. Merry [2] verified Jany's results. He made further experiments to show that the amount of oxygen absorbed depended upon the type of tanning material and that the presence of metals, such as iron and especially copper, also increased the absorption of oxygen. The fact that iron accelerates the absorption of oxygen and that the amount absorbed increases with an increase in pH was later confirmed by W. Grassmann and F. Fohr [3].

[1] Figures in brackets refer to references at the end of this paper.

The present investigation consisted in a study of the deterioration of vegetable-tanned leathers in an atmosphere of oxygen under pressure as preliminary work for the development of an accelerated aging test for leather.

II. MATERIALS AND METHODS

A porcelain-lined oxygen combustion bomb, 5 inches deep and 3 inches in diameter, was used in this work. The quebracho- and chestnut-tanned leathers were prepared in the experimental tannery of the National Bureau of Standards and contained no filling materials except those taken up from the natural commercial extracts. Blocks of these leathers, 6 by 15 inches, which were treated with varying amounts of sulphuric acid so as to have initial pH values ranging from 5 to 2, were cut into smaller pieces which conveniently fitted into the bomb.

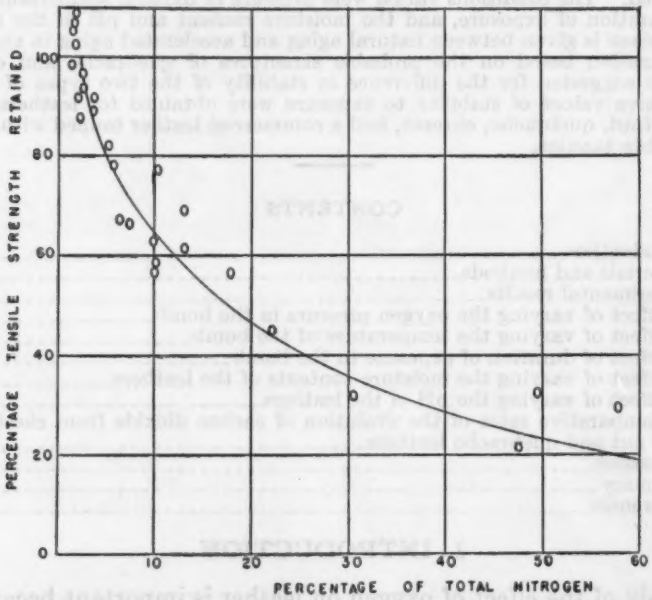

FIGURE 1.—*Comparison of percentage of total nitrogen extracted and loss in tensile strength of leathers aged 2 years under natural conditions.*

Since tensile strength tests could not be made on the small pieces used in the bomb, the effects of the various tests were determined by measuring the chemical deterioration of the leather. The leathers, after being exposed in the bomb, were ground and 3 g of each sample were extracted with five 30-ml portions of water at 50° C. Each portion of water remained in contact with the leather 20 minutes. After being extracted with water, each sample of leather was further extracted by the same procedure with five 30-ml portions of 0.1 *N* sodium carbonate at room temperature. The total nitrogen contents of both the water and sodium carbonate extracts were determined by the Kjeldahl method and from the sum of the two measurements the percentage of the total nitrogen extracted was determined. This method of determining the amounts of soluble nitrogen compounds

in leather is similar to that used by Frey and Beebe [4]. These percentages of the total nitrogen extracted are not a measure of the amount of oxidation occurring in the bomb, but represent the extent of the chemical deterioration in the hide substance under the different conditions of exposure. The mechanism of this deterioration has not yet been studied.

The change in tensile strength with chemical deterioration from results of previous work [5] is shown in figure 1. The percentage tensile strength retained by eight lots of leather was plotted against the total nitrogen extracted from these leathers. The loss in tensile strength is quite rapid at first in comparison with the amount of total nitrogen extracted. However, the results show that a general correlation exists between the physical and chemical deterioration, and for this reason a measurement of chemical deterioration should be as significant as a measurement of physical deterioration.

III. EXPERIMENTAL RESULTS

1. EFFECT OF VARYING THE OXYGEN PRESSURE IN THE BOMB

Preliminary experiments showed that only slightly more deterioration occurred when the oxygen pressure was increased from 50 to 100

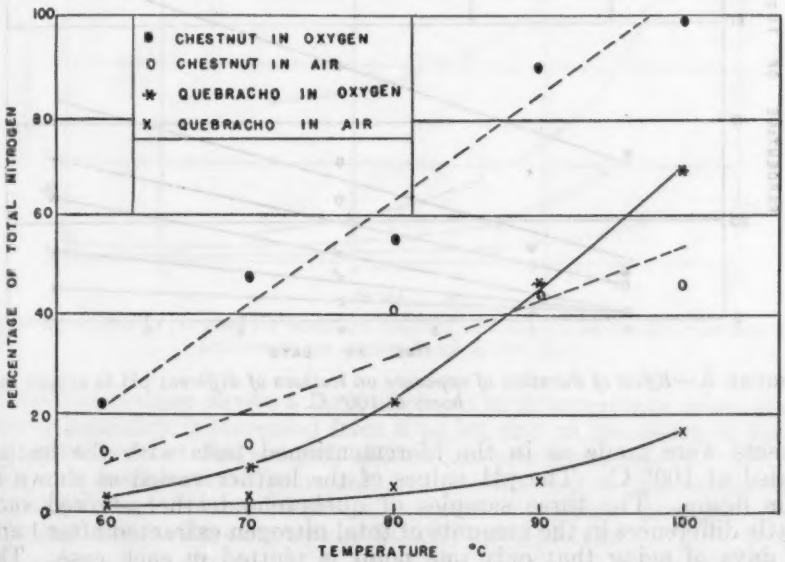

FIGURE 2.—*Effect of varying the temperature on the amount of total nitrogen extracted from leathers at* pH 2.5 *when exposed to air in an oven and to oxygen in a bomb.*

pounds. For this reason the initial pressure of oxygen was held as near to 100 pounds as possible in making all the tests. Two sets of samples at pH values of approximately 2.5 were placed in an electric oven at specified temperatures varying from 60 to 100° C for 24 hours. At the end of this time one set of the samples was placed in the bomb and aged at 100-lb oxygen pressure at the same temperature for 1 week, the other set being allowed to remain in the oven in contact

with air at the same temperature for the same length of time. The effect on the samples of leather on exposure to oxygen in the bomb and on samples exposed to air in the oven is shown in figure 2.

2. EFFECT OF VARYING THE TEMPERATURE OF THE BOMB

The effect of varying the temperature from 60 to 100° C is also shown in figure 2. Chestnut leather shows considerably more deterioration than quebracho leather and the extent of the deterioration for both leathers increases continuously with increasing temperature.

3. EFFECT OF DURATION OF EXPOSURE IN THE BOMB

The increase in deterioration with duration of exposure is shown in figure 3. The time intervals ranged from 1 to 7 days and the experi-

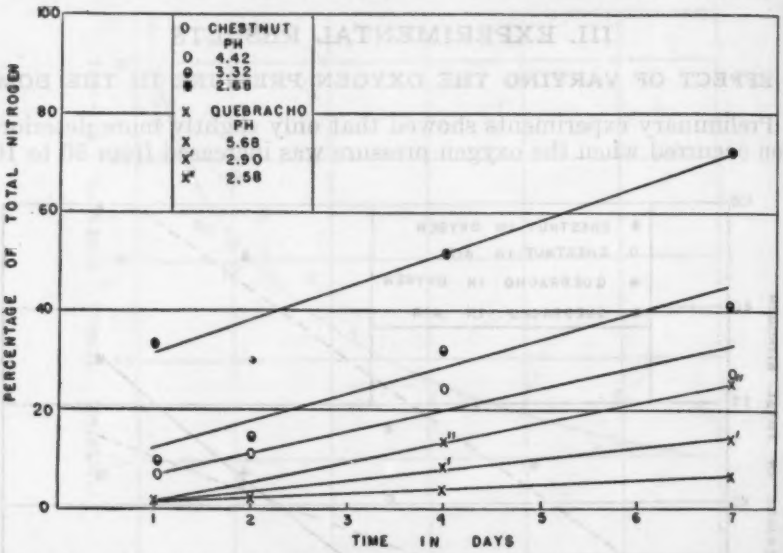

FIGURE 3.—*Effect of duration of exposure on leathers of different* pH *to oxygen in a bomb at 100°* C.

ments were made as in the aforementioned tests with the leather dried at 100° C. The pH values of the leather varied as shown in the figure. The three samples of quebracho leather showed such little differences in the amounts of total nitrogen extracted after 1 and 2 days of aging that only one point is plotted in each case. The deterioration increases at approximately a constant rate. The greater stability of the quebracho leather in comparison with the chestnut leather is again shown by these results.

4. EFFECT OF VARYING THE MOISTURE CONTENTS OF THE LEATHERS

Experiments on the effect of varying the moisture contents of leather aged in the oxygen bomb were all done at 70° C. It was impossible to make tests at a higher temperature because of the tendency of the leather containing high amounts of moisture to char. Even at this

temperature, the chestnut leather conditioned at 60-percent relative humidity and aged 1 week was charred, so that it was impossible to obtain any significant results with it. Tests were made with dried leather and with leather conditioned at 30- and 60-percent relative humidity. The dried leather was obtained by heating the sample in an electric oven at 100° C for 24 hours. The conditioning at 30- and 60-percent relative humidity was done by placing the samples in a desiccator for 2 weeks over sulphuric acid solutions which produced these humidities. The moisture contents of these leathers were 10.8 and 14.3 percent, respectively. The percentages of total nitrogen extracted from leathers of different moisture contents and known pH are shown in figure 4.

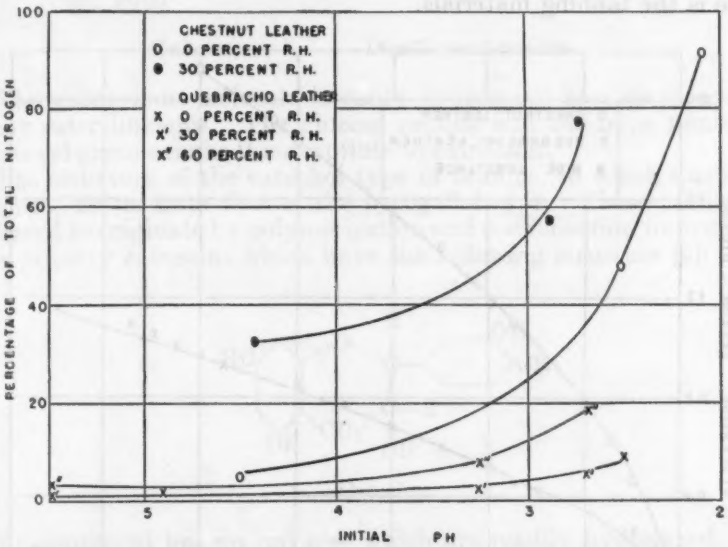

Figure 4.—*Effect of varying the moisture contents and the* pH *on the deterioration of leathers in an oxygen bomb at 70°* C.

Chestnut leather shows a large increase in deterioration when the relative humidity is increased from 0 to 30, and on increasing it further to 60 percent the samples charred as mentioned above. With quebracho leather there is no significant difference in the extent of deterioration at 0- and 30-percent relative humidity; however, an increase occurs in the samples conditioned at 60 percent.

5. EFFECT OF VARYING THE pH OF THE LEATHERS

The influence of pH of the leather on the deterioration produced in the oxygen bomb is shown in figures 3, 4, and 7. The amount of deterioration in all cases increases with decreasing pH. This increase is slow to about pH 3, but it becomes rapid below this point. Chestnut leather shows large amounts of deterioration at comparatively high pH values. In general, the results in regard to the effect of pH are similar to those obtained by Bowker and Wallace [6] in a study of the effect of sulphuric acid on leather.

138329—37——6

6. COMPARATIVE RATES OF THE EVOLUTION OF CARBON DIOXIDE FROM CHESTNUT AND QUEBRACHO LEATHERS

In order to obtain a measure of the relative rates of the oxidation of chestnut and quebracho leathers, dry air free from carbon dioxide was passed over the samples in U-tubes at 100° C, and the amounts of water and carbon dioxide given off were measured by leading the gases through a train of U-tubes containing magnesium perchlorate and Ascarite. The amounts of carbon dioxide evolved are shown in figure 5. Chestnut leather, as shown by the amounts of carbon dioxide given off, is more readily oxidized than quebracho leather. The failure to obtain carbon dioxide when hide substance was treated under the same conditions shows that the source of most of the carbon dioxide is the tanning materials.

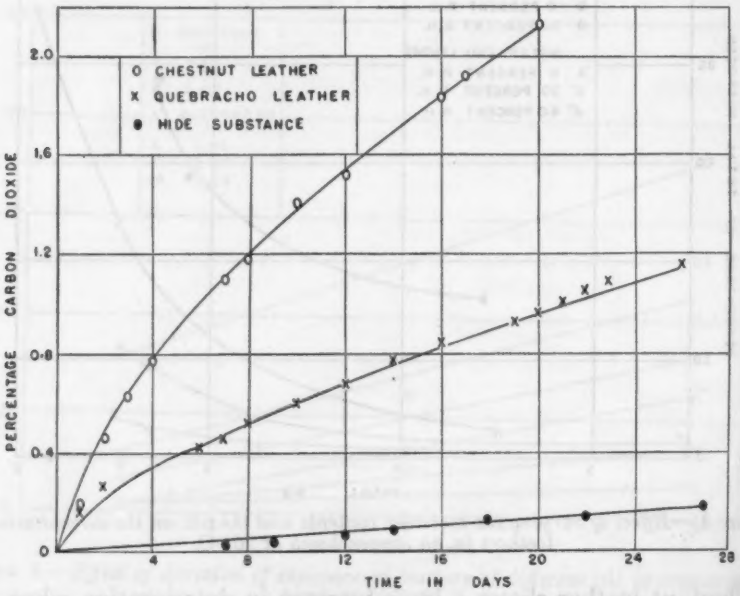

Figure 5.—*Rates of evolution of carbon dioxide from chestnut and quebracho leathers when heated in a stream of air at 100° C.*

IV. DISCUSSION

The results show a large difference between the stability of quebracho- and chestnut-tanned leathers to exposure in the oxygen bomb. Under these conditions the former is quite stable, while the latter is comparatively unstable. An explanation of this difference is suggested by a consideration of the probable structures of the two types of tannins. Chestnut tannin belongs to the pyrogallol type, while quebracho tannin is one of the catechol type. As pointed out by Jany [1], the pyrogallol type should be more easily oxidized because it contains a larger number of hydroxyl groups. Nass and Trimble [7] working independently obtained results which show that chestnut tannin may be considered similar to gallotannin. The formula of gallotannin as determined by Fischer [8] consists of five digallic acid

molecules connected by ester linkages to one molecule of glucose giving the following structure, where R represents one digallic acid residue.

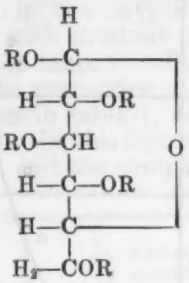

Gallotannin

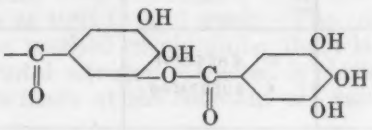

Digallic acid residue

The gallotannin molecule is easily hydrolyzed because it contains many ester linkages. The glucose residue and the large number of hydroxyl groups make it susceptible to oxidation.

The structure of the catechol type of tannins, to which quebracho belongs, differs from that of the pyrogallol type. These tannins are believed to originate by polymerization and condensation from crystalline primary catechins which have the following structure [9]:

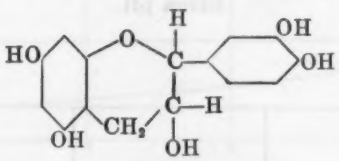

Catechin

This compound has no linkages which are readily hydrolyzed. The resorcinol and catechol residues in this compound are more stable toward oxygen than the pyrogallol residues in gallotannin. The fact that the catechol tannins may be formed by polymerization or condensation gives further evidence of stability.

Although a detailed procedure for an accelerated aging test is not recommended at this time, the results obtained in the present investigation parallel those obtained in natural aging, as shown in figures 6 and 7. In figure 6, the total nitrogen extracted from chestnut- and quebracho-tanned leathers, aged under natural conditions for 8 years, is plotted against pH. Figure 7 shows the results obtained when the same types of leather were dried at 100° C for 24 hours, and aged for 1 week in the oxygen bomb at the same temperature. In each case chestnut leather shows more deterioration than the quebracho leather and the effect of pH is similar for both the accelerated and the naturally aged leathers, except for the fact that more deterioration takes place at the high pH values under the accelerated conditions.

The importance of time of aging for an accelerated test is shown in figure 3. The differences between the amounts of the total nitrogen extracted from the three samples of quebracho leather of known pH increase with increased duration of exposure. The comparative

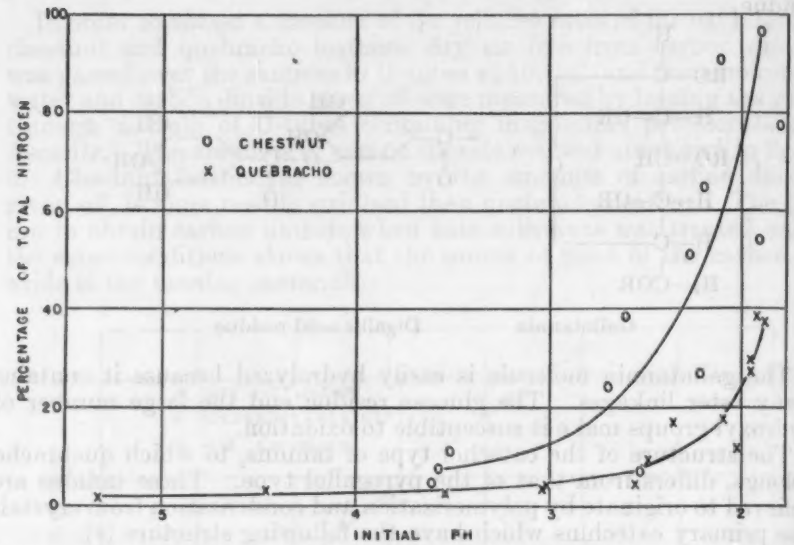

FIGURE 6.—*Effect of aging under natural conditions for about 8 years on leathers of known* pH.

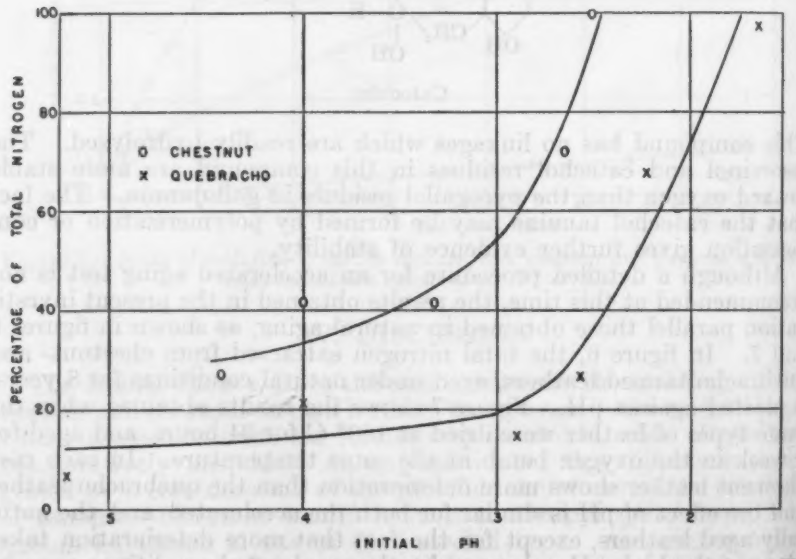

FIGURE 7.—*Effect of accelerated aging for 7 days at 100°* C *on leathers of known* pH.

values for such samples are therefore more significant for the longer times of exposure.

Comparative data on the stability of several types of leather when treated in the oxygen bomb were obtained. These leathers were tanned with chestnut, quebracho, chrome, and a commercial blend of vegetable tannins. The values were determined from the results of aging the oven-dried samples at 100° C for 1 week. The comparisons are given in table 1, and the method of obtaining them is shown in figure 8. In this figure the total nitrogen extracted is plotted against the pH, and the comparisons made at the constant pH value of 2.75.

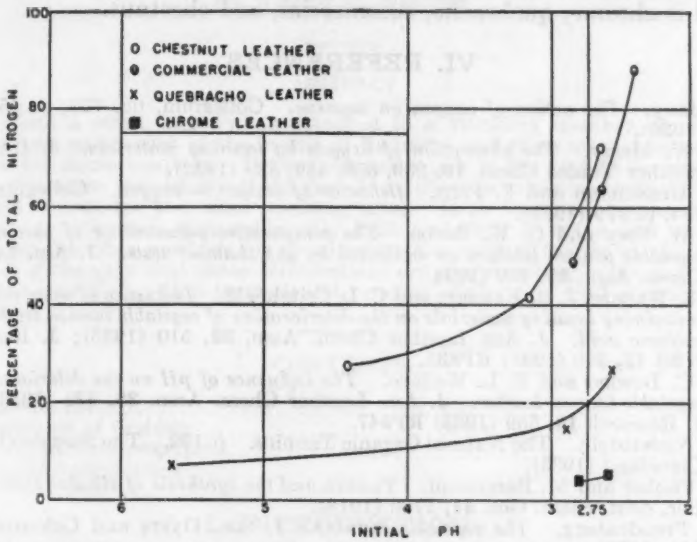

FIGURE 8.—*Method used in obtaining comparative data of the stabilities of leather when exposed to oxygen in a bomb.*

TABLE 1.—*Comparative stabilities of leathers in the oxygen bomb*

Leather	Total nitrogen soluble at pH 2.75
	%
Chestnut	64.8
Commercial	56.5
Quebracho	19.8
Chrome	4.3

The selection of this pH is arbitrary and similar comparisons could be made at any other pH. The most valuable information will probably be obtained by using this or some higher pH. The comparisons point out the degree of protection offered to the leather by the different types of tanning materials. Chrome-tanned leather shows the greatest stability in the oxygen bomb, while the quebracho leather shows considerably more resistance to this treatment than either the chestnut or the commercial leather.

V. SUMMARY

1. Deterioration of leather on treatment in the oxygen bomb increases with increase in oxygen pressure, temperature, duration of exposure, moisture content, and decrease in pH.

2. Quebracho leather is considerably more stable under all conditions of treatment than chestnut leather.

3. Accelerated aging in an atmosphere of oxygen in a bomb compares favorably with natural aging except for the fact that under the former conditions more deterioration takes place at high pH values.

4. The order of decreasing stability of the different types of leather tested is chrome, quebracho, commercial, and chestnut.

VI. REFERENCES

[1] J. Jany. *The action of oxygen on tannins.* Collegium, no. 726, p. 453–460 (1930).

[2] E. W. Merry. *The absorption of oxygen by tanning materials.* J. Int. Soc. Leather Trades Chem. **16,** 239, 358, 489, 529 (1932).

[3] W. Grassmann and F. Fohr. *Behavior of leather to oxygen.* Collegium, no. 784, p. 379 (1935).

[4] R. W. Frey and C. W. Beebe. *The comparative permanence of chrome and vegetable tanned leathers as indicated by gas chamber tests.* J. Am. Leather Chem. Assn. **29,** 489 (1934).

[5] E. L. Wallace, J. R. Kanagy, and C. L. Critchfield. *Influence of some sulphur-containing tanning materials on the deterioration of vegetable tanned leathers by sulfuric acid.* J. Am. Leather Chem. Assn, **30,** 510 (1935); J. Research NBS **15,** 369 (1935) RP835.

[6] R. C. Bowker and E. L. Wallace. *The influence of pH on the deterioration of vegetable-tanned leather.* J. Am. Leather Chem. Assn. **28,** 125 (1933); BS J. Research **10,** 559 (1933) RP547.

[7] M. Nierenstein. The Natural Organic Tannins. p. 192. The Sherwood Press, Cleveland (1935).

[8] E. Fischer and M. Bergmann. *Tannin and the synthesis of similar substances.* Ber. deut. chem. Ges. **51,** 1760 (1918).

[9] K. Freudenberg. *The vegetable tannins.* J. Soc. Dyers and Colourists **45,** 352 (1929).

WASHINGTON, April 2, 1937.

U. S. Department of Commerce National Bureau of Standards

RESEARCH PAPER RP1005

Part of Journal of Research of the National Bureau of Standards, Volume 18, June 1937

COMPENSATION OF STRAIN GAGES FOR VIBRATION AND IMPACT

By William M. Bleakney

ABSTRACT

In general a strain gage, when attached to a vibrating member, undergoes deformations on account of the inertia of its parts, and these may cause serious errors in the strain readings. It has been customary in the past to decrease the mass and increase the rigidity of the gage in an effort to minimize these deformations and correct for the small resulting error. It is, however, frequently not feasible to construct a gage sufficiently light and rigid to make this possible. This paper describes methods for so adjusting the ratio of inertia to rigidity of the parts of the gage that these deformations are compensating. The indication of the instrument may thus be made independent of any acceleration of the gage as a whole.

CONTENTS

	Page
I. Introduction	723
II. Statement of problem	723
III. Compensation principle	725
IV. Proposed application	727

I. INTRODUCTION

The demand for adequate instruments for the measurement of strain in structures in vibration or under impact loads is well known. In the study of vibration in aircraft the Bureau of Aeronautics of the U. S. Navy Department, in cooperation with the Massachusetts Institute of Technology, the Sperry Gyroscope Co., and the Engineering Mechanics Section of the National Bureau of Standards, has been interested in the development of such instruments which may be used to record vibratory strains in aircraft during flight. The severe vibration to which such instruments may be subjected in service requires unusual ruggedness combined with high sensitivity. The present paper is concerned, however, with another desirable attribute; namely, the faithful recording of strain independent of the amplitude and frequency of the vibrating structure under investigation.

II. STATEMENT OF PROBLEM

In general, strain gages consist of two or more parts, one part being attached to each of the two points A and B (fig. 1 and 2), between which the strain is to be determined. These two primary parts, here designated by A' and B', respectively, are restrained to

relative motion of only one degree of freedom, which may be either translational (fig. 1) or rotational (fig. 2), and their relative displacement is indicated by a suitable measuring device C.

Figures 1 and 2 show diagrammatically two simple arrangements which can be used as strain gages. In practice the measuring device may take many different forms, such as a dial micrometer, an optical or mechanical lever, an electric resistance or impedance, an interferometer, or a microscope.

Such systems may be quite satisfactory for strain measurements under static conditions, but when they are applied to the measure-

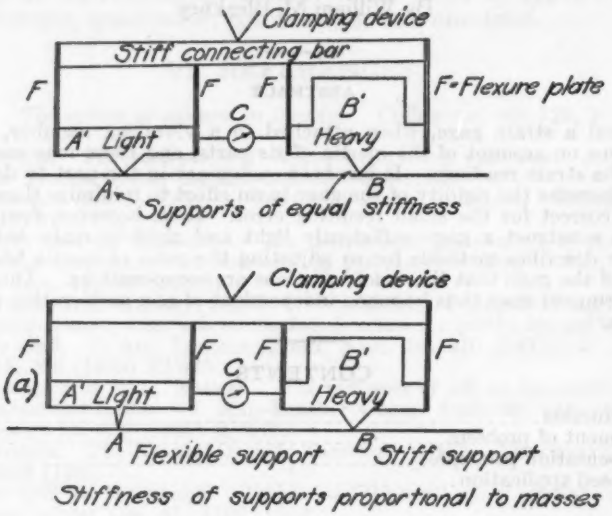

FIGURE 1.—*Strain gage in which the relative motion of the primary parts A' and B' is translational.*

ment of strains in structures in vibration or under impact loads, the accelerations of the systems produce inertia forces which may distort A' and B' and the connecting mechanism, so that the reading of C is in general no longer definitely related to the relative motion of A and B, but varies with the motion of the structure as a whole, and may also vary with the frequency of the vibratory motion.

To avoid this it has been customary in the past to make the parts of the strain-gage system as light and rigid as possible so that these deformations are minimized, and to correct for the small residual

error by various methods, such as reversing the gage and taking the average of readings before and after reversal,[1] or by control experiments to determine the effect of definite accelerations on the reading of the gage. These methods are only partially successful and become entirely inadequate in the study of very high frequency vibrations.

III. COMPENSATION PRINCIPLE

There is, however, another method, so far as we know not previously used, which extends the range of usefulness for these instruments. The method consists in so proportioning the stiffness to the inertia of parts of the system that the inertia forces alone produce no effect

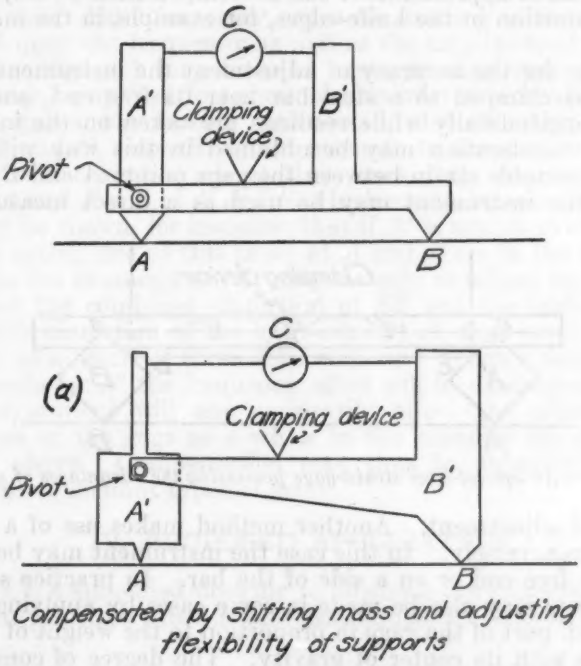

FIGURE 2.—*Strain gage in which the relative motion of the primary parts A′ and B′ is rotational.*

upon the indicating mechanism, although the individual parts of the gage are elastically deformed by these forces.

As a simple illustration of an application of this principle, consider the system represented in figure 1. If the system is accelerated along the line connecting A and B, the knife-edges at these two points, for example, will become distorted and the instrument will in general indicate a strain, although no motion of A relative to B has occurred. If, however, the rigidity is modified as in figure 1(a), or the mass distribution changed as in figure 1(b), and final adjustment obtained by the removal of material at suitable points until no indication of strain is given under these conditions by the indicating mechanism C,

[1] Ramberg, Bailiff, and West. J. Research NBS 14, 189 (1935) RP764.

the gage is then compensated for this type of acceleration, and, of the possible motions of A and B parallel to the line AB, only relative displacements will be indicated by the instrument.

As a second illustration, consider the system represented in figure 2. This system may be modified as shown in figure 2 (a) to provide compensation for longitudinal acceleration of the gage as a whole. The center of mass of the rotating part is shifted below the pivot so that the inertia forces will produce reactions on the knife-edges, which are in the same direction. Distortions in the knife-edges may now be made to compensate by making these reactions proportional to the stiffness of the knife-edges, either by altering the stiffness, or by changing further the mass distribution. If distortion in other parts of the system is appreciable, it can be compensated by adjusting the relative distortion in the knife-edges, for example, in the manner just described.

In testing for the accuracy of adjustment the instrument may, for example, be clamped to a steel bar near its free end, and the bar vibrated longitudinally while readings are taken on the instrument. Since high acceleration may be obtained in this way without producing appreciable strain between the gage points A and B, the indication of the instrument may be used as a direct measure of the

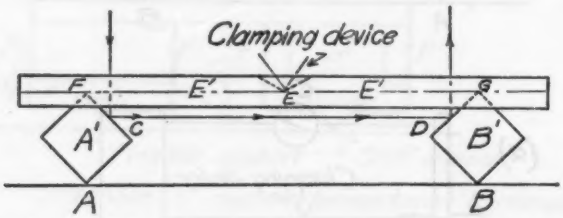

FIGURE 3.—*An optical-lever strain gage possessing the advantages of symmetry.*

accuracy of adjustment. Another method makes use of a thick bar vibrating transversely. In this case the instrument may be mounted either on a free end or on a side of the bar. In practice sufficiently accurate tests may also be made in some cases by applying a steady force to each part of the gage in proportion to the weight of that part, and in line with its center of gravity. The degree of compensation for acceleration in the direction of these forces will then be indicated by the instrument, provided the principal deformations are localized so that the major portion of each part may be considered practically rigid.

Figure 3 illustrates a simple application of the compensation principle to an optical lever strain gage. The strain is indicated by the rotation of A' relative to B', this rotation being measured by reflecting a light beam from these two parts in succession. By making the system symmetrical about a vertical line through E, deformation arising from acceleration of the system parallel to the line AB will be compensating. Thus extension in GE, for example, will be balanced by compression in EF, so that the length GF remains unchanged. Deformation in the knife-edges of A' and B', should it occur, will be compensated in a similar manner.

The effect of vertical acceleration of the system upon the reading of the instrument may also be reduced and practically compensated

by making the points F and G lie on the neutral axis in bending of the member E'. Thus changes in the length of FG are reduced to second order effects with respect to this type of motion. In this way the gage may be compensated for simultaneous effects arising from two different types of inertia forces.

Thus far we have considered inertia forces arising from acceleration of the strain gage as a whole. In general, these are the most troublesome, first because they may be many times larger than the inertia forces arising from the relative motion of the parts of the gage, and second they are not determined by the strain which is to be measured.

In some cases, however, it may be desirable to compensate a gage for distortions arising from the relative motion inherent in the strain itself, for these distortions may cause the reading of the instrument to depend upon the frequency as well as the amplitude of the vibrating strain. Figure 3 may be used again to show how the present method may be applied to reduce or eliminate this frequency effect.

In this system the rocking members A' and B' rotate about axes through F and G, respectively, in response to strain in the line AB, and angular acceleration about these axes gives rise to the inertia forces at A and F and at B and G, which are to be compensated. It may easily be shown, for instance, that if A' is square in cross section the forces acting due to this cause at A and F are in the same direction and in the ratio of 2:1. It remains only to adjust the rigidity of EF so that the combined distortion of EF and the knife-edge at F balances the distortion of the knife-edge at A, thus preventing rotation of A' as a result of these deformations. When a similar adjustment is made for B' the frequency effect will be eliminated.

This adjustment will not necessarily affect the adjustment for acceleration of the gage as a whole in the plane of the drawing, as described above. Compensation may thus be obtained simultaneously for three distinct types of error.

IV. PROPOSED APPLICATION

Figure 4 is a simplified drawing to illustrate the immediate application of this principle which is now contemplated. The relative longi-

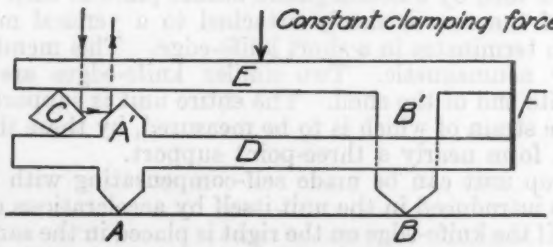

FIGURE 4.—*Compensation principle as applied in figure 5.*

tudinal motion of the horizontal members D and E may be measured by any suitable indicating device. For simplicity an optical system is indicated. The flexure plate F may be designed to carry compressive loads in order to stabilize the system for a constant clamping force applied as indicated. Compensation for acceleration of the

system parallel to the line AB is accomplished in the same manner as that described above. Vertical accelerations will in general produce bending in the horizontal members D and E, which will result in the tipping of the vertical parts A' and B'. This may result in a spurious indication of the instrument. It is clear that by shifting the position of the rocker C the relative bending moments acting on D and E may be so adjusted that the individual effects compensate each other. In practice, the member D, for instance, may be so rigid compared to E that shifting the position of C has little effect. Adjustment may then be made by choosing the proper distance between the point B and the plane of the flexure plate.

This latter method is used in the proposed electromagnetic strain pick-up unit sketched in figure 5. The electrical features of the design were developed by the Massachusetts Institute of Technology and the Sperry Gyroscope Co., who are collaborating in this work.[2]

Figure 5 shows a longitudinal midsection view, which illustrates the essential features of the unit. The core is a permanently magnetized rod of high retentivity and coercivity. Two pairs of soft iron

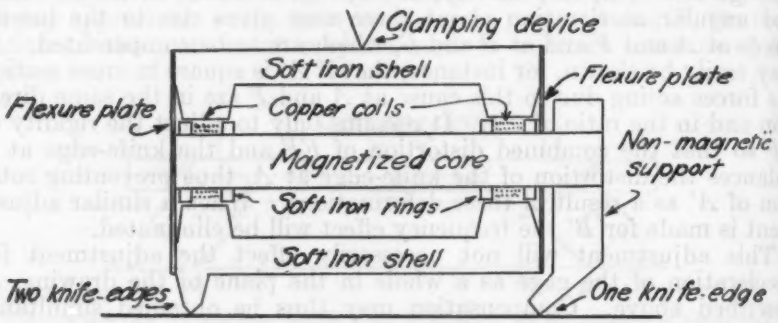

FIGURE 5.—*Electromagnetic and mechanical features of the proposed strain pick-up unit.*

rings are sweated on as shown, and insulated copper coils are wound between the rings of each pair. A cylindrical soft iron shell closes the magnetic circuit. The core is restrained to longitudinal motion relative to the shell by a nonmagnetic flexure plate at each end.

One end of the core is firmly attached to a vertical member, as shown, which terminates in a short knife-edge. This member should be relatively nonmagnetic. Two similar knife-edges are attached to the opposite end of the shell. The entire unit is supported on the structure, the strain of which is to be measured, by these three knife-edges, which form nearly a three-point support.

This pick-up unit can be made self-compensating with respect to deformations introduced in the unit itself by accelerations of the unit as a whole. If the knife-edge on the right is placed in the same vertical plane as the flexure plate at that end, the effect of vertical accelerations will be nearly eliminated. If flexure in the shell and core attributable to vertical accelerations, combined with vertical strain in the flexure plates, is still sufficient to cause appreciable error, this can be compensated by shifting the right knife-edge slightly with respect to

[2] Draper, Bentley, and Willis. J. Aeron. Sci. 4, 281 (1937).

the flexure plate. The optimum position for this knife-edge may be found by trial and henceforth incorporated permanently in the unit.

More serious errors may arise from internal deformations because of longitudinal accelerations of the unit as a whole. These errors, however, may be completely compensated by making the ratio of mass to rigidity the same in the two members. This can be done by trial on each individual unit by removing material at suitable points until strain readings are shown by test to be independent of longitudinal acceleration. This adjustment may be simplified by making the knife-edges similar in shape, but with a length in proportion to the horizontal load they must carry. In making this balance the effects of inertia reactions of the clamping device on the unit should be compensated.

It is desirable to make the unit as rigid as practicable in order to minimize errors caused by incomplete compensation with respect to translational accelerations as just described. For this reason blunt knife-edges are suggested. There remain possible errors caused by rotational acceleration of the unit as whole, and by the small differences in acceleration of the two members arising from the strain which is to be measured. However, the unit as designed is so rigid that these latter errors will not be appreciable in any application contemplated at present.

The methods outlined here for eliminating errors in the measurement of vibratory or transient strains when these errors arise from deformations within the gage itself have not, to our knowledge, been applied or described previously in the literature. It is to be expected that, as improved instruments for making such measurements become available, these methods will become increasingly important.

WASHINGTON, March 31, 1937.

INDEX TO VOLUME 18

A

Page

Abrasion of yarns, RP993 559
Absorptiveness of paper, RP959 41
Accelerated weathering of asphalt shingles, RP1002 669
Acetates of normal aliphatic alcohols, RP989 499
Acetic acid, use in separating mixtures of paraffin and naphthene hydrocarbons, RP967 129
Acid corrosion of stainless steel, RP963 69
Acidity, effect on electrodeposition of iron, RP991 535
Aircraft finishes, resin, permeability to moisture, RP974 235
Air, performance of water current meters in, RP981 351
Airplane camera lens, testing, RP984 449
Alcohols, normal aliphatic, boiling points and densities of acetates, RP989 499
Aldoses, alpha and beta, bromine oxidation and mutarotation measurements, RP969 141
Alloys, aluminum, anodic oxidation {RP961 53 / RP975 251
Alloys, magnesium, anodic coating of, RP964 83
Alpha cellulose in pulps and papers, RP979 333
Alumina, lime, ferric oxide system, RP987 475
Aluminum, anodic oxidation {RP961 53 / RP975 251
Aluminum, atomic weight, RP957 1
Aluminum coatings, corrosion, RP982 361
Anodic oxidation of aluminum alloys {RP961 53 / RP975 251
Anodic treatment of magnesium alloys, RP964 83
Appliances, gas, effect of depth of ports, RP988 485
Asbestos diaphragms in iron deposition, RP991 535
Asphalt shingles, weathering, RP1002 669
Atomic dimension and optical rotation, RP978 315
Atomic weight of aluminum, RP957 1

B

Beij, K. Hilding, Garbis H. Keulegan and, Pressure losses for fluid flow in curved pipes, RP965 89
Beta cellulose in pulps and papers, RP979 333
Bibber, Leon C., George A. Ellinger and, Laboratory corrosion tests of welded low-carbon stainless steel, RP963 69
Binary compounds, composition, RP995 585
Bleakney, William M., Compensation of strain gages for vibration and impact, RP1005 723
Bloom gloss, absence of, RP958 19
Boiling-point-composition diagram dioxane-water system, RP985 461
Boiling points of acetates of normal aliphatic alcohols, RP989 499
Borate-lead system, RP995 585
Branham, Joseph R., Saturation by water in gas analysis compensators, RP962 59
Brauns, Dirk H., Optical rotation and atomic dimension for the four optically active 1-halogeno-2-methylbutanes, RP978 315
Brenner, Abner, Magnetic method for measuring the thickness of nickel coatings on nonmagnetic base metals, RP994 565
Brick and tile walls, compressive strength, RP972 215
Brickwedde, Ferdinand G., Russell B. Scott, Francis B. Silsbee and, A new phenomenon in the superconducting transition of tantalum and of tin, RP977 295
Bright, Harry A., Determination of sulphur occurring as sulphide in portland cement, RP968 137
——, *Herbert C. Vacher, John G. Thompson and,* Cooperative study of methods for the determination of oxygen in steel, RP976 259
Bromine oxidation of heptoses, RP990 505
Bromine oxidation of sugars, RP969 141
Brownmiller, Lorrin T., William Lerch and, Method for approximating the glass content of portland cement clinker, RP997 609
Bunting, E. N., R. F. Geller and, The system PbO–B_2O_3, RP995 585
Burette for testing absorptiveness of paper, RP959 41
Burners, gas, effect of depth of ports, RP988 485
n-Butyl acetate, boiling point and density, RP989 499
Buzzard, R. W., and J. H. Wilson, Anodic coating of magnesium alloys, RP964 83
——, *and J. H. Wilson,* Deterioration of chromic acid baths used for anodic oxidation of aluminum alloys, RP961 53
——, Anodizing of aluminum alloys in chromic acid solutions of different concentrations, RP975 251

C

Calorimeter for saturated steam and water, RP983 389
Calorimetric measurements of heats of combustion of paraffin hydrocarbons, RP966 115
Calorized steel, corrosion, RP982 361
"Camera finish" at the race track, RP986 467
Camera for testing lenses, RP984 449
Camera lenses, testing, RP984 449
Carboloy, thermal expansion, RP960 47
Carson, F. T., A microburette for testing the absorptiveness of thin paper, RP959 41
Case, Frank A., Irvine C. Gardner and, Precision camera for testing lenses, RP984 449
Cellulose, in pulps and papers, RP979 333
Cement clinker, glass content, RP997 609
Cement concretes, stress deformation, RP970 195
Cemented tungsten carbide, thermal expansion, RP960 47
Cement, portland, phase relations, RP987 475
Cement, sulphide sulphur in, RP968 137
Ceramic glasses and glazes, RP995 585
Chromic acid anodizing baths {RP961 53 / RP975 251
Clay brick and tile walls, RP972 215
Cleaves, Harold E., and John G. Thompson, Preparation of iron oxide as a source of high-purity iron, RP996 595
Clinker, portland cement, glass content, RP997 609
Coatings, nonbituminous, soil corrosion of, RP982 361
Cobalt-tungsten carbide mixtures, thermal expansion, RP960 47
Combustion as influenced by gas burner ports, RP988 485
Combustion, heats of, paraffin hydrocarbons, RP966 115
Compensators, gas analysis, RP962 59
Compressibility of fused-quartz glass, RP1003 683
Concrete, effect of temperature on stress-deformation relation, RP970 195
Configuration of pyranoses, RP990 505
Copper sulphate—sulphuric acid corrosion of stainless steel, RP963 69
Corrosion of aluminum {RP961 53 / RP975 251
Corrosion of magnesium alloys, RP964 83
Corrosion of underground structures, RP982 361
Corrosion tests of stainless steel, RP963 69
Cotton yarns, effect of sizing, RP993 559
Critical state of water, RP983 389
Crocidolite diaphragms in iron deposition, RP991 535
Crystal behavior of hydrocarbons, RP1000 639
Current meters, performance, RP981 351
Curve fitting with high precision, RP971 205
Cystine in oxidized wool, RP998 623

D

Densities and boiling points of normal aliphatic alcohols, RP989 — 499
Density, effect on water current meters, RP981 — 351
Density of distilled water as a function of temperature, RP971 — 205
Deterioration of chromic acid baths {RP961 — 53; RP975 — 251}
Deterioration of leather, RP1004 — 713
Diaphragms, use in electrodeposition of iron, RP991 — 535
Dioxane-water system, boiling-point—composition diagram, RP985 — 461
Distilled water, density and refractive index, RP971 — 205
Distinctness-of-reflected-image gloss, RP958 — 19
Drop-measuring apparatus, RP959 — 41

E

Eiseman, John H., and Francis A. Smith, Effect of the depth of drilled ports on the limits of operation of domestic gas burners, RP988 — 485
Elasticity of concrete, RP970 — 195
Electrodeposition baths {RP961 — 53; RP964 — 83; RP975 — 251; RP991 — 535}
Electrodeposition of iron, RP991 — 535
Electrodeposition of rhenium, RP999 — 629
Electrodeposits, measurement of thickness, RP994 — 565
Ellinger, George A., and Leon C. Bibber, Laboratory corrosion tests of welded low-carbon stainless steel, RP963 — 69
Elongation of yarns at rupture, RP993 — 559
Emerson, Walter B., Compressibility of fused-quartz glass, RP1003 — 713
Equilibria in lead-borate system, RP995 — 585
Ethyl acetate, boiling point and density, RP989 — 499
Expansion of Carboloy, RP960 — 47
Expansion of cemented tungsten carbide, RP960 — 47
Expansion of tungsten carbide-cobalt mixtures, RP960 — 47
Ewing, Scott P., Kirk H. Logan and, Soil-corrosion studies, 1934. Field tests of nonbituminous coatings for underground use, RP982 — 361

F

Fabrics, aircraft, permeability to moisture of resin finishes, RP974 — 235
Ferric nitrate, purification, RP996 — 595
Ferric oxide, lime, alumina system, RP987 — 475
Ferric oxide relations in cement clinker, RP987 — 475
Ferrous chloride baths, electrodeposition of iron in, RP991 — 535
Fluid flow, pressure losses in curved pipes, RP965 — 89
Fractionation of petroleum, RP967 — 129
Fused-quartz glass, compressibility, RP1003 — 683

G

Gages, strain, compensation of, for vibration and impact, RP1005 — 723
Gallup, Braxton E., Hubert R. Snoke and, Accelerated weathering tests of mineral-surfaced asphalt shingles, RP1002 — 669
Galvanized steel, corrosion, RP982 — 361
Gamma cellulose in pulps and papers, RP979 — 333
Gardner, Irvine C., and Frank A. Case, Precision camera for testing lenses, RP984 — 449
——, "Camera finish" at the race track, RP986 — 467
Gas analysis, RP962 — 59
Gas burners, effect of depth of ports, RP988 — 485
Gases in metals, RP976 — 259
Gas volume measurements, RP962 — 59
Geib, Martin N. V., Omar C. Moore, Walter T. Schreiber and, Effect of sizing, weaving, and abrasion on the physical properties of cotton yarn, RP993 — 559
Geller, R. F., and E. N. Bunting, The system PbO–B_2O_3, RP995 — 585
Gilliland, Theodore R., Samuel S. Kirby, Newbern Smith, and Stephen E. Reymer, Characteristics of the ionosphere and their application to radio transmission, RP1001 — 645
Ginnings, D. C., H. F. Stimson, N. S. Osborne and, Calorimetric determination of the thermodynamic properties of saturated water in both the liquid and gaseous states from 100 to 374° C, RP983 — 389
Glass, compressibility of fused-quartz, RP1003 — 683
Glass content of portland cement clinker, RP997 — 609
Glasses and glazes, ceramic, RP995 — 585
Glazes and glasses, ceramic, RP995 — 585
Gloss, review of methods of measurement, RP958 — 19

H

1-Halogeno-2-methylbutanes, optical rotation and atomic dimension, RP978 — 315
Harris, Milton, and Arthur L. Smith, State of the sulfur in oxidized wool, RP998 — 623
——, *Ralph T. Mease, and Henry Rutherford*, Reaction of wool with strong solutions of sulfuric acid, RP980 — 343
Heats of combustion of normal paraffin hydrocarbons, RP966 — 115
Heuer, Wilson W., Robert T. Leslie and, Study of the crystal behavior of hydrocarbons, RP1000 — 639
Hidnert, Peter, Thermal expansion of cemented tungsten carbide, RP960 — 47
Hoffman, James I., and G. E. F. Lundell, Redetermination of the atomic weight of aluminum, RP957 — 1
Hollow tile walls, compressive strength, RP972 — 215
Humphreys, Curtis J., William F. Meggers and, Interference measurements of wave lengths in the ultraviolet spectrum of iron, RP992 — 543
Hunter, Richard S., Methods of determining gloss, RP958 — 19
Hydraulics, flow in pipe bends, RP965 — 89
Hydraulics (see water current meters), RP981 — 351
Hydrocarbons, crystal behavior, RP1000 — 639
Hydrocarbons, heats of combustion, RP966 — 115
Hydrocarbons, in petroleum, RP967 — 129
Hydrochloric acid corrosion of stainless steel, RP963 — 69
Hydrogen in steel, RP976 — 259

I

Impact and vibration, compensation of strain gages for, RP1005 — 723
Interference measurements of wave lengths, RP992 — 543
Ionosphere, characteristics, RP1001 — 645
Iron, electrodeposition, RP991 — 535
Iron oxide, pure, RP996 — 595
Iron, pure, RP996 — 595
Iron spectrum measurements, RP992 — 543
Isbell, Horace S., and William W. Pigman, Bromine oxidation and mutarotation measurements of the alpha- and beta-aldoses, RP969 — 141
——, Configuration of the pyranoses in relation to their properties and nomenclature, RP990 — 509

J

Jessup, Ralph S., Heats of combustion of the liquid normal paraffin hydrocarbons from hexane to dodecane, RP966 — 115

K

Kanagy, Joseph R., Behavior of leather in the oxygen bomb, RP1004 — 713
Kasper, Charles, Rapid electrodeposition of iron from ferrous chloride baths, RP991 — 535
Kennelly-Heaviside layer (see ionosphere) RP1001 — 645
Keulegan, Garbis H., and K. Hilding Beij, Pressure losses for fluid flow in curved pipes, RP965 — 89
Kirby, Samuel S., Newbern Smith, Stephen E. Reymer, Theodore R. Gilliland and, Characteristics of the ionosphere and their application to radio transmission, RP1001 — 645
Kline, Gordon M., Permeability to moisture of synthetic resin finishes for aircraft, RP974 — 235
Knowles, Howard B., G. E. F. Lundell and, A contribution to the chemistry of rhenium RP999 — 629

L

Page

Launer, Herbert F., Simplified determination of resin in papers and pulps, RP973 227
—, Simplified volumetric determination of alpha, beta, and gamma cellulose in pulps and papers, RP979 333
Lead-borate system, RP995 585
Lead-coated steel, corrosion, RP982 361
Leather, deterioration, RP1004 713
Lenses, method of testing, RP984 449
Lerch, William, and Lorrin T. Brownmiller, Method for approximating the glass content of portland cement clinker, RP997 609
Leslie, Robert T., and Wilson W. Heuer, Study of the crystal behavior of hydrocarbons, RP1000 639
Lime, ferric oxide, alumina system, RP987 475
Liquids, microburette for measuring small drops of, RP959 41
Logan, Kirk H., and Scott, P. Ewing, Soil-corrosion studies, 1934. Field tests of nonbituminous coatings for underground use, RP982 361
Lundell, G. E. F., and Howard B. Knowles, A contribution to the chemistry of rhenium, RP999 629
—, *James I. Hoffman and*, Redetermination of the atomic weight of aluminum, RP957 1

M

Magnesium alloys, anodic coating, RP964 83
Magnetic measurement of thickness of nickel coatings, RP994 565
Mason, Martin A., Galen B. Schubauer and, Performance characteristics of a water current meter in water and in air, RP981 351
Masonry, structural tile, strength of, RP972 215
McMurdie, Howard F., Studies on a portion of the system: CaO–Al_2O_3–Fe_2O_3, RP987 475
Mease, Ralph T., Henry Rutherford, Milton Harris and, Reaction of wool with strong solutions of sulfuric acid, RP980 343
Meggers, William F., and Curtis J. Humphreys, Interference measurements of wave lengths in the ultraviolet spectrum of iron, RP992 543
Metallic coatings for underground structures, RP982 361
Metallic rhenium, oxidation, RP999 629
Metals, acid corrosion tests, RP963 69
Metals, determination of gases in, RP976 259
Metals, measurement of electrodeposits, RP994 565
Metals, protection against corrosion { RP961 53; RP964 83; RP975 251; RP994 565
Meters, water current, performance of, RP981 351
Methyl acetate, boiling point and density, RP989 499
Methylbutanes, 1-halogeno-2-, optical rotation and atomic dimension, RP978 315
Microburette for testing absorbent paper, RP959 41
Mineral-surfaced asphalt shingles, accelerated weathering, RP1002 669
Moisture, permeability of resin finishes to, RP974 235
Moore, Omar C., Martin N. V. Gelb, Walter T. Schreiber and, Effect of sizing, weaving, and abrasion on the physical properties of cotton yarn, RP993 559
Mutarotation of sugars { RP969 141; RP990 505

N

Naphthene hydrocarbons, separation from paraffin hydrocarbons, RP967 129
n-Butyl acetate, boiling point and density, RP989 499
Nickel plating, thickness measurements, RP994 565
Nitric acid corrosion of stainless steel, RP963 69
Nitrogen in steel, RP976 259
n-Propyl acetate, boiling point and density, RP989 499

O

Objective, photographic, method of testing, RP984 449
Optical properties of water, RP971 205
Optical rotation and atomic dimension, RP978 315
Optical rotation of sugar { RP969 141; RP990 505
Osborne, N. S., H. F. Stimson, and D. C. Ginnings, Calorimetric determination of the thermodynamic properties of saturated water in both the liquid and gaseous states from 100 to 374° C, RP983 389
"Overshoot" phenomenon in tantalum and tin, RP977 295
Oxidation of aluminum alloys { RP961 53; RP975 251
Oxidation of metallic rhenium, RP999 629
Oxidation of sugars { RP969 141; RP990 505
Oxidation of wool, RP998 623
Oxygen, effect on leather, RP1004 713
Oxygen in steel, RP976 259

P

Paper, resin content, RP973 227
Papers and pulps, determination of cellulose in, RP979 333
Paper-testing microburette, RP959 41
Paraffin hydrocarbons, heats of combustion, RP966 115
Paraffin hydrocarbons, separation from naphthene hydrocarbons, RP967 129
Parsons, Douglas E., and David Watstein, Compressive strength of structural tile masonry, RP972 215
Permeability to moisture of resin finishes, RP974 235
Perrhenic acid, formation, RP999 629
Petroleum, fractionation, RP967 129
Petroleum hydrocarbons, crystal behavior, RP1000 639
Phase relations of lead-borate equilibria, RP995 585
Phase relations of portland cement, RP987 475
"Photo finish" at the race track, RP986 467
Photographic objective, testing, RP984 449
Pigman, William W., Horace S. Isbell and, Bromine oxidation and mutarotation measurements of the alpha and beta aldoses, RP969 141
Pipe bends, pressure losses for liquid flow in, RP965 89
Pipe, nonbituminous coatings for, RP982 361
Plastic flow of concrete, RP970 195
Prepared roofing, accelerated weathering, RP1002 669
Pressure losses in curved pipes, RP965 89
Printing plates, electrodeposition of iron in production, RP991 535
Protective coating on magnesium alloys, RP964 83
Portland cement clinker, glass content, RP997 609
Portland cement, phase relation, RP987 475
Portland cement, sulphides in, RP968 137
Ports for gas burners, RP988 485
Potentiometric titration of reduced compounds of rhenium, RP999 629
n-Propyl acetate, boiling point and density, RP989 499
Pulps and papers, determination of cellulose in, RP979 333
Pulps, paper, determination of resins in, RP973 227
Pyranoses, configuration as related to properties, RP990 505

R

Race track, "camera finish", RP986 467
Radio measurement, ionosphere, RP1001 645
Reflectance methods of determining gloss, RP958 19
Refractive index of distilled water as a function of temperature, RP971 205
Resin finishes for aircraft, permeability to moisture, RP974 235
Resin in paper, RP973 227
Resolving power of lenses, RP984 449
Reymer, Stephen E., Samuel S. Kirby, Newbern Smith, Theodore R. Gilliland and, Characteristics of the ionosphere and their application to radio transmission, RP1001 645
Rhenium, properties, RP999 629
Roofing, asphalt-shingle, RP1002 669
Rutherford, Henry, Ralph T. Mease, Milton Harris and, Reactions of wool with strong solutions of sulfuric acid, RP980 343

S

Page

Schicktanz, Sylvester T., Separation of constant-boiling mixtures of naphthene and paraffin hydrocarbons by distillation with acetic acid, RP967 129
Schreiber, Walter T., Martin N. V. Geib, and Omar C. Moore, Effect of sizing, weaving, and abrasion on the physical properties of cotton yarn, RP993 559
Schubauer, Galen B., and Martin A. Mason, Performance characteristics of a water current meter in water and in air, RP981 351
Scott, Russell B., Ferdinand G. Brickwedde, Francis A. Silsbee and, A new phenomenon in the superconducting transition of tantalum and of tin, RP977 295
Silsbee, Francis B., Russell B. Scott, and Ferdinand G. Brickwedde, A new phenomenon in the superconducting transition of tantalum and of tin, RP977 295
Sheen, description, RP958 19
Shingles, asphalt, accelerated weathering, RP1002 669
Silt in streams as affecting accuracy of current meters, RP981 351
Sizing of yarns, RP993 559
Smith, Arthur L., Milton Harris and, State of the sulfur in oxidized wool, RP998 623
Smith, Edgar R., and Mieczyslaw Wojciechowski, Boiling-point-composition diagram of the system dioxane-water, RP985 461
——, *Mieczyslaw Wojciechowski and*, Boiling points and densities of acetates of normal aliphatic alcohols, RP989 499
Smith, Francis A., John H. Eiseman and, Effect of the depth of drilled ports on the limits of operation of domestic gas burners, RP988 485
Smith, Newbern, Stephen E. Reymer, Samuel S. Kirby, Theodore R. Gilliland and, Characteristics of the ionosphere and their application to radio transmission, RP1001 645
Snoke, Hubert R., and Braxton E. Gallup, Accelerated weathering tests of mineral-surfaced asphalt shingles, RP1002 669
Soil corrosion of metallic coatings, RP982 361
Spectrum of iron, RP992 543
Specular gloss, description, RP958 19
Stainless steel corrosion tests, RP963 69
Starch sizing on yarns, RP993 559
Steam, thermodynamic properties, RP983 389
Steel, determination of gases in, RP976 259
Steel, stainless, corrosion tests, RP963 69
Stimson, H. F., D. C. Ginnings, N. S. Osborne and, Calorimetric determination of the thermodynamic properties of saturated water in both the liquid and gaseous states from 100 to 374° C, RP983 389
Strain gages, compensation of, for vibration and impact, RP1005 723
Stream measurements with current meters, RP981 351
Strength of structural tile masonry, RP972 215
Stress-deformation relation for concrete, RP970 195
Sugars, preparation, nomenclature, mutarotation, and oxidation {RP969 ..... 141; RP990 ..... 505}
Sulfuric acid, effect on leather, RP1004 713
Sulfuric acid solutions, effect on properties of wool, RP980 343
Sulfur in wool, RP998 623
Sulphides in portland cement, RP965 137
Sulphur in portland cement, RP968 137
Superconducting transition of tantalum and tin, RP977 295
Surface texture, discussion, RP958 19
Sweet-potato starch sizing of yarns, RP993 559
Synthetic resin finishes for aircraft, permeability to moisture, RP974 235
System CaO–Al_2O_3–Fe_2O_3, RP987 475

T

Tannins, stability, RP1004 713
Tantalum, superconducting transition, RP977 295
Taylor, John K., Leroy W. Tilton and, Accurate representation of the refractivity and density of distilled water as a function of temperature, RP971 205
Temperature, effect on stress-deformation of concrete, RP970 195
Thermal expansion of Carboloy, RP960 47
Thermal expansion of cemented tungsten carbide, RP960 47
Thermal expansion of tungsten carbide-cobalt mixtures, RP960 47
Thermodynamic properties of saturated steam and water, RP983 389
Thermomutarotations of sugars, RP969 141
Theuer, Arthur U., Effect of temperature on the stress-deformation of concrete, RP970 195
Thickness of electrodeposits, RP994 685
Thompson, John G., Harold E. Cleaves and, Preparation of iron oxide as a source of high-purity iron, RP996 593
——, *Herbert C. Vacher, and Harry A. Bright*, Cooperative study of methods for the determination of oxygen in steel, RP976 259
Tile walls, compressive strength, RP972 215
Tilton, Leroy W., and John K. Taylor, Accurate representation of the refractivity and density of distilled water as a function of temperature, RP971 205
Tin, superconducting transition, RP977 295
Transition, superconducting, of tantalum and tin, RP977 295
Tungsten carbide-cobalt mixtures, thermal expansion, RP960 47

U

Ultraviolet spectrum of iron, RP992 543
Underground corrosion of metallic coatings, RP982 361

V

Vacher, Herbert C., Harry A. Bright, John G. Thompson and, Cooperative study of methods for the determination of oxygen in steel, RP976 259
Vibration and impact, compensation of strain gages for, RP1005 723
Volumetric gas analysis, RP962 69

W

Walls, brick and tile, compressive strength, RP972 215
Water current meters, performance, RP981 351
Water-dioxane system, boiling-point—composition diagram, RP985 461
Water, distilled, density and refractive index, RP971 205
Water, properties, RP983 389
Water-vapor in gas-analysis compensators, RP962 69
Watstein, David, Douglas E. Parsons and, Compressive strength of structural tile masonry, RP972 215
Wave lengths in spectrum of iron, RP992 543
Weathering of asphalt shingles, RP1002 669
Weaving of yarns, RP993 559
Welded stainless steel, acid corrosion, RP963 69
Welded steel corrosion tests, RP963 69
Wilson, J. H., R. W. Buzzard and, Anodic coating of magnesium alloys, RP964 83
——, *R. W. Buzzard and*, Deterioration of chromic acid baths used for anodic oxidation of aluminum alloys, RP961 53
Wojciechowski, Mieczyslaw, and Edgar R. Smith, Boiling points and densities of acetates of normal aliphatic alcohols, RP989 499
——, *Edgar R. Smith and*, Boiling-point—composition diagram of the system dioxane-water, RP985 461
Wool, effect of solutions of sulfuric acid on properties, RP980 343
Wool, oxidation, RP998 623

Y

Yarns, effect of sizing on properties, RP993 559

Z
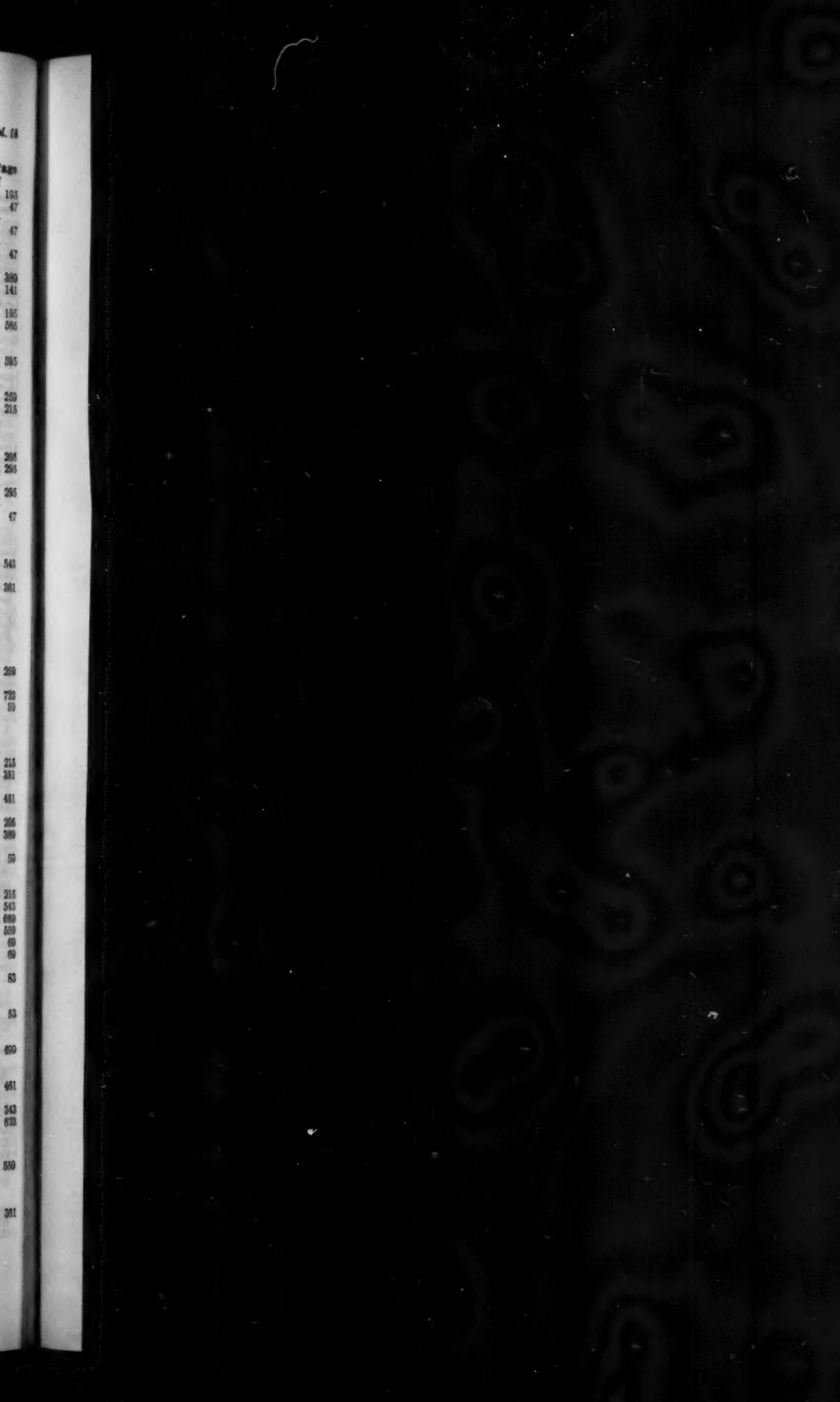
Zinc-coated steel, corrosion, RP982 361